THE
UNIVERSITY OF WISCONSIN–
MILWAUKEE

COLLEGE OF ENGINEERING
AND
APPLIED SCIENCE

DISCLAIMER

INTERFACIAL AREA AND INTERFACIAL TRANSFER IN TWO-PHASE FLOW SYSTEMS

Volume II. Chapters 6 – 10

T. Guo, J. Park and G. Kojasoy

Department of Mechanical Engineering
University of Wisconsin-Milwaukee, Milwaukee
Milwaukee, Wisconsin 53201

March 2003

Prepared for
U.S. DEPARTMENT OF ENERGY
Under Contract No. DE-FG02-87ER13764

TABLE OF CONTENTS

VOLUME I

VOLUME II

VOLUME III

VOLUME IV

EXECUTIVE SUMMARY

Advances in the study of two-phase flow increasingly require detailed internal flow structure information upon which theoretical models can be formulated. The void fraction and interfacial area are two fundamental parameters characterizing the internal flow structure of two-phase flows. However, little information was available on these parameters, and it is mostly limited to vertical flow configuration. Particularly, there was virtually no database for the local interfacial area concentration in spite of its necessity in multidimensional two-fluid model analysis.

In view of the above, a research program, which has been sponsored by the DOE/BES, has been underway at the University of Wisconsin-Milwaukee. The overall objectives of the research program were to develop instrumentation methods, an extensive database and analysis leading to predictive models for describing the internal flow structure and behaviors of two-phase flow in horizontal configurations.

Experimental efforts were directed at developing instrumentation technique for measurements of the local interfacial area concentration and void fraction in the bubbly flow, plug/slug flow, stratified smooth and stratified wavy and annular flow patterns encountered for two-phase flows in horizontal configurations. Chapters 5 through 12 describe several conductivity probe techniques that have been developed under this research program. More specifically:

- Chapters 5 and 6 present the development and utility of the two-sensor conductivity probe for a bubbly flow,
- Chapter 7 describes the utility of hot-film anemometry method for a bubbly flow whereas Chapters 9 and 10 documents the development of hot-film probe method for a plug/slug flow,
- Chapter 8 describes the four-sensor conductivity probe design for measuring the large bubble interfacial area concentration in a plug/slug flow-pattern,
- Chapter 11 summarizes the development and utility of a two-sensor parallel-wire conductivity probe for the stratified, i.e., stratified-smooth,

stratified-wavy and stratified-atomizing, flow patterns encountered in horizontal two-phase flows, finally,

- Chapter 12 involves with the development of eight-sensor parallel-wire probe method designed for a horizontal annular flow-pattern.

Analytical efforts were focused on deriving predictive mechanistic models describing the interfacial structure in various adiabatic two-phase flow patterns as well as predicting fluid particle behavior in boiling channels. Chapters 13 through 18 summarize these efforts. More specifically, they are summarized as follows:

- Chapter 3 deals with the derivation of the interfacial area transport equation and discusses the basic mechanisms affecting the source and sink terms appearing in the interfacial transport equation.
- Chapter 13 is devoted to studies of interfacial instabilities of horizontal stratified flows,
- Chapter 14 describes mechanistic scaling methodologies and derivation of similarity requirements for two-phase flow-regime transitions,
- Chapter 15 presents an analysis of the spherically symmetric phased change (moving boundary) problem to describe the bubble growth and/or collapse in boiling channels,
- Chapter 16 describes several droplet disintegration mechanisms and offers droplet size and size distributions model for an annular flow-pattern, whereas Chapter 17 is devoted to bubble break-up processes and describes a detailed mechanistic model describing the averaged bubble size and size distributions in bubbly flow, finally,
- Chapter 18 deals with modeling of void fraction and interfacial area concentration and concludes that the core break-up is a dominant break-up mechanism, which determines the interfacial area concentration in the core whereas the Taylor break-up mechanism becomes dominant around the pipe perimeter.

LIST OF FIGURES

VOLUME I

VOLUME II

VOLUME III

VOLUME IV

LIST OF TABLES

VOLUME I

VOLUME III

VOLUME IV

6. INTERNAL STRUCTURE AND INTERFACIAL VELOCITY DEVELOPMENT FOR BUBBLY TWO-PHASE FLOW

G. Kojasoy, W.D. Huang
Department of Mechanical Engineering
University of Wisconsin-Milwaukee,
Milwaukee, WI 53201, USA

ABSTRACT

This paper describes an experimental study of the internal structure of air-water flowing horizontally. The double-sensor resistivity probe technique was applied for measurements of local interfacial parameters, including void fraction, interfacial area concentration, bubble size distributions, bubble passing frequency and bubble interface velocity. Bubbly flow patterns at several flow conditions were examined at three axial locations, L/D = 25, 148 and 253, in which the first measurement represents the entrance region where the flow develops, and the second and third may represent near fully developed bubbly flow patterns. The experimental results are presented in three-dimensional perspective plots of the interfacial parameters over the cross-section. These multi-dimensional presentations showed that the local values of the void fraction, interfacial area concentration and bubble passing frequency were nearly constant over the cross-section at L/D = 25, with slight local peaking close to the channel wall. Although similar local peakings were observed at the second and third locations, the internal flow structure segregation due to buoyancy appeared to be very strong in the axial direction. A simple comparison of profiles of the interfacial parameters at the three locations indicated that the flow pattern development was a continuous process. Finally, it was shown that the so-called "fully developed" bubbly two-phase flow pattern cannot be established in a horizontal pipe and that there was no strong correspondence between void fraction and interface velocity profiles.

6.1 Introduction

The bubbly two-phase flow pattern is characterized by the presence of bubbles, with the maximum size being much smaller than the diameter of the containing channel

size, dispersed in a continuous liquid phase. This two-phase flow pattern appears in a wide range of energy conversion devices, such as nuclear reactors, liquid metal MHD generation systems and chemical reactors. In order to improve the efficiency and/or to analyze the safety of such systems, it is important to know the detailed internal structure of bubbly two-phase flow.

The void fraction, interfacial area concentration and mean bubble size are three fundamental parameters describing local internal structure for the bubbly two-phase flow. The void fraction represents the local phase distributions, whereas the interfacial area describes the available interfacial area for the interfacial transport of mass, momentum and energy. Finally, the bubble size serves as a link between the void fraction and interfacial area concentration. An accurate knowledge of local distributions of these internal geometric parameters is of great importance to the eventual understanding and modeling of the interfacial transfer terms, which are required in a multi-dimensional two-fluid model analysis of a two-phase flow field.

For the purpose of providing basic information on the internal structure and interfacial transfer mechanisms in bubbly two-phase flow, a considerable number of experimental studies have been carried out in recent years. Since the fundamental work of Serizawa et al. (1975) and Herringe and Davis (1976), continuous progress has been made with respect to the degree of experimental profoundness in studying local two-phase flow structures (Delhaye, 1991; Ishii, 1991; Kataoka, 1990; Kocamustafaogullari, 1991; Liu, 1989, 1991; Wang, 1987). Also, in parallel with these experimental efforts, there has been significant progress in the analysis of phase separation and phase distribution phenomena in bubbly flows (Beyerlein, 1985; Kataoka, 1991; Lahey, 1989; Zun, 1990). It is to be recognized that with the exception of the work of Kocamustafaogullari and Wang (1991), all of the bubbly flow experiments were carried out in vertical flow channels. Even in the case of well-studied vertical flow configurations, experimental results from fairly diverse sources are controversial regarding the lateral void fraction distributions and the effects of bubble size and flow conditions causing void profile transformation from a saddle shape into a convex shape. The difficulties in obtaining completely similar general results undoubtedly stem from our lack of understanding of scaling the entrance effects as well as the mechanisms

involved in determining the internal structure of bubbly two-phase flow. The problem of phase distributions is further complicated by the fact that gas-liquid mixture pipe flows do not exhibit the fully developed equilibrium condition that is characteristic of single-phase flows. The expansion of the gas phase associated with the frictional pressure gradient causes a continuous acceleration of the mixture, and, consequently, a continuous flow development in the axial direction.

In view of the above discussion, it is evident that much experimental work is still necessary to attain a thorough physical understanding of the transverse and axial phase distribution mechanisms in bubbly two-phase flows. In this context, an experimental investigation has been under way at the University of Wisconsin-Milwaukee to study the transverse distribution and axial development of local air-water bubbly two-phase flow characteristics along horizontal flow channels.

The experimental work is directed at establishing a comprehensive database for model development to describe interfacial area concentration and interfacial transfer terms. In these experiments, a double-sensor resistivity probe technique was employed to measure the local void fraction, bubble interface velocity and local interfacial area concentration in an air-water bubbly flow in a 50.3 mm ID horizontal channel. In addition to these, the local Sauter mean diameter of bubbles, bubble passing frequency and bubble chord length distribution have also been measured simultaneously by the same probe. In order to determine whether some type of fully developed or equilibrium condition does exist after an adequate entrance length, the local measurements of the internal flow structure were made at three axial locations, L/D = 25, 148 and 253 downstream of the air-water mixing chamber. In the following, the test facility is described, and some results are discussed in terms of transverse distributions and axial development of local void fraction, interfacial area concentration, bubble passing frequency and bubble interface velocity.

6.2 Experimental setup and procedure

6.2.1 Description of the flow loop

The overall flow loop schematic is illustrated in Fig. 1. The loop consists of two parallel lines of 50.3 mm ID and 25.2 mm ID circular Pyrex glass tubings with pressure

taps installed between them. The entire test section is about 15.4 m in length and is all transparent, so that flow visualization, high-speed photography and high-speed cinematography are possible. It is designed such that various local instrumentations for two-phase flow measurements and different mixing chambers can be easily accommodated.

The air and water are used as coupling fluids. The air to the test section is supplied from the University of Wisconsin-Milwaukee central air system. It is, however, regulated through a 0.95 m^3 capacity high-pressure storage tank, and metered by a series of turbine flowmeters. The water is recirculated. It is pumped from a 1.9 m^3 capacity storage tank by a stainless steel centrifugal pump and regulated from 0 to 100% of the pump capacity by a transistor inverter. The water flow rate is measured by a series of paddlewheel flowmeters assembled in a parallel configuration. As shown in Fig. 2, the air enters the mixing chamber from a 90° vertical leg and is injected into the water flow through a cylindrical porous media of 100 μm porosity to achieve a uniform mixing. The two-phase mixture from the test section is directed to an air-water separator. The air is vented to the atmosphere, and the water is returned to the water storage tank.

The last 1.5 m of the test section incorporates two quick-closing valves, which are pneumatically operated and electronically controlled, have a very rapid response time (of the order of milliseconds) and are synchronized through a common electrical switch to ensure simultaneous operation. The distance between the valves is long enough to minimize any experimental error in measuring the average void fraction. For the purpose of obtaining a significant and consistent value of the average void fraction, the void fraction measurements by the quick-closing valves were repeated at least two times. On some occasions, it was repeated more than twice.

Pressure transducers of the diaphragm type are utilized for both absolute pressure and differential pressure measurements, and a series of U-tube manometers are also used for differential pressure measurements. The test section differential pressure is measured at six intervals with high-frequency transducers, with a natural frequency of 5 kHz, located 1.53 m apart from each other. Their range is from 0 to 34.4 kPa with an accuracy of ± 0.3% of the full scale. The absolute pressure transducers are located at two locations

in the test section, 6.70 and 8.22 m downstream of the mixing chamber, respectively. They have a range of 0 to 172 kPa with an accuracy of ± 0.25% of the full scale.

6.2.2 Experimental procedure

The experiments were carried out under bubbly flow conditions by using double-sensor resistivity probes. Liquid and gas volumetric superficial velocities ranged from 3.74 to 6.59 m/s and 0.21 to 1.34 m/s, respectively, and averaged void fractions ranged from 3.73 to 21.5%. The temperature was about 21-23 °C, and the system pressure was about atmospheric. Details of the experimental conditions are summarized in Table 1. It is to be noted that the gas superficial velocities listed in Table 1 refer to the values at L/ D = 253 measurement station. At each preset liquid superficial velocity, the gas superficial velocity was increased as long as the flow pattern was bubbly. Evidence of slug or plug flow was indicated by the output signals and verified by visual observations; such flows were discarded from evaluation. During the operation of the quickclosing valves, the pressure reached sizeable proportions of the transparent loop pressure limitations. The system is protected against pressure surges. The temperature of the water was maintained at room temperature by adding tap water to the storage tank.

The rotary mounting and traversing mechanism for the probe are shown in Fig. 3. The probe was inserted through a probe support located at the bottom of a rectangular Plexiglas test section. The test section was 15 cm in length, 15 cm in height and 7.5 cm in width. The test section was affixed to the flow channel by rotary seals. The seal provided a watertight joint, yet allowed the test section to rotate freely. A spring- loaded locking pin was an integral part of the forward seal. This locking pin provided a "click action" setting to the rotation of the test section, locking it into position every 22.5°. The locking pin was spring preloaded to 2 lb_f for a solid, positive action.

A Vernier, with graduations to an accuracy of 0.01 mm, was used to traverse the probe in a direction perpendicular to the axis of the tube. The position of the probe was read on a digital slide position transducer. The high resolution was necessary to evaluate probe positions in the flow stream accurately and to ensure reproducible results. As shown in Fig. 4, 23 locations were selected through the pipe diameter of 50.3 mm ID. The increments were smaller as the probe traversed toward the wall at the upper half of

the tube. For the majority of experiments, the double-sensor resistivity probe was traced through the vertical axis of the pipe as illustrated in Fig. 4. The local values of void fraction, interfacial area concentration, bubble interface velocity, Sauter mean bubble diameter and bubble passing frequency were measured at each probe stop. In order to investigate the variations of the interfacial parameters over the cross-section of the pipe, for several experimental conditions, the test section was rotated with 22.5° intervals, and the probe was traced at 108 selected points, as illustrated in Fig. 5.

For each preset experimental condition the data, including 23 probe locations, pressure drops at six intervals and the absolute system pressure at two locations, were recorded. As indicated above, at several experimental conditions, the probe was traced through 108 locations. At the end of each experimental run the quick-closing valves were operated to measure average void fraction, which was used to check the validity of local void fraction measurements. Experiments were interfaced with a data acquisition system utilizing a Zenith PC/AT computer with a Metrabyte DASH-16F 16 channel mufti-function high-speed analogue/ digital I/O expansion board, and Labtech Notebook software.

Owing to the large volume of data generated, the sampling rate was kept at 20 kHz for each sensor, and the sampling time was 1 s. It was found that this combination provided a sufficiently large volume of data for any statistical analysis. It is to be noted that the total sampling time may seem to be very short when compared with earlier investigations carried out on vertical bubbly two-phase flows. However, it is important to note that in a horizontal bubbly two-phase flow pattern the velocities are very high, and thus it becomes essential to have a sampling rate as high as possible to record all the bubbles. This simultaneously leads to a shorter sampling time due to overall limitations on the data acquisition system. For more information concerning the flow loop, air-water mixing, experimental procedure and signal processing, see Kocamustafaogullari et al. (1990, 1991).

6.3 Results and discussion

6.3.1 Description of interfacial parameters

In Fig. 6, radial profiles of the local void fraction at $\theta = 0°$, 45° and 90° together with three-dimensional perspective plots of the void fraction distribution over the cross-section of a 50.3 mm ID pipe are presented. The angle θ was measured from the top. These data were taken with a double-sensor resistivity probe traced as shown in Fig. 5 at the axial distance of L/D = 253 from the air-water mixing chamber. The radial profiles shown in Figs. 6(a), (b), (c) and (d), respectively, represent the average gas superficial velocities of $\langle j_g \rangle$ = 0.213, 0.419, 0.788 and 1.21 m/s at a common liquid flow rate, $\langle j_f \rangle$ = 4.67 m/s.

From these figures, it is evident that buoyancy provokes the migration of gas bubbles toward the top of the pipe and the void fraction distribution becomes highly non-symmetric in the pipe cross-section. With an increase in gas flow, the local void fraction at a given location increases. Irrespective of the gas velocity, the internal flow structure has a general similarity at $\theta = 0°$ in terms of local peaking toward the top of the channel wall occurring at about r/R ~ 0.8-0.9. The most distinctive character of the void fraction profiles, however, is the appearance of a bubble boundary layer for all angles. A number of bubbles migrate toward the tube wall, yielding a non-uniform void fraction profile at a given horizontal slice of pipe cross-section. The evolution of such a void profile can be described by the bubble deposition model described by Zun (1990). According to this model, the bubble penetrates in the transverse direction due to lift and diffusion, while on the other hand, large-scale turbulent eddies act as a restraining field to this penetration. Depending on the location in the tube cross-section, the above process may be accelerated or decelerated by the buoyancy. Based on the vertical bubbly flow observations, Zun (1990) correlated the intensity of lift and diffusion with the periodic structure of bubble intrinsic motion. Because of the high bubble population and high bubble passing frequencies, it was not possible to justify Zun's argument by quantitative observations.

The perspective plots always show local peaks toward the tube wall, although the wall peaking is not as strong as that observed for vertical bubbly flows (Liu, 1991; Zun, 1991). As 0 increases, the location of wall peaking moves toward the center making a thicker bubble boundary layer. It is interesting to note from Figs. (b), (c) and (d) that as the gas superficial velocity increases the maximum value of void fraction at 0 = 0°

steadily increases and, also, that the bubble segregation due to buoyancy depletes the bubble population toward the bottom of the pipe until the local maximum at $\theta = 0°$ reaches a value of 0.65-0.70, which corresponds to the maximum packing condition of spherical solid particles. After this value is reached, as shown in Fig. 6(c), the bubble population build-up starts moving toward the bottom of the tube, as indicated in Fig. 6(d). It is also interesting to note from these figures that at $\theta = 90°$, which may locally reflect the vertical bubbly flow configuration, the void fraction profile develops gradually from a saddle-type of profile to a parabolic profile with a single maximum at the pipe center as the gas superficial velocity increases.

Based on experimental observations in a vertical flow channel, Serizawa and Kataoka (1987) described four major void fraction distribution patterns in a two-dimensional $\langle j_f \rangle$-$\langle j_g \rangle$ flow pattern map. Later, Liu (1991) illustrated that the void fraction distribution patterns may not completely be characterized by $\langle j_f \rangle$ and $\langle j_g \rangle$ alone. By changing the initial bubble size, Liu indicated that more than one phase distribution pattern may appear under the fixed volumetric flux combinations of $\langle j_f \rangle$ and $\langle j_g \rangle$. This phenomenon was found to be especially significant under low liquid flow conditions.

Only one bubble generation mechanism was used during the present experimentation. Therefore, effects of initial bubble size were not systematically investigated. However, fundamental photographic studies regarding the initial bubble size effects were undertaken in horizontal bubbly two-phase flow configurations with very low bubble number densities. These visual studies indicated that irrespective of initial bubble size, the maximum and mean bubble sizes were uniquely defined in a distance of $L/D \cong 30$ downstream of the mixing chamber. Similar observations were also made by Sevik and Park (1973). As shown by Kocamustafaogullari et al. (1994) the local turbulence in the core and bubble interactions results in a relatively uniform bubble size distribution due to coalescence and break-up processes. For example, for the cases illustrated in Figs. 6(a)-(d), the average Sauter mean bubble diameter varied from 2.92 mm to 3.93 mm as the gas superficial velocity increased. Although the bubble size is inversely affected by the liquid flow rate and directly proportional to the gas flow, the sample void fraction distributions shown in Fig. 6 are typical distributions of other flow conditions. We were not able to justify four bubbly flow patterns as described by

Serizawa and Kataoka (1987). This discrepancy in experimental observations may be explained in terms of major differences between vertical and horizontal bubbly flow processes.

There are two basic dissimilarities between vertical upflow and horizontal bubbly flow patterns. In the vertical flow, there exists a significant positive relative velocity between bubbles and continuous liquid phase, whereas a small but negative average relative velocity was observed in the horizontal flow. The bubbly flow pattern in horizontal flow appears at much larger liquid velocities than those observed for vertical flow. Higher continuous phase velocities may be responsible for the more homogeneous bubble size distribution that is observed in a horizontal bubbly flow configuration. The bubble size is mainly determined by the turbulence in the core, and the initial bubble size probably is not an important parameter that affects the bubbly flow patterns in a horizontal flow configuration.

Figs. 7 and 8 describe the interfacial area concentration and bubble passing frequency profiles for the corresponding flow conditions of Fig. 6. The interfacial area concentration and the bubble passing frequency profiles very closely follow the void fraction distributions. With the assumption that bubbles are spherically shaped, it can be shown that there exists a very simple relation among the local void fraction, a, local interfacial area concentration, a;, and the local Sauter mean diameter, d_{sm}, as follows:

$$a_i = \frac{6\alpha}{d_{sm}} \tag{1}$$

As demonstrated by Kocamustafaogullari et al. (1994), the Sauter mean bubble size distribution is nearly uniform for a given flow condition. Thus, from Eq. (1) the observed similarity in profiles of the void fraction, interfacial area concentration and bubble passing frequency is not surprising.

For the horizontal flow, the observed local void fraction can reach 0.65-0.70, which corresponds to the maximum packing condition of solid spherical bubbles, whereas the peak interfacial area concentration can go up to 900-1000 m^2/m^3. Since the local transport of mass, momentum and energy are directly proportional to the interfacial area concentration, the figures point to the existence of a highly non-symmetric interfacial transport in a horizontal two-phase flow configuration. As indicated above, the

wall peaking in void fraction and bubble passing frequency has already been observed in vertical flow configurations by several investigators. However, the numerical values of local peaks of void fraction and frequency reported here are much larger than those observed in vertical flow configurations.

The axial components of bubble interface velocities measured by the double-sensor resistivity probe technique are illustrated in Fig. 9 for various gas injection rates. The figure shows that changes in the velocity profile shape are very small compared with changes in the void fraction, interfacial area concentration and bubble passing frequency profiles. There are no peaks in bubble interface velocity profiles corresponding to those observed toward the top wall peaking in void fraction and interfacial area concentration profiles. On the contrary, the velocity profiles show a fairly uniform distribution over a large portion of the flow area, except for the wall region.

In order to quantify the changes of shape, and to provide a simple comparison with single-phase turbulent velocity profiles, the measured curves were fitted by a least squares regression to an empirical equation of the form

$$u_{bi}(r) = \frac{(1+n)(1+2n)}{2n^2}\bar{u}_{bi}\left(1-\frac{r}{R}\right)^{1/n} \qquad (2)$$

where $u_{bi}(r)$ is the local bubble interface velocity and $\bar{u}_{bi}$ is the weighted mean gas velocity defined by

$$\bar{u}_{bi} \equiv \frac{\int_A \alpha(r)u_{bi}(r)da}{\int_A \alpha(r)dA} \qquad (3)$$

The above procedure was performed for all flow conditions of 52 bubbly flow runs. It was noted that the power law indices, n, were grouped about a 1/7th power law, whereas the $\bar{u}_{bi}$ value was grouped slightly smaller than the average liquid velocity by a ratio of 0.85 to 0.98. The lower end of the ratio was observed for the lowest liquid velocity of $\langle j_f \rangle$ = 3.74 m/s, whereas the higher ratio was common for higher liquid superficial velocities. Fig. 10 illustrates several comparisons between locally measured bubble interface velocity and the liquid velocity distribution predicted from the I/7th power law turbulent flow velocity profiles. The liquid velocity profiles were calculated from Eq. (2) by replacing $\bar{u}_{bi}$ by the mean liquid velocity, which is defined by

$$\bar{u}_f = \frac{\langle j_f \rangle}{1 - \langle \alpha \rangle} \tag{4}$$

where $\langle j_f \rangle$ is the average liquid superficial velocity, and $\langle \alpha \rangle$ is the average void fraction defined by

$$\langle \alpha \rangle = \frac{1}{A} \int_A \alpha(r) dA \tag{5}$$

By comparing the measured bubble interface velocity and predicted liquid velocity profiles, it can be observed that the predicted liquid velocity profiles are always slightly greater than the bubble interface velocity. This observation indicates that the bubbles are accelerated by liquid inertia in a very short distance after mixing and closely follow the local liquid phase velocity, and that there is no evidence to suggest a strong proportionate correspondence between void fraction and velocity profiles, as suggested by Beanie (1972). Detailed experimental studies on the average velocity and drift velocity are given elsewhere (Kocamustafaogullari, 1994).

6.3.2 Axial flow pattern development

In order to examine the flow pattern development in the axial direction, additional test sections were built. The local measurements of interfacial parameters were conducted at three axial locations, L/D = 25, 148 and 253 downstream of airwater mixing chamber, in which the first measurement represents the entrance region where the internal flow structure develops, and the second and the third measurements are presumably representative of the near fully developed flow region where the cross-sectional profiles do not change appreciably as the flow moves along the axial direction.

Figs. 11, 12 and 13 compare the local void fraction interfacial area concentration and bubble frequency at two gas velocities. The first (part (a) of each figure), represents low gas flow and the second (part (b)), is representative of high gas flows. Average void fractions shown on these figures indicate these values at L/D = 253. At upstream locations, void fractions are slightly lower due to the pressure gradient; this was taken into account in generating these figures. The following observations can be made from these figures:

- The bubbly flow is maintained throughout the channel.

- Values of the interfacial parameters in the radial direction are nearly constant at L/D = 25 except near the wall, where slight local maxima can be observed irrespective of the gas superficial velocities. This behavior is very similar to the bubbly flow in a vertical tube observed recently by Liu (1991), Ishii and Revankar (1991) and Leung et al. (1993). This is not surprising, because close to the mixing chamber at L/D = 25 the bubble residence time was very small, and the transverse phase segregation due to the gravity has not been established yet. The bubble behavior at this section is very similar to that reported in vertical flow. However, a very significant segregation due to the buoyancy can be observed toward the second and third locations.
- Although large differences can be observed from the first location to the second or third location, there are still appreciable changes that can be observed from the second location to the third one. The changes from the second section to the third one can be partially explained through the expansion of the gas phase associated with the frictional pressure gradient, causing a continuous acceleration of the mixture, and consequently a continuous flow development. However, the flow segregation due to the buoyancy is still effective from the second to the third location. Qazi et al. (1993) reported that the axial development of void fraction profiles in vertical two-phase flow can be achieved at L/D - 22. Recently, Leung et al. (1993) reported similar observations at L/ D =60. However, as demonstrated by Figs. 11(a) and (b), substantial changes occur from L/D = 22 to 60 in the horizontal flow configuration. At high liquid superficial velocities Leung et al. always observed a wall peaking similar to the present observations.
- The internal structure development from the first section to the third section and the gravitational segregation are more gradual in the high gas flows than in the low gas flows.
- For large gas flow rates, local peakings in the void fraction, interfacial area concentration and bubble frequency become more pronounced.
- Finally, the bubbly flow pattern development is a continuous process, and the so-called "fully developed" bubbly two-phase flow pattern cannot be established in a

horizontal pipe. The lag of profile development becomes more significant in higher gas velocities.

Fig. 14 illustrates the axial component of bubble interface velocity profile development for the corresponding flow conditions of Figs. 11, 12 and 13. As the internal flow structure distribution goes through significant changes along the flow direction, the velocity profile stays nearly the same for a given flow condition. A slight change in the numerical values of the velocity can be attributed to the expansion of the gas phase associated with the frictional pressure gradient causing a continuous acceleration of the mixture in the axial direction. The indications of this experimental study are that air-water mixture bubbly flows tend to develop towards a nearly equilibrium velocity profile, independent of the axial location. This was evidenced by the velocity profiles, which appeared to be grouped around a 1/7th power law distribution.

6.4 Summary and conclusions

The internal phase distributions of air-water bubbly two-phase flow in a 50.3 mm ID transparent horizontal pipeline have been experimentally investigated. The local values of the void fraction, interfacial area concentration, bubble passing frequency and axial velocity components were measured by using the double-sensor resistivity probe technique. The axial development of bubbly flow structure for several flow conditions was examined at three axial locations, L/D = 25, 148 and 253, in which the first measurement represents the entrance region where the flow develops, and the second and third represent near fully developed bubbly flow pattern.

The experimental results were presented in the three-dimensional perspective plots of the interfacial parameters over the flow channel cross-section. The indications of this experimental study are that air-water mixture flows tend to develop towards a near equilibrium structure at about L/D = 148, although slight changes are still possible from L/D = 148 to L/D = 253. The continuous changes of the flow structure in terms of void fraction, interfacial area concentration and bubble passing frequency were partially explained in terms of the expansion of the gas phase due to the continuous phase. The

flow structure development was a continuous process, and the so-called "fully developed" bubbly two-phase flow pattern cannot be established in a horizontal pipe.

As the internal flow structure distribution goes through significant changes in the axial direction, the velocity profile stays nearly the same for a given flow condition. The velocity profiles tend to develop towards a nearly equilibrium profile, which appeared to be grouped around 1/7th turbulent flow power law distribution. Finally, there was no evidence to suggest a strong proportionate correspondence between void fraction and velocity profiles, as suggested by early investigators.

6.5 Acknowledgements

The work reported in this paper was supported by the US Department of Energy, Office of Basic Energy Science, under Grant No. DEFG0287ER13764. The authors would like to express their sincere appreciation for the encouragement, support and technical comments on this program from Drs O.P. Manley and D. Frederic of the US DOE/BES.

Dedication

This paper is dedicated to my former graduate adviser, Dr Novak Zuber, whose persuasive interest in two-phase flow started me on the study of interfacial phenomena.

Appendix A: Nomenclature

a_i interfacial area concentration (m^2/m^3)

A pipe cross-sectional area (m^2)

D pipe diameter (m)

d_{sm} Sauter mean diameter (m)

j superficial velocity (m s-')

L axial length (m)

r radial coordinate (m)

R pipe radius (m)

u_{bi} bubble interface velocity (m/s)

$\bar{u}_{bi}$ weighted mean gas velocity (m /s)

$\bar{u}_f$ weighted mean liquid velocity (m/s)

Greek letters

α void fraction

θ angle

Subscripts

B bubble

F liquid phase

G gas phase

I bubble interface

Symbols

$< >$ area-averaged value

$\bar{}$ void fraction weighted mean value

6.6 References

1. D.R.H. Beattie, Two-phase flow structure and mixing length theory, J. Nucl. Eng. Des. 21 (1972) 46-64.
1. S.W. Beyerlein, R.K. Cossman and H.J. Richter, Prediction of bubble concentration profiles in vertical two-phase flow, Int. J. Multiphase Flow 11 (5) (1985) 629-641.
2. J.M. Delhaye and P. Bricard, Interfacial area in bubbly twophase flow experimental data and correlations, ANS Thermal Hydraulics Proceedings, Nat. Heat Transfer Conf., Minneapolis MN, July 28-31, 1991, pp. 3-13.
3. R.A. Herringe and MR. Davis, Structure development of gas-liquid mixture flows, J. Fluid Mech. 73 (1) (1976) 97-123.
4. M. Ishii and S.T. Revankar, Multi-sensor probe method for local measurements in two-phase flow, Proc. 9th Symp. Energy Engineering Sciences, Argonne National Laboratory, 1991.

5. Kataoka and A. Serizawa, Interfacial area concentration in bubbly flow, J. Nucl. Eng. Des. 120 (1990) 163-180.
6. I. Kataoka and A. Serizawa, Statistical behaviors of bubbles and its application to prediction of phase distribution in bubbly two-phase flow, Proc. Conf. Multiphase Flow, Tsukuba, Japan, Vol. 1, 1991, pp. 459-462.
7. G. Kocamustafaogullari, Z. Wang and W.D. Huang, Interfacial characteristic measurements in horizontal bubbly twophase flow, University of Wisconsin-Milwaukee Report, DOE/NE/13764-4, 1990.
8. G. Kocamustafaogullari and Z. Wang, An experimental study on local interfacial parameters in a horizontal bubbly twophase flow, Int. J. Multiphase Flow 17 (5) (1991) 553-572.
9. G. Kocamustafaogullari, W.D. Huang and J. Razi, Measurement and modeling of average void fraction, bubble size and interfacial area, Nucl. Eng. Des. 148 (1994) 437-453.
10. R.T. Lahey, The analysis of phase separation and phase distribution phenomena using two-fluid models, J. Nucl. Eng. Des. 122 (1989) 17-40.
11. W. Leung, S.T. Revankar, Y. Ishii and M. Ishii, Interfacial area and two-phase flow structure development in bubbly flow measured by double sensor probe, ANS Proc. 1993 National Heat Transfer Conf., Atlanta, Vol. 7, 1993, pp. 51-58.
12. T.J. Liu, Experimental investigation of turbulence structure in two-phase bubbly flow, Ph.D. Thesis, Northwestern University, Evanston IL, 1989.
13. T.J. Liu, The effect of bubble size on void fraction distribution in a vertical channel, Proc. Conf. Multiphase Flow, Tsukuba, Japan, Vol. 1, 1991, pp. 453-457.
14. M.K. Qazi, G. Guido Lavelle and A. Clausse, Axial development of void fraction profiles in vertical two-phase flow, Int. J. Multiphase Flow 19 (1993) 385-389.
15. Serizawa, I. Kataoka and I. Michiyoshi, Turbulence structure of air-water bubbly flow, Part II: local properties, Int. J. Multiphase Flow 2 (1975) 235-246.
16. Serizawa and I. Kataoka, in H. Afgan (ed.), Phase Distribution in Two-Phase Flow, Transient Phenomena in Multiphase Flow, Hemisphere, 1987.

17. M. Sevik and S.H. Park, The splitting of drops and bubbles by turbulent fluid flow, J. Fluids Eng. 95 (1973) 53-60.
18. S.K. Wang, S.J. Lee, O.J. Jones and R.T. Lahey, 3-D turbulence structure and phase distribution measurements in bubbly two-phase flows, Int. J. Multiphase Flow 13 (1987) 327-343.
19. Zun, Mechanism of bubble nonhomogeneous distribution in two-phase shear flow, Nucl. Eng. Des. 118 (1990) 155-162.
20. Zun, I. Kljenak and S. Moze, Space-time evaluation of bubble non-homogeneous distribution in upward flow, Proc. Conf. Multiphase Flow,. Tsukuba, Japan, Vol. 1, 1991, pp. 463-467.

HORIZONTAL TWO-PHASE FLOW LOOP

A - Interchangeable Air-Water mixing chambers
B - Water flow meters of appropriate size
C - Water flow meter control valves
D - Air flow meters of appropriate size
E - Air flow meter control valves
F - Air flow regulating valves
G- Air pressure regulator
H - Air filter
I - Water pressure relief valves
J - Water flow regulating valves
K - Pneumatic operated ball valves
L - Motor control
M - computer and data acquisition system
N - 250 gal. Air tank
P - 500 gal. Water tank
Q - Air-Water separator, with internal baffles
R - Water shut-off valve
S - 20 hp. 750 gpm Water pump
T - Glass pipe couplings with pressure taps

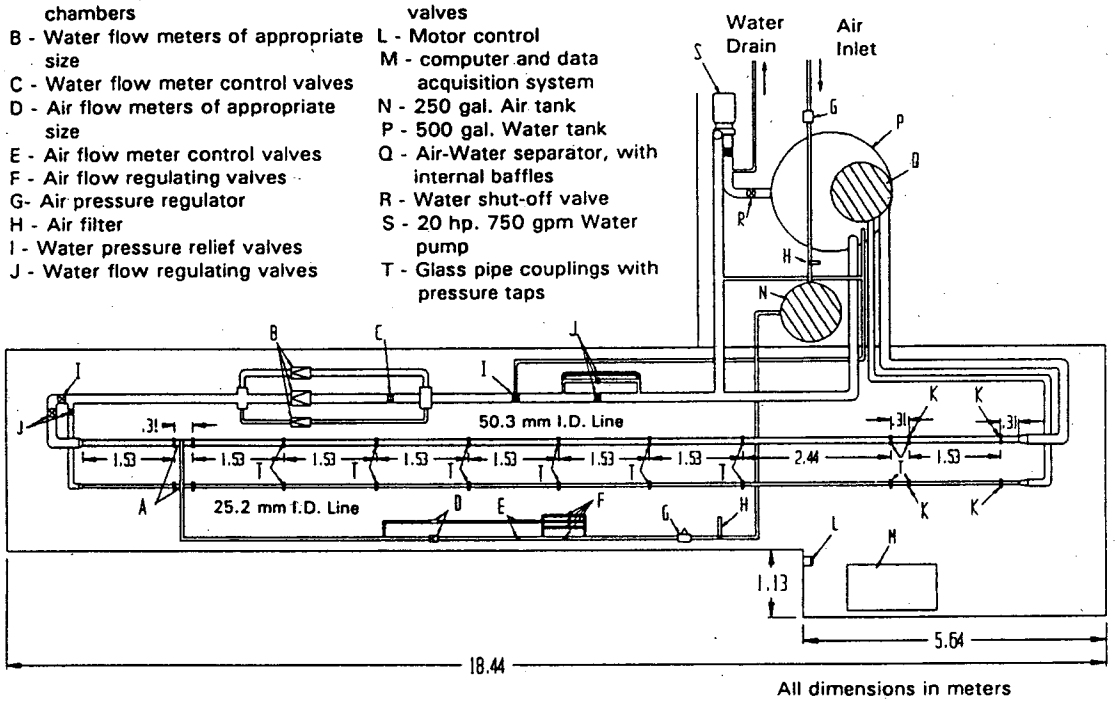

Fig. 1. Schematic of the experimental flow loop.

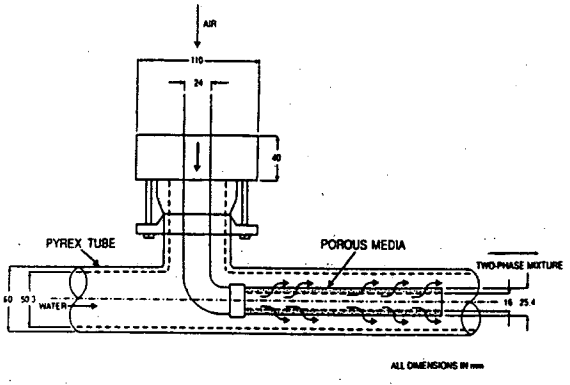

Fig. 2. Schematic of the air–water mixing chamber.

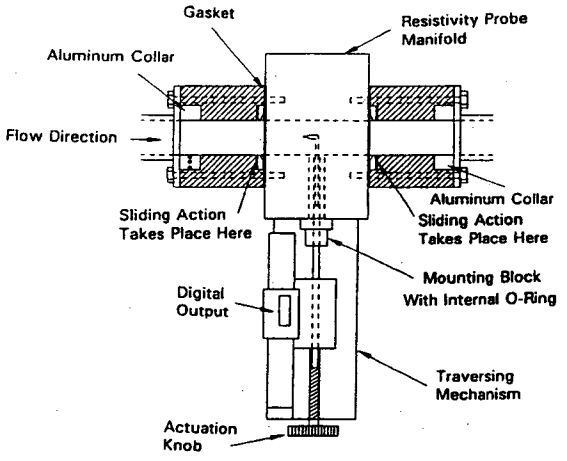

Fig. 3. Mounting and traversing mechanism.

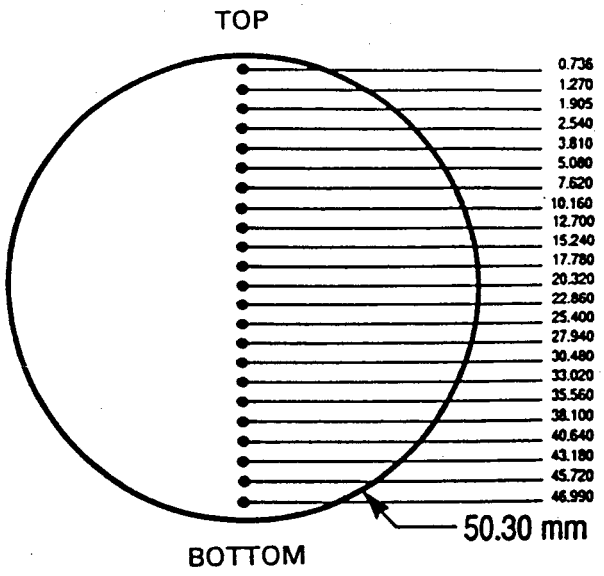

Fig. 4. Probe positions along vertical axis of test section.

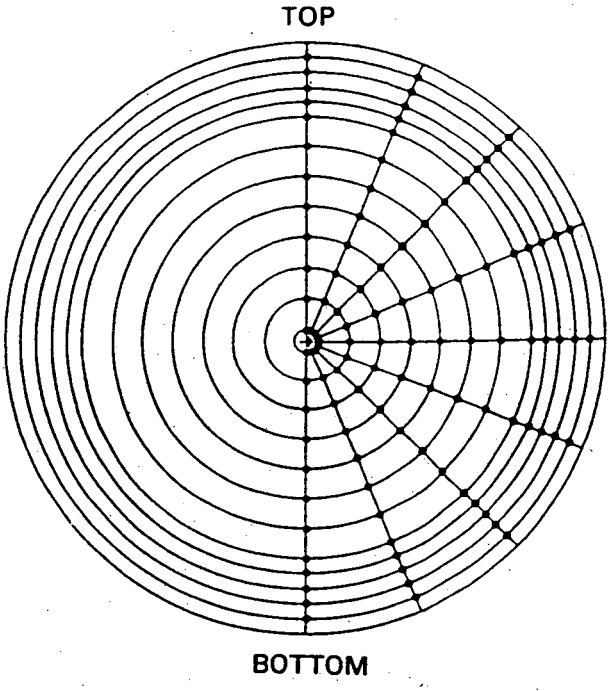

Fig. 5. Probe positions across test section.

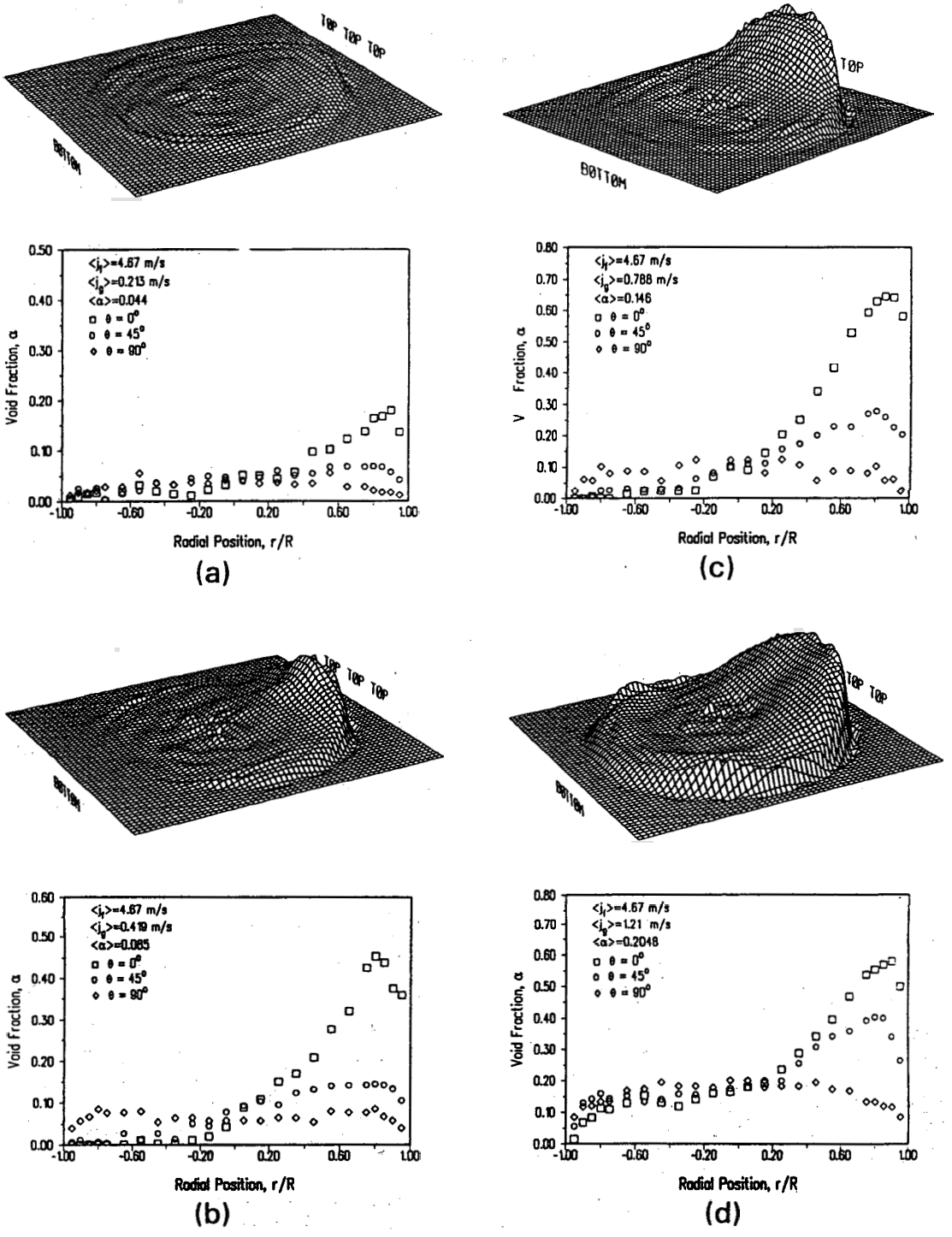

Fig. 6. Void fraction distribution over pipe cross-section at $L/D = 253$ with increasing gas flow.

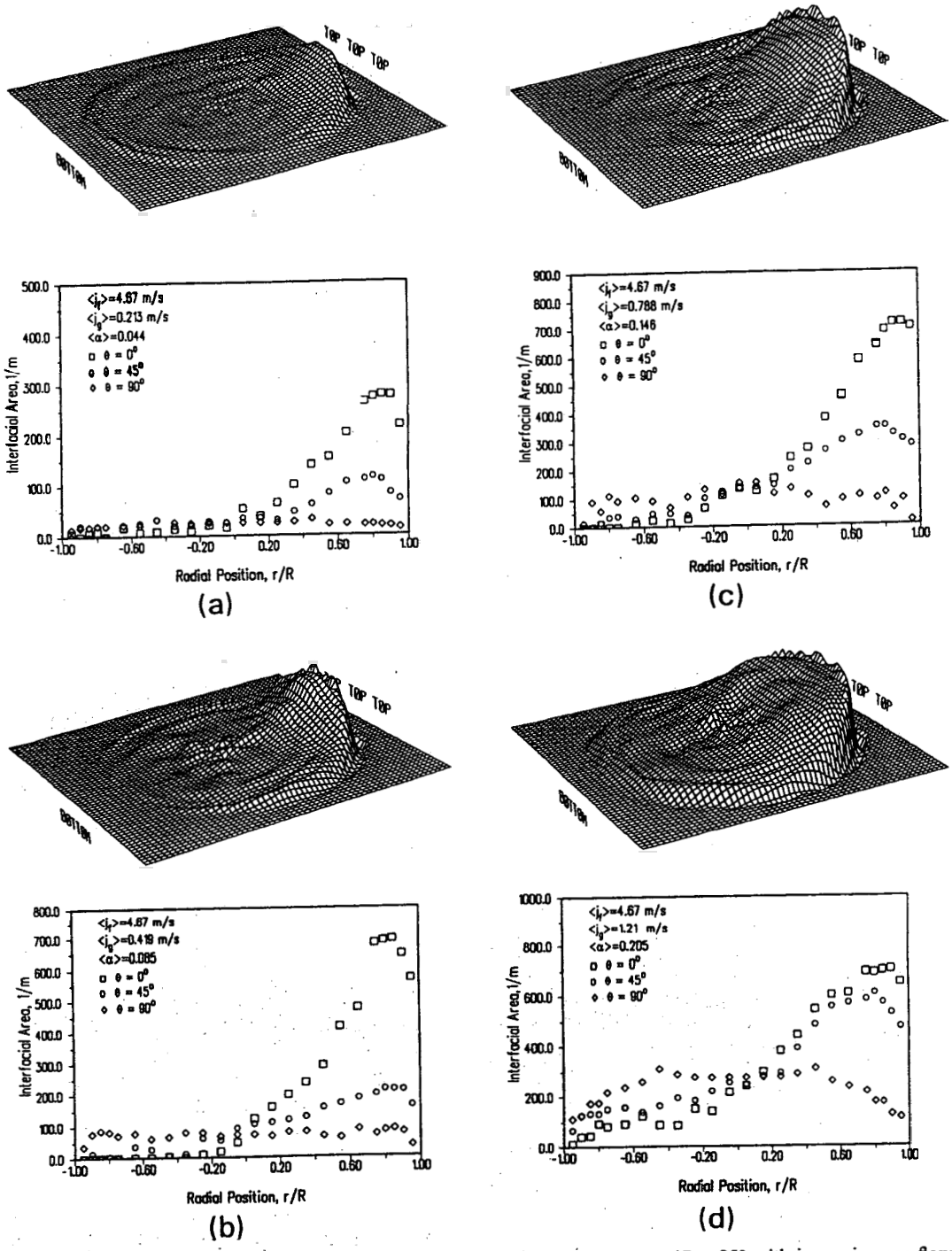

Fig. 7. Interfacial area concentration distributions over pipe cross-section at $L/D = 253$ with increasing gas flow.

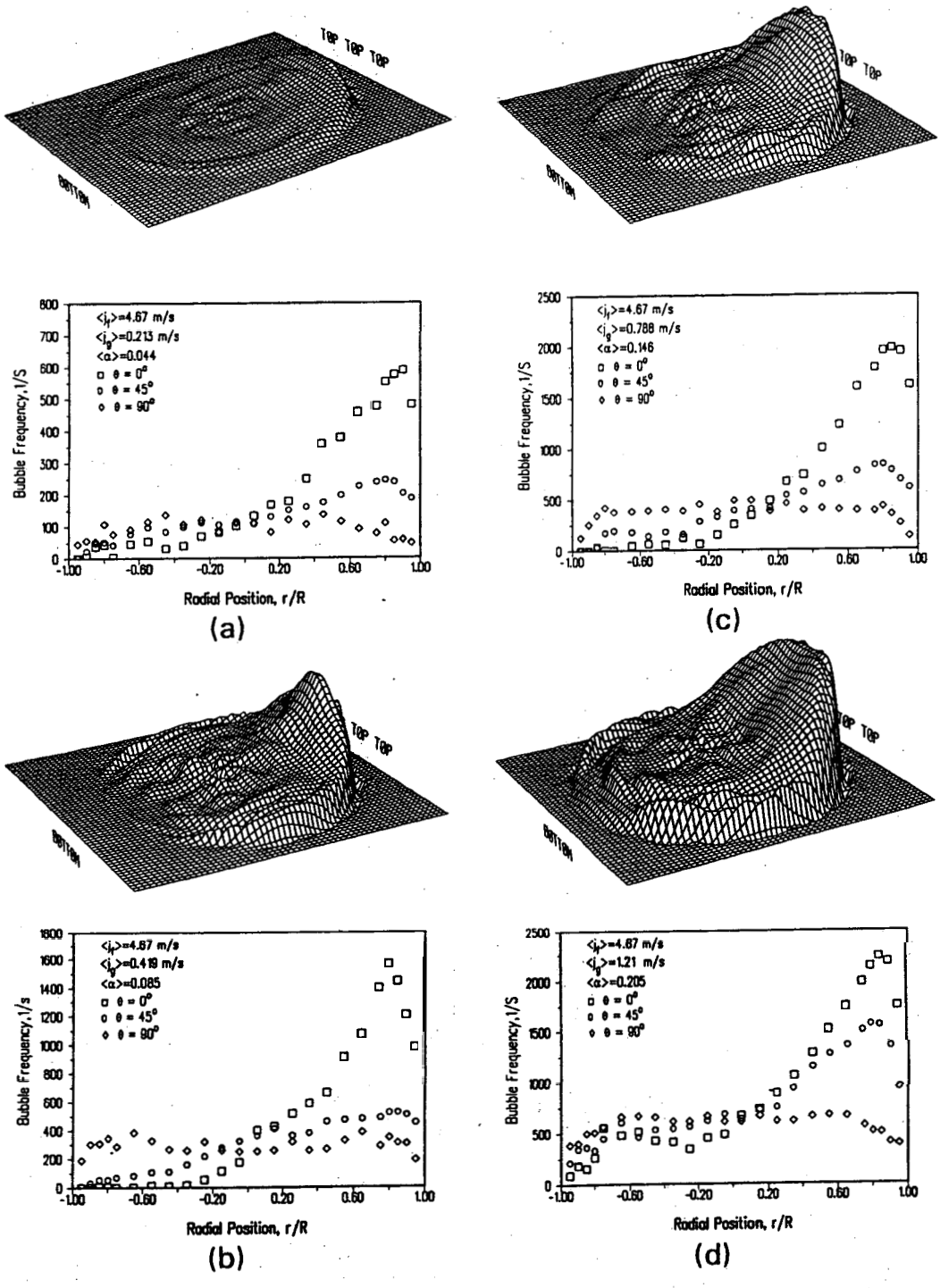

Fig. 8. Bubble frequency distributions over pipe cross-section at $L/D = 253$ with increasing gas flow.

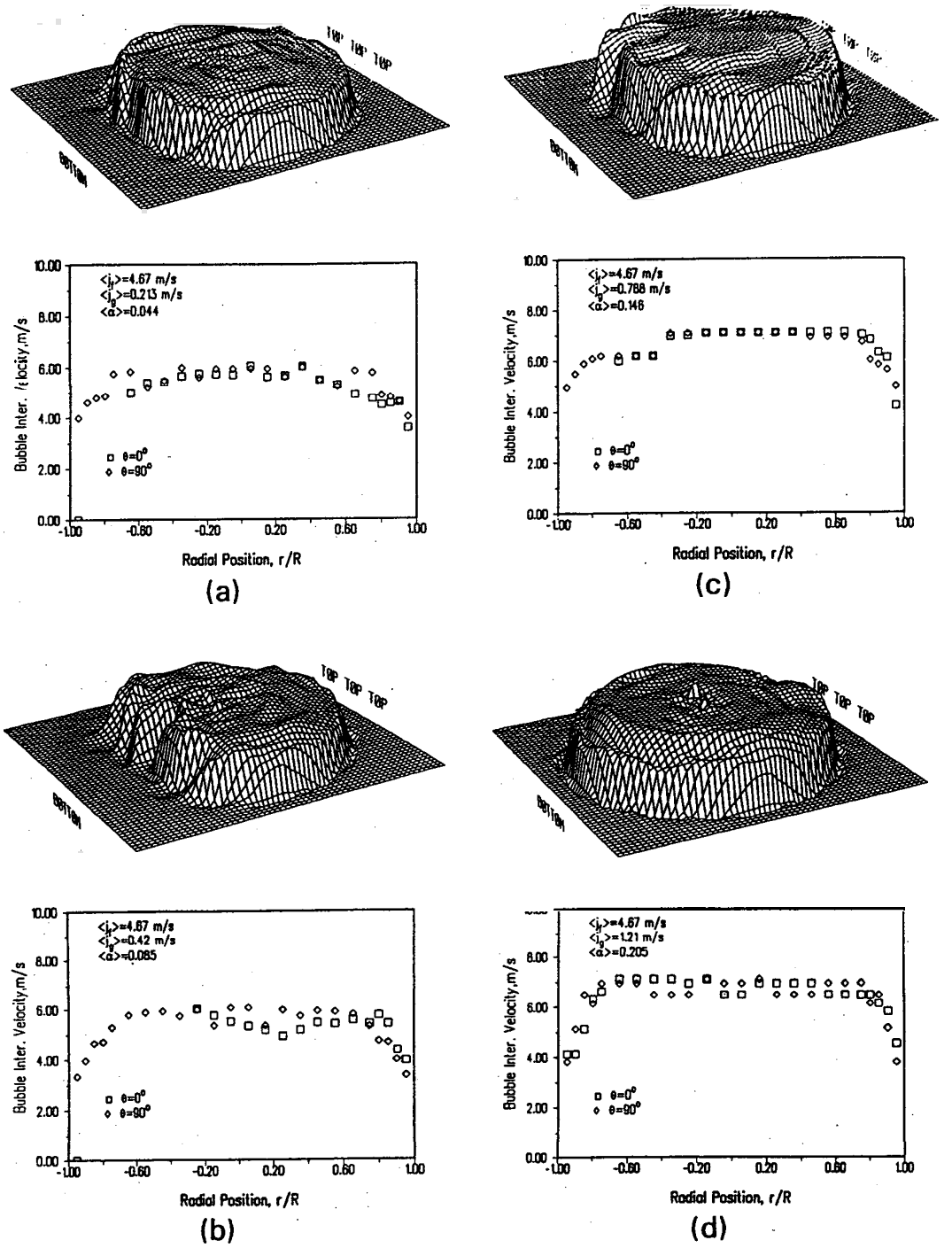

Fig. 9. Bubble interface velocity profiles over pipe cross-section at $L/D = 253$ with increasing gas flow.

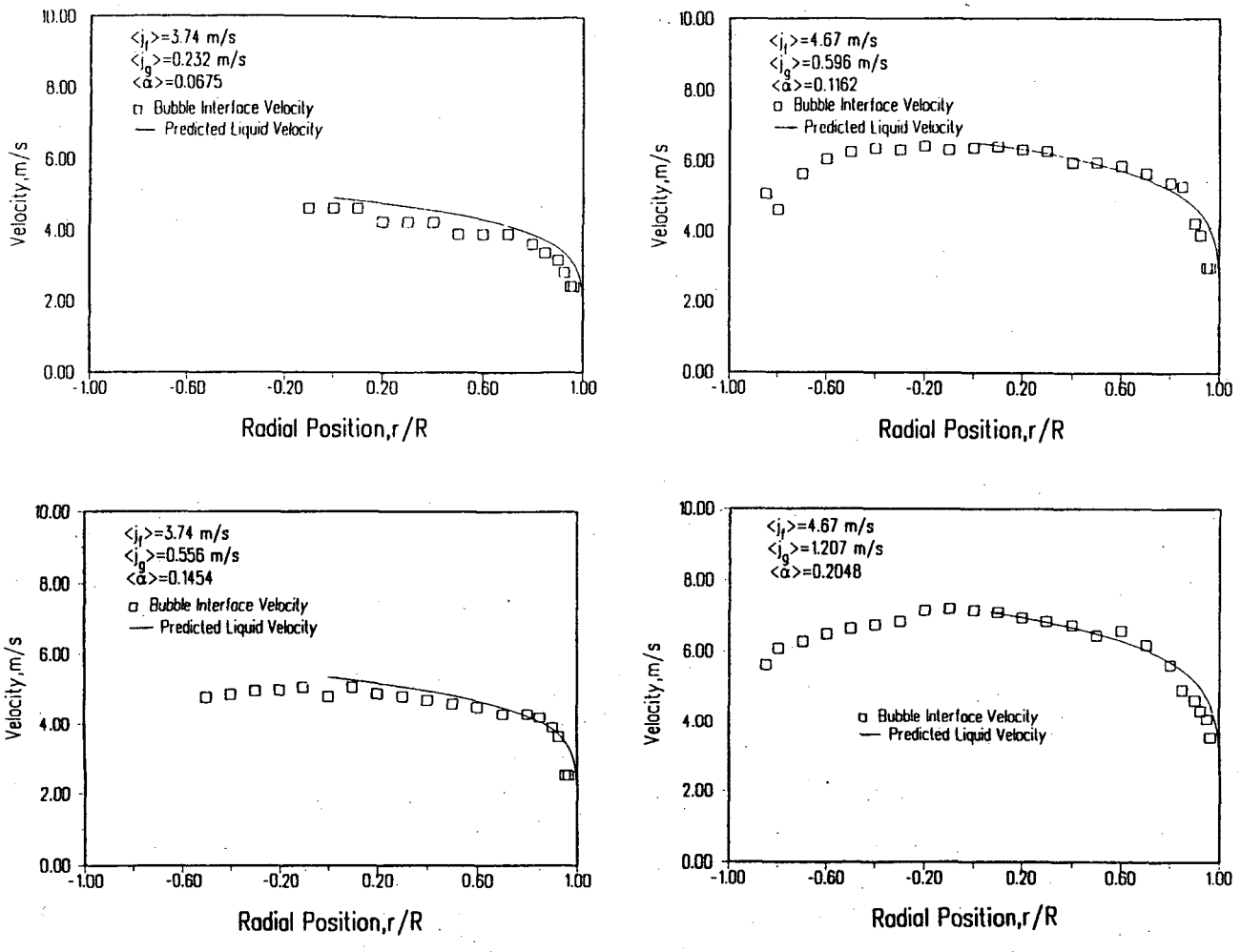

Fig. 10. Comparison of bubble interface velocity with predicted liquid velocity.

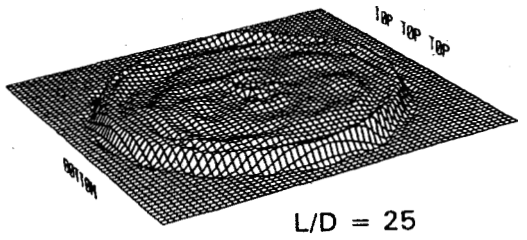

L/D = 25

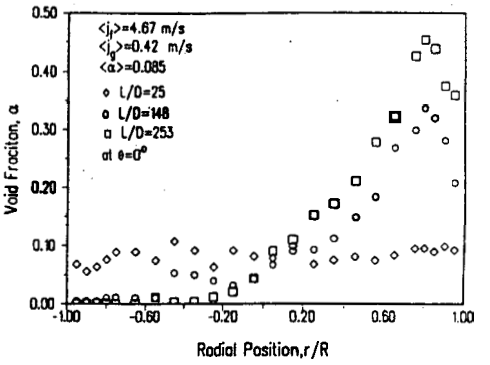

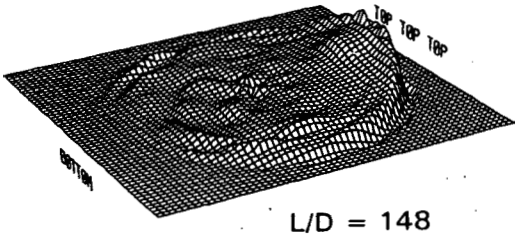

L/D = 148

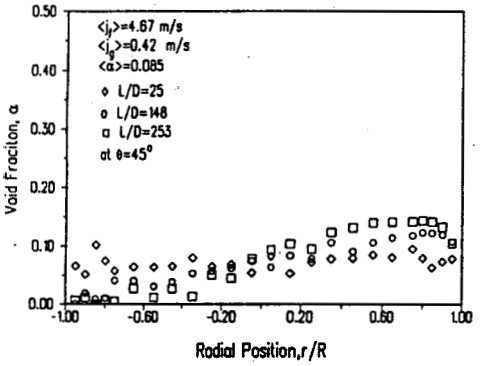

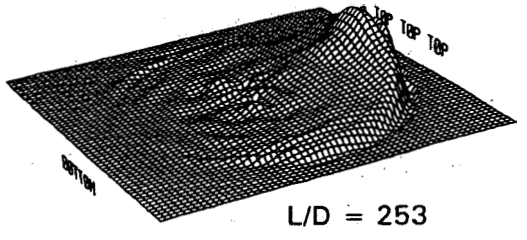

L/D = 253

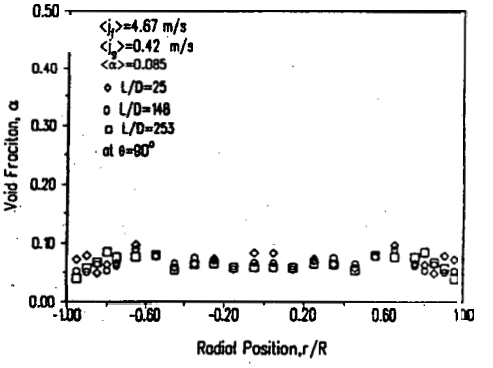

Fig. 11(a).

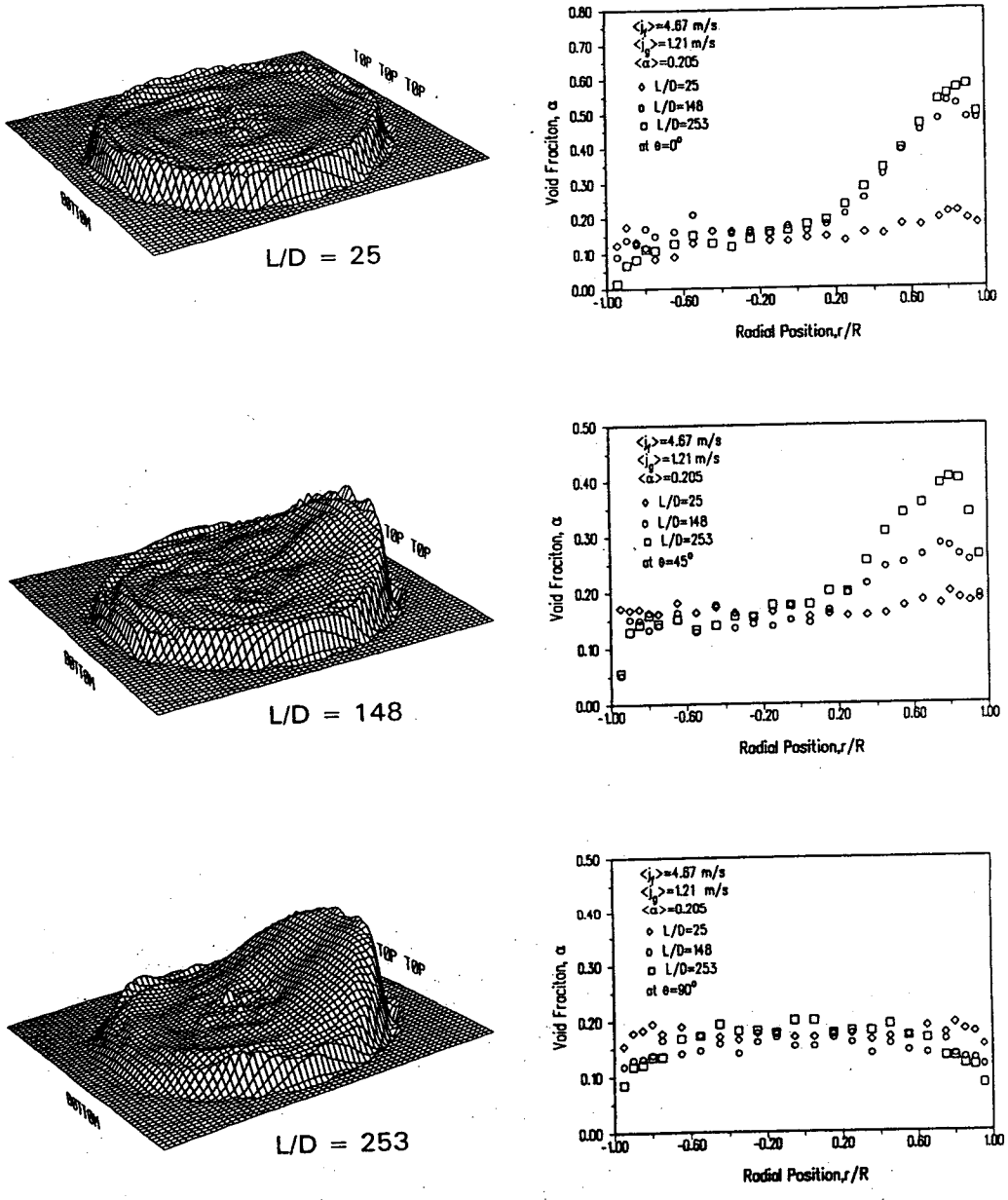

(b)

Fig. 11. Void fraction development in axial direction. (a) Low gas flow; (b) high gas flow.

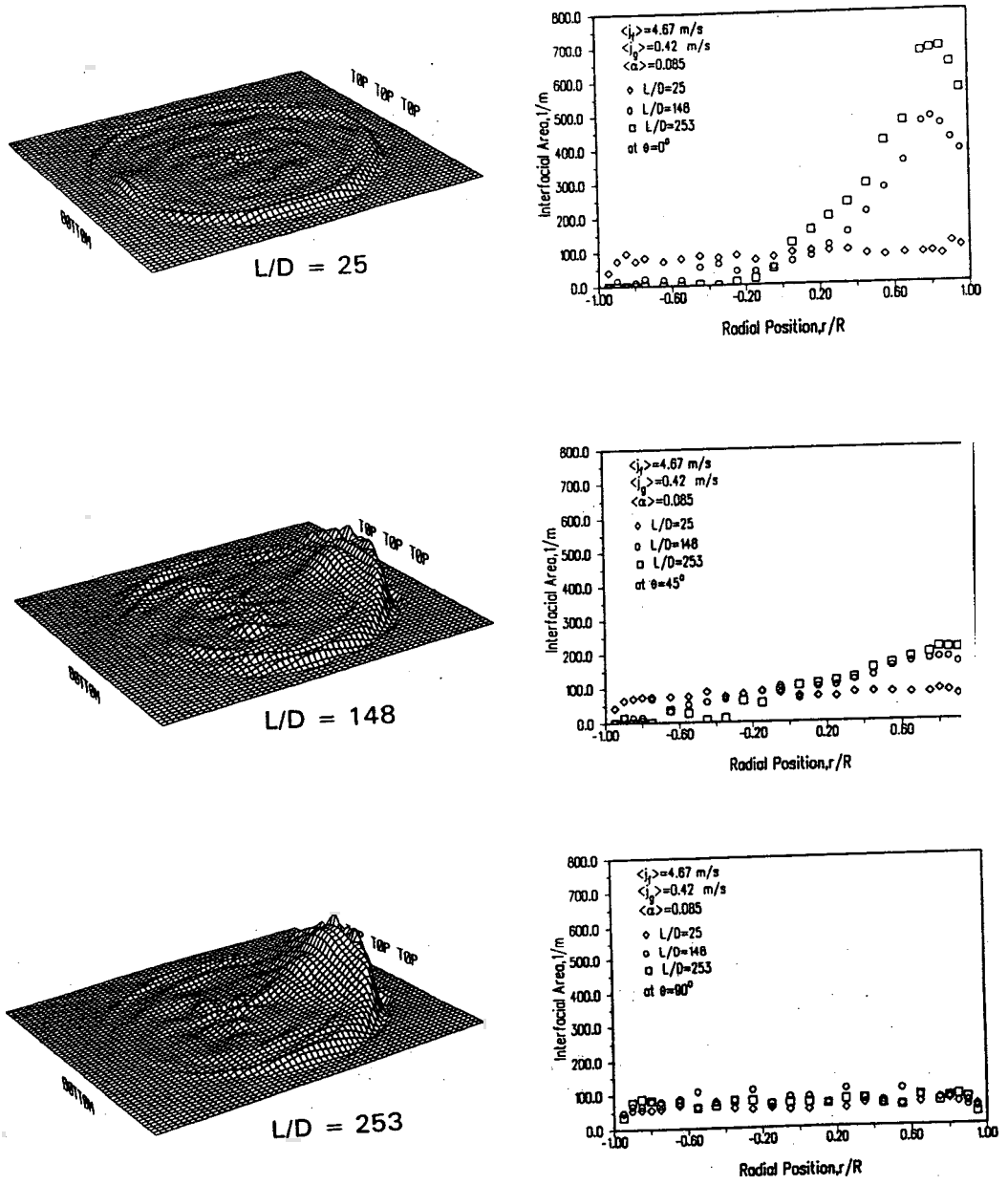
Top
Top
Top
Bottom
L/D = 25
<j_f>=4.67 m/s
<j_g>=0.42 m/s
<α>=0.085
◇ L/D=25
○ L/D=148
□ L/D=253
at θ=0°
Interfacial Area,1/m
Radial Position,r/R
L/D = 148
at θ=45°
L/D = 253
at θ=90°

Fig. 12(a).

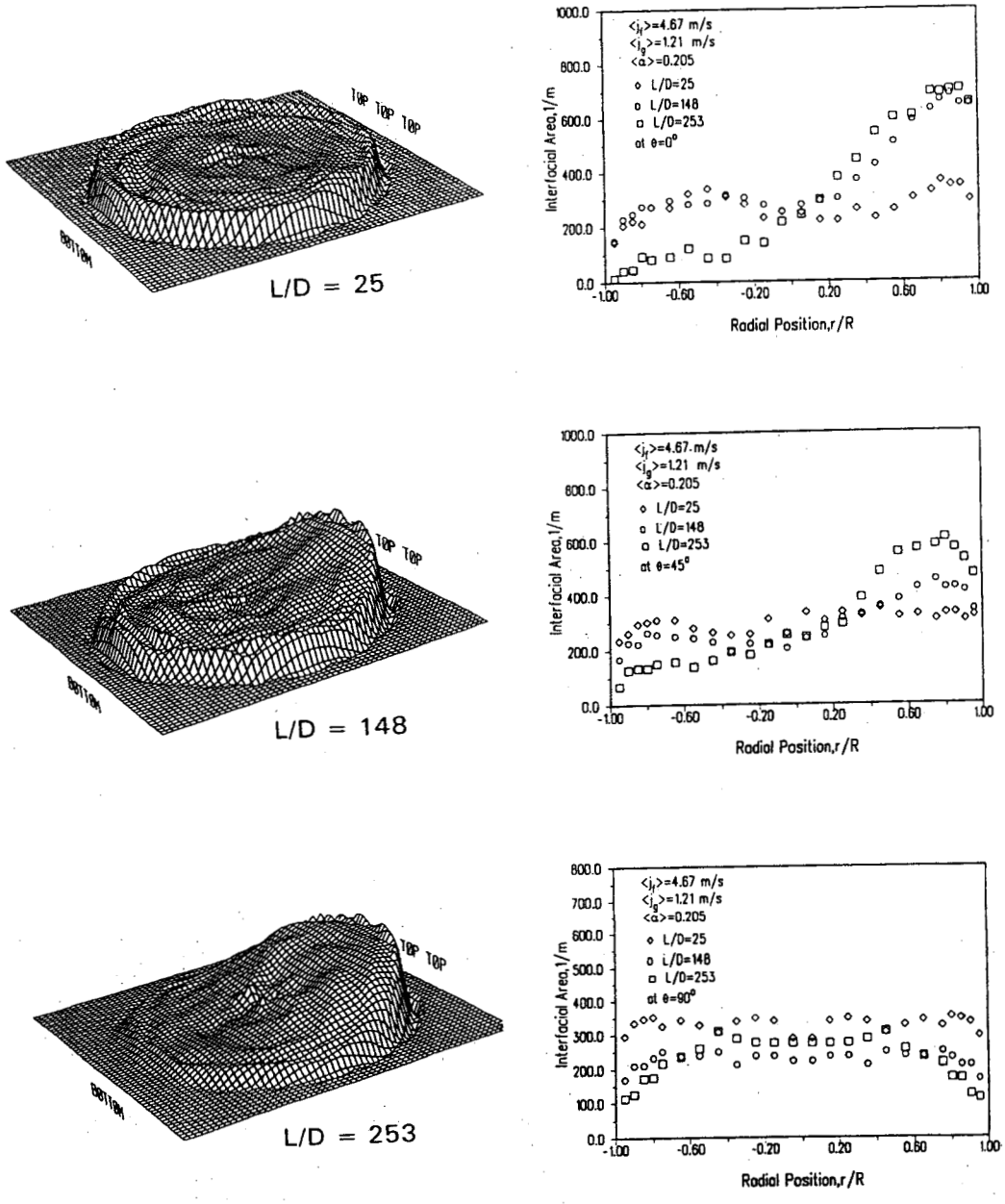

(b)

Fig. 12. Interfacial area concentration development in axial direction. (a) Low gas flow; (b) high gas flow.

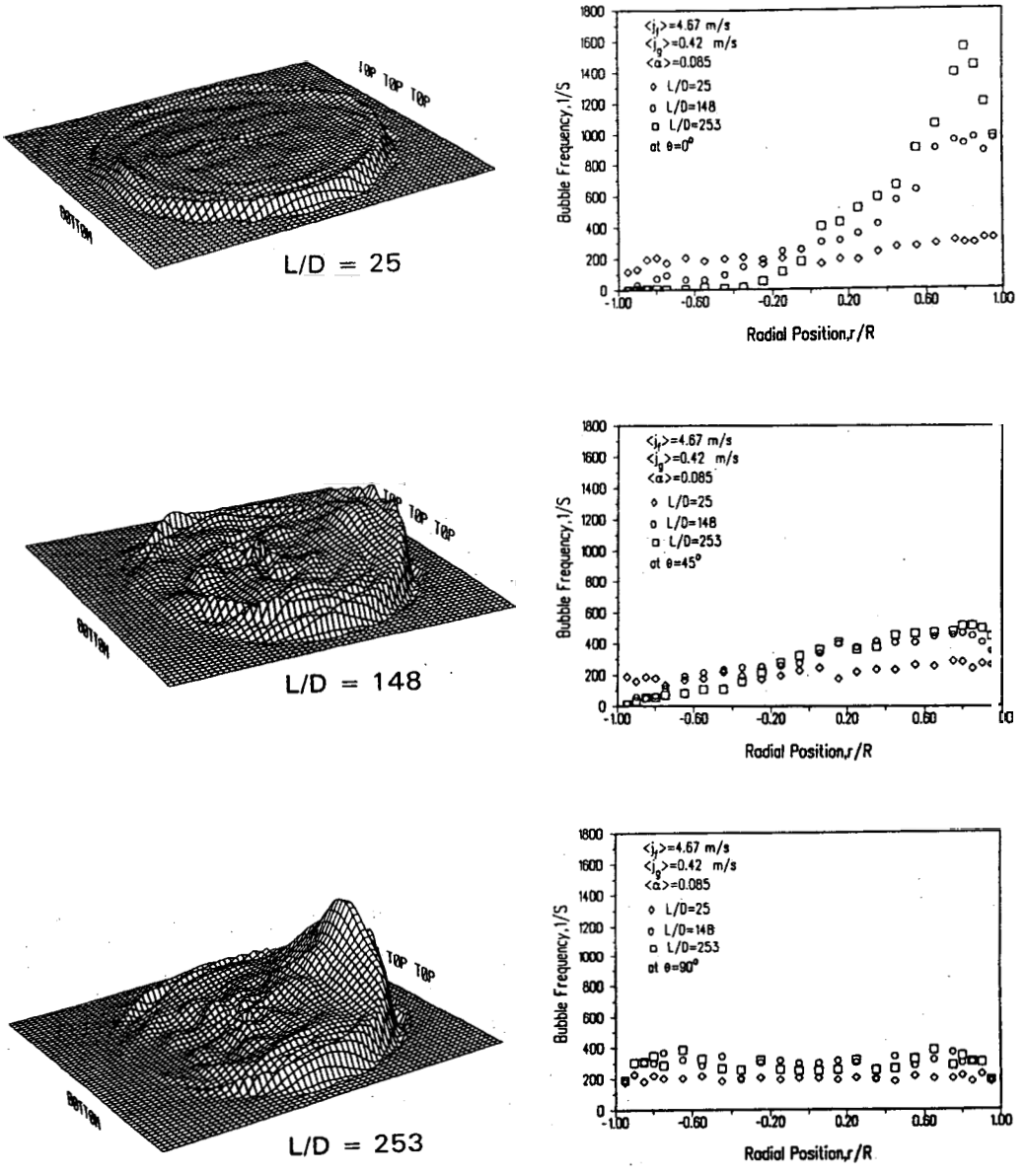
L/D = 25
L/D = 148
L/D = 253
<j_f>=4.67 m/s
<j_g>=0.42 m/s
<α>=0.085
◇ L/D=25
○ L/D=148
□ L/D=253
at θ=0°
at θ=45°
at θ=90°
Bubble Frequency,1/S
Radial Position,r/R

Fig. 13(a).

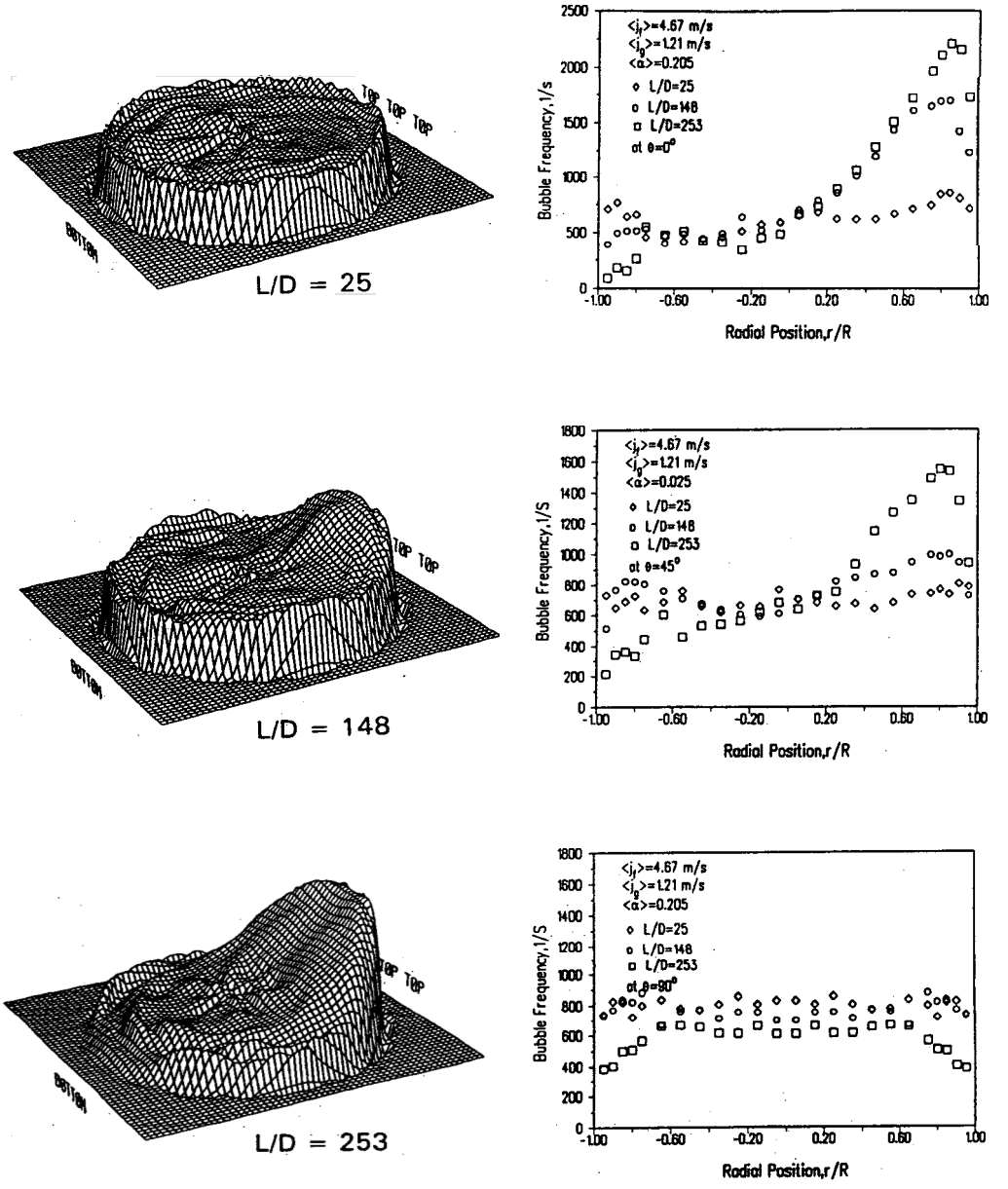

Fig. 13. Bubble frequency behaviour in axial direction. (a) Low gas flow; (b) high gas flow.

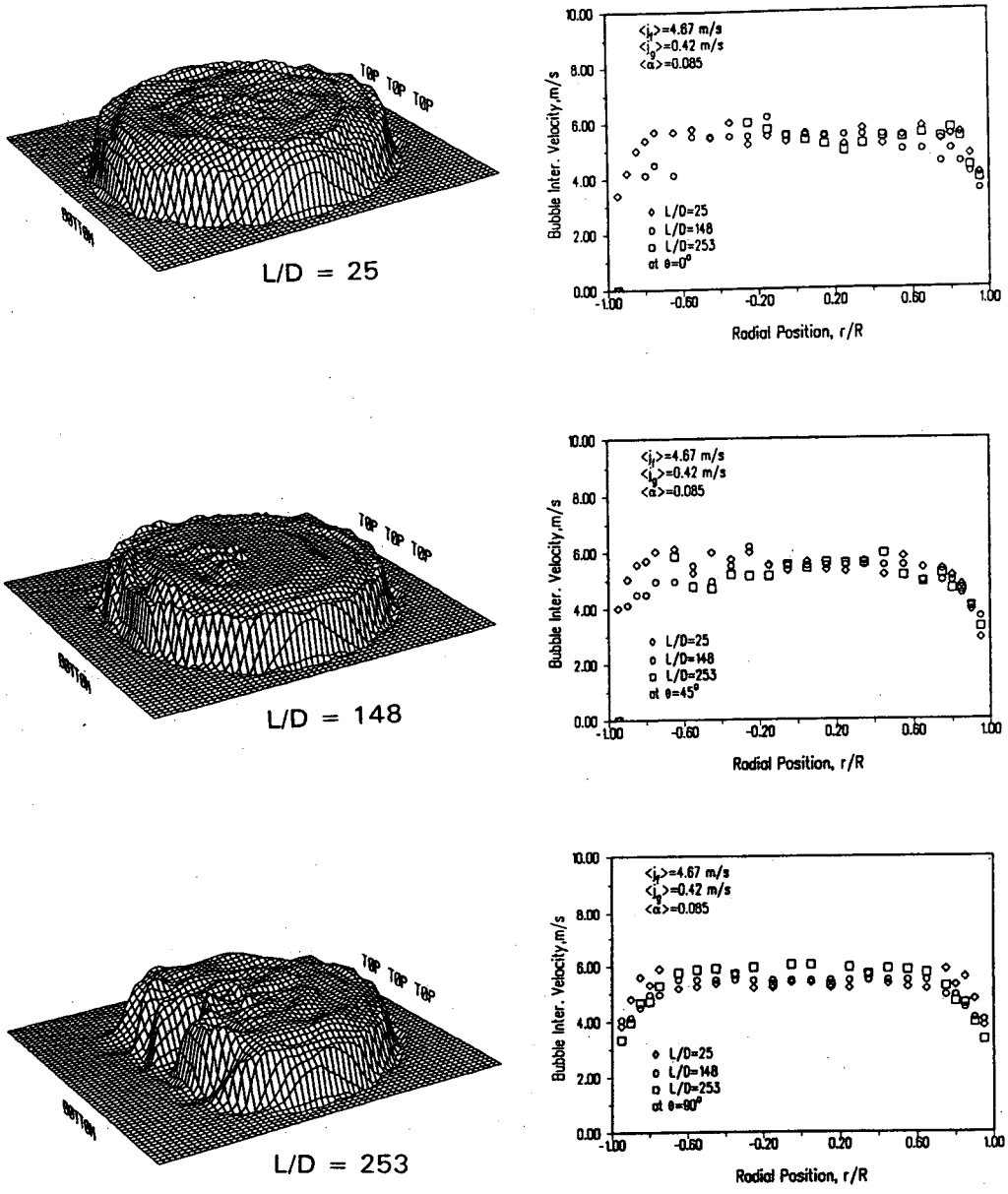
Top
Bottom
L/D = 25
L/D = 148
L/D = 253
<j_f>=4.67 m/s
<j_g>=0.42 m/s
<α>=0.085
L/D=25
L/D=148
L/D=253
at θ=0°
at θ=45°
at θ=90°
Bubble Inter. Velocity,m/s
Radial Position, r/R
10.00
8.00
6.00
4.00
2.00
0.00
-1.00
-0.60
-0.20
0.20
0.60
1.00

Fig. 14(a).

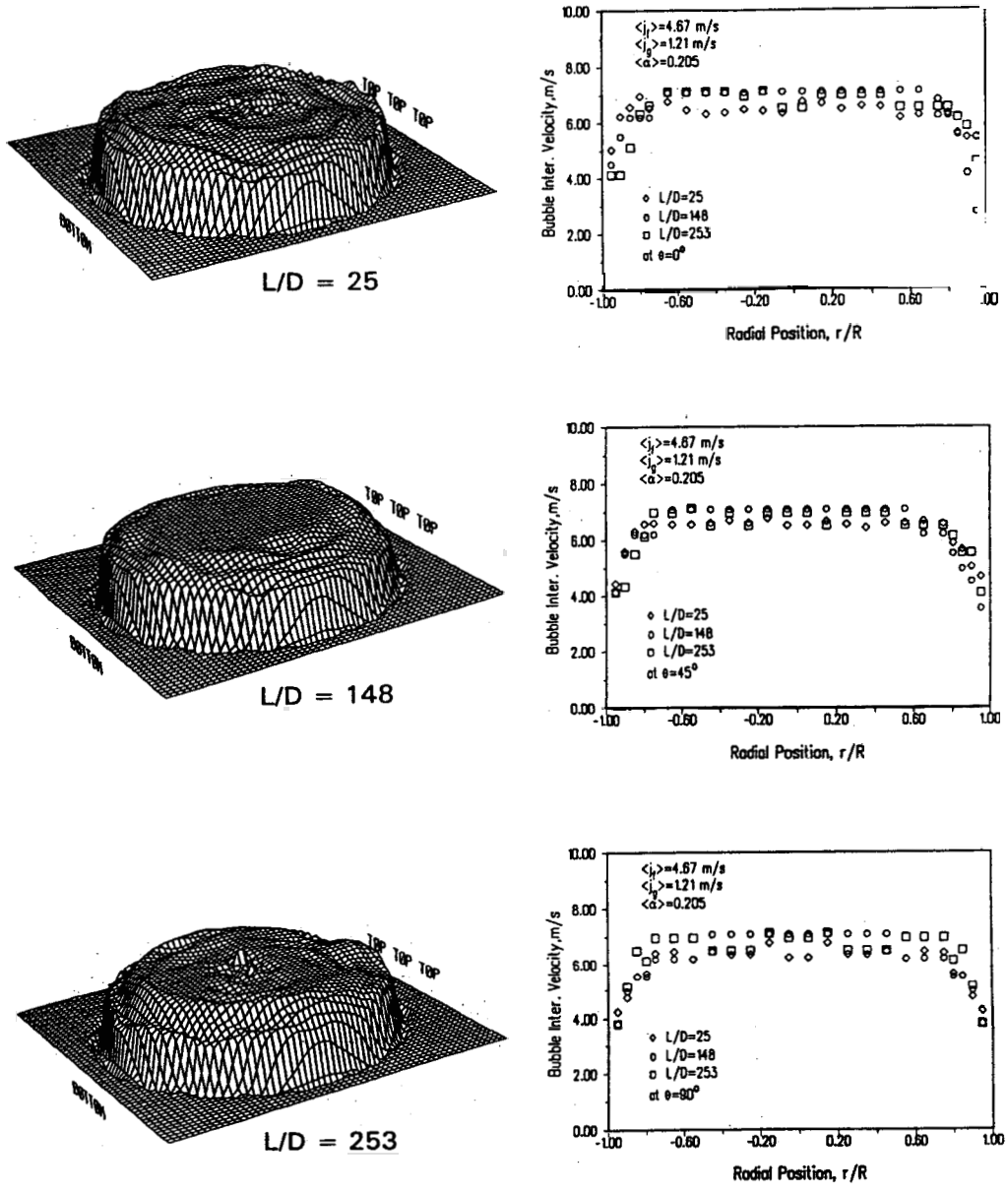

(b)

Fig. 14. Bubble interface velocity behaviour in axial direction. (a) Low gas flow; (b) high gas flow.

7. USE OF HOT-FILM ANEMOMETRY TECHNIQUE IN HORIZONTAL BUBBLY TWO-PHASE FLOW MESUREMENTS

Ala Iskandrani and Gunol Kojasoy

Department of Mechanical Engineering, University of Wisconsin-Milwaukee
Milwaukee, Wisconsin 53201, U. S. A.

ABSTRACT

Utility of the hot-film anemometry technique in a horizontal bubbly flow-pattern is examined. It is shown that a single probe can be used for identifying the gas and liquid phases. Analyzing the nature of the voltage signal, a signal processing scheme is developed for measurements of time-averaged local void fraction distribution as well as for the measurements of local mean axial velocity and turbulent intensity in the liquid phase. The signal processing scheme is optimized so it can be used in a very high void-fraction region toward the top of the pipe, which is the unique characteristic of bubbly two-phase flow in horizontal channels. To verify the accuracy of the proposed method combined effects of the local void fraction and liquid velocity measurements are checked against the global measurements of liquid flow rate. The results are found to be satisfactory within the experimental uncertainties. Furthermore, the area-averaged void fraction obtained from the hot-film probe measurements compared well with the quickclosing valve technique measurements. The results show that the hot-film probe method is accurate and reliable for the local measurements of void fraction, liquid velocity and turbulent intensity in horizontal bubbly flow provided that the data is processed properly. Some results of the local measurements of time-averaged void fraction, axial mean velocity and turbulent intensity at relatively low and high gas flows are also presented for a horizontal air-water bubbly flow in a 50.3 min ID pipe.

7.1 Introduction

Void fraction is considered one of the most important parameters in gas-liquid two-phase flows from an engineering point of view. Several methods are available at present to measure void fraction. These are photographic, light attenuation, ultrasonic attenuation, double-sensor probe, impedance tomography, and Laser Doppler Anemometer (LDA). These methods for measuring the void fraction are effective only in certain idealized cases. The photographic and light attenuation methods cannot be used with opaque walls and are limited to transparent dispersed two-phase flows with volumetric void fraction less than a few percent [1]. The ultrasonic method is not restricted to such conditions, and thus expands the measurement of the void fraction beyond the presently available range of fluids and non-opaque systems [2]. However, the ultrasonic attenuation method has a major limitation due to the reduction of the measurement certainty because of the scattering echoes, and thus it is restricted to low void fraction bubbly systems. The X-ray computed tomography, impedance tomography and ring-type conductance transducer were used to determine the cross-sectional or volume averaged void fraction [3]. However, the local void fraction cannot be measured by such technique.

Several attempts have been made to extend the use of LDA to bubbly flows [1,4]. In a very recent work of Suzanne et al. [5], it was concluded that at void fraction greater than about 2% the LDA signal is no longer suitable because of the increase of the beam interruption rate by the bubble crossing. In this case the hot-film anemometry was recommended.

It is to be noticed that with the exception of the work of Kocamustafaogullari and Wang [6], all of the bubbly flow experiments were carried out in vertical flow channels. Even in the case of well-studied vertical flow configurations, experimental results from fairly diverse sources are controversial regarding the void fraction distributions and the effects of the bubble size and flow conditions causing void profile transformation from a saddle shape into a convex shape. The difficulties in obtaining completely similar general results undoubtedly stem from our lack of understanding of the mechanisms involved in determining the internal structure of bubbly flow. Furthermore, due to basic internal

structural differences between the vertical and horizontal bubbly flows, it is impossible to extend the vertical bubbly flow results to horizontal bubbly flows.

In light of the above discussion, it is evident that much experimental work is still necessary to attain a thorough physical understanding of the internal stricture of horizontal bubbly two-phase flows. In view of the intention to measure local variables in a horizontal bubbly two-phase flow with local void fraction possibly ranging from 0 - 65%, it is unavoidable that a probe method must be used. In this context, an experimental investigation has been underway at the University of Wisconsin-Milwaukee to study the air-water bubbly two-phase flow characteristics along horizontal flow channels using the hot-film probe technique.

The primary purpose of this research is to show that the hot-.film anemometry technique can be successfully used in horizontal bubbly two-phase flows

- to identify liquid and gas phases (phase separation), from which the local volume fraction can be evaluated,
- to evaluate the local time-averaged, axial liquid phase mean and turbulent fluctuating velocities,
- to measure the local void fraction and local bubble passing frequency of the two-phase flow, and finally,
- to investigate the dependence of the local parameters on other flow variables.

7.2 Hot-Film Anemometry Technique

7.2.1 Principle of Measurement

Hsu et al. [7] and Delhaye [8] were the first to study the response of hot-film probes in a liquid-gas two-phase flow. Since then, this technique has been used extensively [9-14] in vertical bubbly flow pattern. However, only limited efforts were made to examine two-phase flow characteristics in large scale experimental programs in horizontal bubbly flow channels.

In principle, the hot-film probe provides information about the flow field by relating the changes in this field to changes in the heat transfer at the probe tip surface. As the fluid flows past the constant temperature hot-film probe, changes in the fluid velocity, including turbulence fluctuations, cool the sensor at different rates. These

changes in cooling rates result in voltage changes in the anemometer. In the case of an air-water two-phase flow, very sharp variations occur in the anemometer voltage output as the probe tip goes through a gas-liquid interface because the heat-transfer characteristics of air is completely different than water. A typical sensor output for two-phase bubbly flow is illustrated in Fig. 1. As seen in this figure the sensor encounters both liquid and small gas bubbles several times in a very short period. After the sharp initial drop, caused by the probe piercing the front of a bubble, the voltage gradually continues to decrease while the sensor stays inside the bubble. This is due to the evaporation of a thin film of liquid that remains on the sensor. On the other hand, the output signal from the probe shows a very sharp increase to the previous voltage level upon exiting the gas bubble due to wetting of the sensor. It is interesting to notice that, when the liquid wets the sensor, the signal rebuilds after a very short period during which it exhibits an overshoot. This is usually the case because the hot-film anemometer circuitry tends to overcompensate the voltage increase when liquid suddenly envelopes the tip of the probe.

In the upper portion of the pipe, the probe encounters plenty of bubbles, or partial bubbles hits, where the residence time in gas bubbles and liquid is too short to show the basic output characteristics of the probe and consequently becomes harder to analyze such signals. When the probe is in the gas, the signal is no longer representative of the velocity, it is thus necessary to remove this part of the signal as discussed in the next section.

7.2.2 Signal Processing

7.2.2.1 Phase Separation

The first requirement in evaluating a two-phase flow with a hot-Olin probe is the ability to identify and differentiate the gas and liquid phases on a record of the anemometer signal. A number of investigators have reported utility of the hot-film anemometry in two-phase flows. In these investigations a variety of bubble detection techniques, consisted of detecting the voltage changes associated with a change in phase, have been used.

In the present investigation, Farrar et al. [15] and Lewis [16] methods were combined to develop a reliable detection technique based on an interactive amplitude and threshold procedure. This new technique tackled the inherent problems in high-speed, high void fraction bubbly flows. Serious problems associated with previous methods when applied to a horizontal bubbly flow can be summarized as follows: Firstly, very small bubbles or partial bubble hits produce signals that do not fall below the voltage level corresponding to the lowest continuous liquid phase velocity fluctuations. Therefore, they cannot be detected. Secondly, the overshoot in the hot-film signal results in a significant negative slope during the decay process following the overshoot. This may be interpreted as being due to the passage of a bubble front interfaces. The overshooting may cause serious errors in time-averaged void fraction calculation or it might cause major incorrect evaluation of turbulence.

The voltage output was recorded on disk. The derivative of this output signal with respect to time was then calculated. This derivative represents the slope of the output signal. By plotting the anemometer output and the slope on the same time scale, the effects of a bubble striking the probe can be seen as in Fig. 2a & b. For each bubble passage, the slope signal shows a sharp negative spike for the nose of the bubble followed by a sharp positive spike for the tail of the bubble. The power required to heat the sensor in the gas phase is considerable less than in the liquid phase. Similarly, the positive spike in the slope signal is a result of the increase in power required to maintain the sensor temperature as the probe reenters the liquid phase. From here, it is a matter of determining the proper threshold values to detect the spikes in the slope signal.

The first threshold is used to determine the rear of the gas bubble. Its value must be positive. This slope threshold value is the most important because it has the largest magnitudes and is unaffected by any of the flow characteristics. Therefore, it is the easiest to detect. Its value should distinguish between the peaks caused by liquid interface and those from the turbulent fluctuations. The turbulence slope values were of a magnitude of less than 250. By plotting the anemometer output voltage data and the corresponding slope, as seen in Fig. 2a & b, the positive value of the slope can be recorded for each liquid slug occurrence by visual inspection. This was done for experimental data covering the entire range of gas and liquid flow rates. The rear of

bubble was found to cause a positive peak with a magnitude greater than 500. This value was used as the threshold for the bubble rear detection or liquid slug beginning. When this threshold value is reached or exceeded, in the positive plane, the phase separation step signal, 8, is set equal to unity indicating the liquid phase (Fig. 2c).

Similarly, a second threshold value was found for the negative spike caused by the probe hitting a gas bubble. These negative peaks were found to have a magnitude greater than 300 in the negative plane. It is obvious from Fig. 2b that the magnitude of this slope is usually smaller than the previous one, because the drop in the voltage occurs gradually. So it is harder to detect and easier to be feigned by the turbulence fluctuations. This is why a conservative value of -500 has been used as a bubble front detection threshold. This value is used to identify the bubbles only with relatively clear tail voltage signal. The principal slope is going to be incorporated to double check the validity of the negative slope as discussed later.

To ensure that all bubbles have been detected and to take care of the overshooting, the program works backward whenever the first threshold occurs to indicate a start of liquid phase. Since this threshold is very distinct and impossible to miss, it sets up the base for the further signal analysis. The signal processing program works backwardly forcing all data to be gas until another first threshold value or a third threshold event (whatever comes first) takes place. The third assigned slope threshold value is of importance when the second threshold bubble start detection fails. Because some bubbles, small ones in particular, introduce intermediate negative slope, which may be hard to differentiate from velocity fluctuations negative slopes, the third slope threshold makes the detection of gas phase more lenient. Therefore its value is set to -250. This, in its absolute plane, is much less than the slope associated with interface passage but slightly greater than the slope of most velocity fluctuations. In this way we get a narrower band of liquid voltage signal, which results in detecting smaller bubbles. The third threshold works in conjunction with an amplitude threshold, which will be discussed in the next section.

When the entire data signal has been analyzed in this way, the program returns the phase separation step signal. This signal is used for the void fraction analysis and helps to assign the liquid phase data used for velocity analysis. One problem with the above

method, and any other method involving an immersed probe in the two-phase flow, is as described by Wang et al. [17], the probe deforms and deflects the bubbles prior to piercing. This would lead to an underestimation of the void fraction.

7.2.2.2 Determination of Proper Data Set for Velocity Analysis

In the preceding section it was demonstrated that the proposed bubble detection technique can identify the starting and ending times of virtually every bubble event within hot-film signal. Nevertheless, using all identified liquid phase data for velocity analysis causes significant error. Similar to the phase separation method another method has been developed to identify the proper data set that should be used in liquid velocity data processing. The back-bone threshold value for this task is the voltage amplitude threshold. Unlike the previous technique, this one is only of practical use if a method of automatically determining suitable values for the amplitude can be identified. This was achieved by using the probability density function (pdt). Fig. 3 shows the digitized pdf corresponding to a large sample of hot-film probe data obtained at a certain probe position in a typical bubbly flow. A sample of the hot-film signal from which it was obtained is also shown in the figure. The pdf is observed to have a bimodal shape consisting of two peaks separated by a low level plateau region. The upper peak represents the high voltage associated with liquid phase, while the lower peak represents the low voltage associated with gas phase. In the current program the lower peak, which is located near the bottom of the hot-film signals, is not determined and thus our pdf is truncated to accommodate only the large peak. This peak corresponds to the voltage/velocity associated with the continuous phase turbulence. A point on the voltage scale of the pdf slightly below that corresponding to position "c" on Fig. 3 is an ideal choice for voltage amplitude threshold since it will be low enough to avoid mistaking any turbulence velocity fluctuations and high enough to detect the majority points in gas phase.

After identifying the amplitude threshold value internally by the computer program, the points with voltage higher than this threshold value and their slopes within the first and second threshold slopes are only considered for velocity analysis. The data points associated with over-shooting, at the rear of bubbles, are excluded again by

proceeding backwards. By working backwards, the current point is compared with the previous few points. If the current point voltage is higher than the voltage threshold value and its slope is lower than the second slope, then it is identified as overshooting provided that the immediate preceding points have the massive positive slope. In Fig. 2d, the velocity evaluation step signal is shown for the corresponding anemometer output voltage, slope, and phase separation. In this figure, unity indicates acceptable data point for velocity analysis, zeros are not admissible points and should be excluded from any further velocity analysis.

7.2.3 Statistical Processing of the Data

Although the actual voltage change in a hot-film probe signal due to the probe encountering the bubble is not important or accurate, the time that the probe is exposed to the bubble can be used to determine the local time-averaged void fraction, a, at any point, r. It is defined as a time-average of the concentration, δ(r,t), by:

$$\alpha(r) \equiv \lim_{T\to\infty} \int_0^T (1-\delta(r,t))dt \qquad (1)$$

where, δ, as a function of the space coordinate, r, and time, t, is equal to 0 if the probe sensor is in the gas phase and equal to 1 if the sensor is in the liquid phase. Equation (1) can be written in discrete form as follows:

$$\alpha(r) = \frac{1}{T}\sum_{i=1}^{N}(t_{2i} - t_{2i-1}) \qquad (2)$$

where i indicates the i^{th} gas bubble and t_{2i-1}, and t_{2i} define the time when the probe enters into the gas bubble and liquid, respectively, the number of gas bubbles passing the probe sensor in the total sampling time, t, is n.

The local mean axial liquid velocity and the values of turbulent fluctuations were calculated by using

$$U_{mean}(r) = \frac{1}{N}\sum_{k=1}^{N} u_k(r,t) \qquad (3)$$

and

$$u^r(r) = \sqrt{\left(\frac{1}{N}\left[\sum_{k=1}^{N}\left[u_k(r,t) - U_{mean}(r)\right]^2\right]\right)} \qquad (4)$$

respectively. In Eqs. (3) and (4), $u_k(r,t)$ is the instantaneous axial velocity for the k^{th} data point in the liquid phase, and N is the total number of data points in the liquid phase of the digital sample, k = 1 ....N. To remove the error caused by the intermittent wave motion, the time-based filtering process was developed in calculating turbulence fluctuations, Iskandrani [18].

7.3 Experimental Set-up and Procedure

7.3.1 Experimental set-up

The experimental flow loop consists of a horizontal line of 50.3 mm i.d. Pyrex glass tubing with pressure tabs installed between them. The entire test section is about 15.4 m in length and is entirely transparent, so that flow visualization, high-speed photography and cinematography are possible.

The air and distilled water are used as coupling fluids. The air is supplied to the test section from the university central air system. It is, however, regulated through a 0.95 m^3 capacity high-pressure storage tank, and metered by a series of turbine flowmeters. The water is recirculated. It is pumped from a 1.9 m^3 capacity storage tank by a stainless steel centrifugal pump and regulated from 0 to 100% of the pump capacity by a transistor inverter. The water flow rate is measured by a series of paddlewheel flowmeters assembled in a parallel configuration. The air enters the mixing chamber from a 90° vertical leg and is injected into the water flow through a cylindrical porous media of 100-~μm porosity to achieve uniform mixing and quick development of a bubbly two-phase flow pattern. The water enters the mixing chamber from an axially aligned upstream section of the mixing chamber. The two-phase mixture from the test section is discharged to an air-water separator. The air is vented to the atmosphere, and the water is returned to the water storage tank.

Seven pressure taps are mounted along the flow loop. Six diaphragm-type pressure transducers along the six U-tube manometers are used to measure the pressure drop. The pressure transducers have a natural frequency of 5 Hz with a range of 0-34.4 kPa, and accuracy of ± 0.3% of the full scale. The pressure of the air at the location of the

flowmeter and the two-phase flow system pressure at the test section are both measured and used to correct for the compressibility effects of air.

7.3.2 Experimental procedure

The experiments were carried out under fully developed bubbly flow conditions using conical shaped (TSI 1231-V) hot-film probes. The liquid and gas volumetric superficial velocities ranged from 3.8 to 5.0 m/s and 0.25 to 0.8 m/s, respectively, and average void fractions ranged from 4.2 % to 15.2 %. For all the flow conditions, the system pressure was near atmospheric and the temperature about 20-22 ° C. The software compensates for the temperature changes of the water automatically. The local values of void fraction, bubble frequency and liquid velocity measurements were made at L/D= 253 downstream of the air-water mixing chamber. Twenty-one probe locations were selected through the vertical pipe diameter and at each location, local instantaneous liquid velocity and void fraction were measured. For more information concerning the details of experimental procedure, see Iskandrani (1997)

The data from the probe was collected by the anemometer and stored in a PC computer. The data sampling rate was set to 20 kHz, which allowed a statistically meaningful sampling time. Once the data were stored in the memory of the computer, a FORTRAN program was developed to process the data, separating phases, converting the voltages to velocities, and calculating the essential parameters.

The experimental uncertainties in this research were mainly caused by random electric fluctuations in the used instruments. The uncertainties calculated for void fraction, turbulent velocity and bubble frequency, were 7.4, 10.0 and 4.0%, respectively. Moreover, in order to check the accuracy of both local void fraction and the mean axial liquid velocity measurements, the area-averaged liquid superficial velocity was compared to corresponding liquid superficial velocity as given by the flow meter. It was observed that the calculated superficial velocity, using two types of area segments, is consistently within the margin of 0-9% difference compared with the experimental water flow meter reading. These comparisons and the single-phase measurements benchmarked with data from Laufer (1954) are discussed in detail in Iskandrani (1997).

7.4 Experimental results and discussions

A sample of the time-averaged local void fraction, α, liquid-phase mean axial velocity, U_{mean}, and the turbulence structure as presented by the turbulent velocity, u', and turbulent intensity, defined as $(u'/ U_{mean,local})$, are described in Figs. 1-3. Here, r/R represents the ratio between the hot-film sensor location, r, measured along the vertical axis from the pipe center, and the pipe radius, R, thus defining the dimensionless radial position of the probe in the pipe. r/R = - 1 identifies the bottom of the pipe, whereas, r/R = 1 refers to the top. The single-phase liquid flow measurements of axial velocity and turbulence structure corresponding to the same liquid flow rates, i.e. the same superficial velocity, $<j_f>$, as the respective two-phase flow, are also shown on these figures for reference. When respective two-phase flow profiles are compared in these figures, it is evident that the void fraction, mean axial velocity, and turbulence structure distributions have similar behaviors. These results demonstrate interesting characteristics of a horizontal, bubbly flow. More detailed observations can be made as follows:

7.4.1 Local void fraction description

As observed in Figs. 1-3(c), the void fraction distribution shows a sharp decrease toward the bottom of the pipe and practically becomes zero at a certain probe position r/R. This general behavior indicates the existence of a liquid layer free of voids except near the wall of the pipe, where the profile of void fraction starts to build up again. Such build up adjacent to the wall points to the fact that there is a bubble boundary layer. The liquid layer thickness decreases by increasing gas flow rates at a given liquid flow, as explained in Section 4.4. It covers a liquid region between r/R = 0.3 and - 0.2 at $<j_f>$ = 3.8 m/s and between r/R = - 0.2 and - 0.8 at $<j_f>$ = 5.0 m/s. This behavior shows that gas bubbles are distributed more homogeneously as the liquid flow rate increases.

Bubbles tend to migrate toward the upper wall under the dominant influence of buoyancy force. Thus, the void fraction under all test conditions generally showed a distinct peak near the top wall at about r/R $\approx$0.8-0.9. This range corresponds to 2.5-5.0 mm distance from the wall. This observation is more pronounced at relatively high gas flow rates. This peak that appears in most cases, can be attributed to the increased hydraulic resistance of the liquid path between the bubble and wall, which may cause a

sharp decline in void fraction. This phenomenon is identical to that observed in vertical bubbly two-phase flows by Serizawa et al. (1975a,b), Wang (1985) and Wang et al. (1987) and in horizontal bubbly flow by Kocamustafaogullari and Wang (1991).

Although void fraction distributions tend to flatten as the liquid flow rate increases, the distinct peak always occurs at relatively the same location. The fact that the peak void fraction in all cases never exceeds 65% indicates that a maximum packing void fraction exists in the channel. Above the maximum packing limit, coalescence of bubbles occurs resulting in larger slug bubbles.

The most distinctive character of the void fraction profiles, however, is the appearance of a bubble boundary layer for all angles even in the bottom of the pipes as we observe in Figs. 1-3(c). A number of bubbles migrate toward the tube wall, yielding a non-uniform void fraction profile at a given horizontal slice of pipe. A similar trend with void fraction profile has been reported by Kocamustafaogullari and Wang (1991) using a do le sensor probe in horizontal bubbly flow.

7.4.2 Mean liquid velocity description

The mean velocity profiles (Figs. 1-3(a)) show asymmetric character with the largest velocities located in the bottom part of the pipe. The degree of asymmetry decreases with increasing liquid flows or decreasing gas flow.

An interesting feature of the velocity profile is that the velocity distribution within the bottom liquid layer exhibits a fully-developed turbulent flow character as demonstrated by the 1/7th power law profile. The 1/7th power law was fitted by the experimentally measured maximum velocity located in the liquid layer. Obviously, the maximum velocity in this `liquid layer' occurs slightly off the pipe centerline (i.e. $-0.2 < r/R < 0$). It is interesting to note that although the value of this maximum velocity increases as either the gas or liquid flow rate increases, the location of the maximum remains unchanged.

It is evident that within the high population bubble region at the upper portion of the pipe, the mean liquid velocity decreases sharply towards the upper pipe wall. Its value goes even below the single-phase profile. This sharp drop in the liquid velocity may be attributed to two reasons. Firstly, when the bubbles appear they induce additional

turbulence that is called the bubble-induced turbulence. As a result a sharp increase in turbulence due to the presence of bubbles naturally reduces the mean local velocity. Secondly, increased bubble population toward the top of the pipe creates an additional resistance to liquid flow resulting in retardation of the liquid mean velocity in this region. This combined retardation of increased bubble population turbulence and the resistance to the liquid flow results in considerable reduction of the mean liquid velocity toward the top of the tube. On the other hand, the reduction of the liquid mean velocity in this region causes a considerable increase of velocity in the rest of the pipe to maintain the overall continuity requirement. This observation is most pronounced at low liquid flow rates, since in this case bubbles are concentrated at the uppermost part of the pipe and with plenty of room for the liquid (i.e. easier path) to flow. Since as mentioned earlier in the discussion of void fraction, the bubbles tend to spread out as liquid flow increases.

It is interesting to note that the opposite happens in vertical flows. In two-phase vertical bubbly flows, the presence of voids tends to flatten the liquid velocity profile for both upward and downward flows. Moreover, for high flows in the upward direction the higher vapor concentration near the wall causes the liquid to move faster due to bubble-induced drag as reported by Wang et al. (1987).

7.4.3 Turbulence structure description

The turbulence structure is presented in terms of the root-mean-square values of the axial turbulent fluctuation in Figs. 1-3(b) and the turbulent intensity ($u'/U_{mean,local}$) in Figs. 1-3(d). The turbulence fluctuations, u', always increase when the gas is introduced. In the lower part of the pipe, the slight increase is compared to the single-phase profile. However, at the upper part of the pipe where the population of bubbles is high, it substantially increases until it peaks and then drops down abruptly in the region next to the wall.

It is interesting to note that the location where u' starts to build up is exactly the location where the void fraction distribution initiated take off. Moreover, the level of void fraction profile, determines the level of turbulence velocity, i.e. the more gradual the profile of the void fraction, a, the more gradual the profile of turbulent fluctuation, u'. This indicates that the liquid turbulent velocity, u', is a strong function of bubble

population, i.e. bubble-induced turbulence. This observation is similar to what is observed in vertical bubbly flow by Lance and Bataille (1991) and others that turbulent kinetic energy increases strongly with void fraction.

Kocamustafaogullari and Wang (1991) measured the bubble gas velocity distribution for horizontal bubbly flows using a double sensor probe. Their experimental observations demonstrated clearly that the bubble velocity profile is quite uniform in the core of the pipe, i.e. - 0.7 < r/R < 0.7, and it drops gradually next to the pipe wall. This drop, however, is not as pronounced as U_{mean} of the liquid in the region adjacent to the wall. Therefore, the difference in velocities between the two phases, air and water, decreases and thus the two-phase flow gradually resembles the homogenous flow as it approaches the wall. The decay of the relative velocity between the gas bubbles and liquid happens in the wall region due to the fact that the effect of the wall to reduce the liquid velocity is significantly more than gas because of the high viscosity of liquids compared to gases. As the relative velocity diminishes the liquid turbulence also drops. Therefore, as we move radially to the upper wall, there are two main competing factors affecting the turbulence. First, the void fraction, as it increases, it enhances u'. Second, the consistent drop in U_{mean} makes the relative velocity approach zero since the bubble velocity almost remains constant while the liquid velocity drastically decreases. Thus the u' profile experiences a transition zone (it dwells as shown in the figures) when both effects are even. Then it drops as the relative velocity decays. Around r/R = 0.9, it drops even more sharply because of the drop in void fraction, yet not strong enough to the liquid level because of the combined effect of the induced-wall turbulence present in that region and the presence of bubbles. Briefly from the above discussion, the turbulence fluctuations are a function of availability of bubbles (presented by void fraction) as well as the relative velocity between bubbles and surrounding liquid. This hypothesis can explain all the observations as will be demonstrated later. In spite of the presence of the bubble boundary layer in the bottom of the pipe, it does not enhance u' since this zone (next to the wall) has low relative velocity, and thus, the sole dominating effect is due to the wall-induced turbulence.

Figs. 1-3(d) of turbulence intensity ($u' / U_{mean,\ local}$) further verify our results of root-mean-square values. The identical trend of turbulence intensity in the lower part of

the pipe between single-phase and two-phase confirms the existence of a fully developed liquid layer almost completely free of appreciable bubble density. That means the introduction of air has no effect on turbulence intensity in this liquid layer. On the other hand, the intensity increases rapidly as the void fraction increases. It is very interesting to note that $u'/U_{mean,\ local}$ is a very strong function of α for a certain setting of $<j_g>$ and $<j_f>$ unlike u' which is also a function of the relative velocity. This result is similar to that reached by Lance and Bataille(1991) for vertical bubbly flows. The $u'/U_{mean,\ local}$ profiles peaks next to the wall very similar to void fraction profiles. However, next to the lower pipe wall, the $u'/U_{mean,\ local}$, local profile is negligibly higher than single phase because of the interactions of bubble-induced and wall-induced turbulence.

Probably not the most distinctive, but certainly the most surprising observation is the variation of turbulence intensity in the lower part of the pipe. With careful inspection of the graphs in that region, we notice that the turbulence intensity ($u'/U_{mean,\ local}$) within that region is consistently slightly lower than the single-phase. It seems the very small values of void fraction (i.e. < 0.5%) tend to lower the turbulence intensity. However, above a certain value of void fraction, its effect is to strongly increase the turbulence intensity. This explains the retardation in the profile of turbulence intensity to build up, compared to void fraction or u' profiles. This `lubrication' effect of a very small bubble population was observed in vertical bubbly flow by Serizawa et al. (1975a), Wang et al. (1987) and Liu and Bankoff (1993a,b) for high liquid flows. However, unlike the vertical configuration, this phenomenon is not observed in the root-mean-square, u', profiles, probably because of the counteracting effect of $U_{mean,\ local}$, (or relative velocity) on u'. This phenomenon observed in horizontal bubbly flow configuration seems to confirm the vertical bubbly flow configurations of Serizawa et al. (1975a) and Lance and Lopez de Bertodano (1996).

7.4.4 Effect of flow variables

The effects of gas flow on the profiles of the local void fraction, bubble-passing frequency, mean velocity, turbulent velocity, and turbulent intensity are shown in Figs. 4-7, respectively. In these figures, the liquid flow is kept constant, and the gas flow rate is used as a parameter. The void fraction increases with increasing gas flow. However, the

liquid layer thickness, which is, identified y practically zero void in the bottom part of the pipe decreases with increasing gas flow. The void fraction peak increases about 65% for the higher two gas flow rates. It confirms our result that this is the packing value of the void fraction. Similar trends are shown in Fig. 5 for bubble-passing frequency.

In the uppermost region the bubble frequency increases significantly from $\langle j_g \rangle$ = 0.25 to 0.5 m/s, while the increase from $\langle j_g \rangle$ = 0.5 to 0.8 m/s is comparatively smaller. That means the higher the gas flow rate the larger the bubble sizes. As can be seen from Fig. 6, the introduction of gas into a water flow generally accelerates the velocities all over the pipe except at the most upper portion of the pipe (r/R > 0.5) where mean velocities decelerates relative to single-phase profile. The peaks of all plots are at the same location (r/R $\approx$ -0.1) a little off the pipe centerline. As indicated in Fig. 7, the turbulence fluctuations increased strongly upon increasing the gas flow, which is attributed to the phenomenon of bubble-induced turbulence. This is quite similar to the result of Liu and Bankoff (1993a,b) in bubbly vertical flow. At the lower portion, the increase is negligible because of the weak bubble-induced turbulence due to low local relative velocity. In the upper part, the turbulence velocity increases significantly and peaks before the upper wall because of the competition between the void fraction and relative velocity effects. It is evident that the wall-induced turbulence is always accompanied by bubble-induced turbulence, however, for horizontal two-phase flow, it is the dominant type in the next-to-wall region. At the bottom liquid layer, the relative turbulence, as characterized by the turbulence intensity, follows very closely to single-phase intensity. However, after the liquid layer, the turbulence is strongly enhanced with increasing gas flow. That leads to the fact that there is a value of void fraction above which the increase of $\langle j_g \rangle$ causes considerable increase in turbulence structure. All three cases of $u'/U_{mean,\ local}$ peak at the same location indicating that the turbulence is significantly affected by the void fraction.

The influence of increasing liquid flow at a constant gas flow is demonstrated in Figs. 8-11. As can be observed from Fig. 8, the effect of increasing liquid flow rate is to disperse bubbles and flatten the void fraction distribution and thus shrinking the liquid layer. The void fraction peak decreases drastically as the liquid flow rate increases. However, there is no noticeable difference in the peak positions. It is evident that the

bubble boundary layer is most pronounced at high liquid flow rates. The same trend is evident in Fig. 9 where the bubble-passing frequency tends to flatten out as $<j_f>$ increases. Fig. 10 shows that the increase in $<j_f>$ tends to help the liquid mean velocity profile develop toward a symmetric behavior. As can be inferred from Figs. 10 and 11, the liquid velocity fluctuations at all probe locations increase as liquid flow rate increases. This effect. is more pronounced toward the bottom of the pipe than the highly populated bubble zone. In Fig. 11, it is quite obvious that at the upper part of the pipe (r/R >0.5), increasing liquid flow at constant gas flow decreases the turbulence intensity (similar to results of Liu and Bankoff, 1993a,b). However, in the lower part of the pipe (r/R <0.2) introduction of liquid seems to slightly decrease the turbulence intensity. This is attributed to the phenomenon that a very small amount of void fraction tends to decrease turbulence intensity. Between r/R = 0.5 and –0.2, there is a transition zone, since as explained earlier, increasing $<j_f>$ leads to distribution of the bubbles.

7.5 Summary and conclusions

The internal phase distribution of air-water bubbly two-phase flow in a 50.3-mm i.d. transparent horizontal pipeline was experimentally investigated. The local values of void fraction, bubble frequency and liquid velocity were measured.

The experimental results indicate that the void fraction and bubble-passing frequency have local maxima near the upper pipe wall, and the profiles tended to flatten with increasing liquid flow rate. For the horizontal bubbly flow, the observed time-averaged local void fraction can reach 65%, whereas the bubble frequency may reach a value of 1400 s^{-1}. The fact that the peak void fraction in all cases never exceeds 65% indicates that maximum packing exists within the channel. It was found that increasing the gas flow rate at a fixed liquid flow rate would increase the local void fraction and bubble-passing frequency.

The axial liquid mean velocity showed a relatively uniform distribution except near the upper pipe wall, where a sharp reduction in velocity was noticed. The local mean liquid velocity and turbulence fluctuations increased with gas flow rate. An interesting feature of the liquid velocity distribution is that it tends to form a fully-developed turbulent pipe-flow profile in the lower part of the pipe.

At very low local void fractions, the turbulent intensity consistently tended to be slightly lower than the single-phase. A similar case was observed in vertical bubbly flows. However, at high void fractions (i.e. high bubble population), introduction of gas strongly enhances the turbulence structure as characterized by the turbulent velocity fluctuation and turbulent intensity behavior. In general, it was concluded that the local turbulence intensity is mainly a function of the local void fraction.

Acknowledgements

The work reported in this paper was supported by a grant from the US Department of Energy, Office of Basic Energy Science. The authors would like to express their sincere appreciation for the encouragement, support and technical comments on this program from Drs R. Price and R. Goulard of the US DOE/BES.

Nomenclature

j	Superficial Volumetric Flux
N	Total number of data points
R	Pipe radius
r	Radial distance
t	Time
U	Axial velocity
u	Instantaneous axial velocity
u'	Axial component of velocity fluctuations

Greek Symbols

α	Void fraction
δ	Delta function

Subscripts

f	Liquid phase
g	Gaseous phase
i	i^{th} gas bubble

References

1. Abel, R., Resch, F.J., 1978. A method for the analysis of hot film anemometer signals in two-phase flows. Int. J. Multiphase Flow 4, 523-533.
2. Delhaye, J.M., 1969. Hot-film anemometry in two-phase flow. In: Le Tourneau, B.W., Bergles, A.E. (Eds.), Two-Phase Flow Instrumentation. ASME, New York, pp. 58-69.
3. Grossetete, C., 1995. Experimental investigation and preliminary numerical simulation of void profile development in a vertical cylindrical pipe. Proceedings of the 2nd International Conference on Multiphase Flow, Kyoto, Japan.
4. Hibiki, T., Hogsett, S., Ishii, M., 1997. Local measurement of interfacial area, interfacial velocity and liquid turbulence in two-phase flow. DECD Meeting on Instrumentation, Santa Barbara, CA.
5. Hsu, Y.Y., Simon, F.F., Graham, R.W., 1963. Application of hot-wire anemometry for two-phase flow measurements such as void fraction and slip velocity. Proceedings of the ASME Winter Meeting, Philadelphia, PA.
6. Iskandrani, A., 1997. Use of Hot-Film Anemometry in Horizontal Two-Phase Bubbly Flow. M.S. thesis at the University of Wisconsin Milwaukee.
7. Iskandrani, A., Kojasoy, G., 1999. Utility of hot-film anemometry technique in horizontal bubbly two-phase flow. National Heat Transfer Conference.
8. Kocamustafaogullari, G., Wang, Z., 1991. An experimental study on local interfacial parameters in a horizontal bubbly two-phase flow. Int. J. Multiphase Flow 17, 553-572.
9. Kocamustafaogullari, G., Huang, WK., Razi, J., 1994. Measurement and modeling of average void fractions, bubble size and interfacial area. Nucl. Eng. Des. 148, 437-453.
10. Lance, M., Bataille, J.M., 1991. Turbulence in the liquid phase in a uniform bubbly air-water flow. J. Fluid Mech. 222, 95-118.
11. Lance, M., Lopez de Bertodano, M.A., 1996. Phase distribution phenomena and wall effects in bubbly two-phase flows. Multiphase Sci. Technol. 8, 69-123.

12. Laufer, J., 1954. The Structure of Turbulent in Fully-Developed Pipe Flow. NACA Report 1174.
13. Liu, T.J., Bankoff, S.G., 1993a. Structure of air-water bubbly flow in a vertical pipe - I. Liquid mean velocity and turbulence measurements. Int. J. Heat Transf. 36, 10491060.
14. Liu, T.J., Bankoff, S.G., 1993b. Structure of air-water bubbly flow in a vertical pipe. II. Void fraction, bubble velocity and bubble siga distribution. Int. J. Heat Transf. 36, 1061-1072.
15. Ohba, K., Itoh, T., 1978. Light attenuation technique for void fraction measurement in two-phase bubbly flow - II. Experiment. Technol. Rep. Osaka Univ. 28 (1449), 495506.
16. Serizawa, A., Kataoka, I., Michiyshi, L, 1975a. Turbulence structure of air-water bubbly flow - I: measuring techniques. Int. J. Multiphase Flow 2, 221-233.
17. Serizawa, A., Kataoka, I., Michiyshi, I., 1975b. Turbulence structure of air-water bubbly flow - II. Local properties. Int. J. Multiphase Flow 2, 235-246.
18. Suzanne, C., Ellingsen, K., Risso, F., Roig, V., 1998. Local measurement in turbulent bubbly flows. Nucl. Eng. Des. 184, 319-327.
19. Theofaneous, T.G., Sullivan, J., 1982. Turbulence in two-phase dispersed flows. J. Fluid Mech. 116, 343-362.
20. Wang, S.K., 1985. Three-dimensional Turbulence Structure Measurements in Air/water Two-phase Flow. Ph.D. Thesis, Rensselaer Polytechnic Inst., Troy, NY.
21. Wang, S.K., Lee, S.J., Jones, O.C., Jr, Lahey, R.T., Jr, 1987. Three-dimensional turbulence structure and phase distribution measurements in bubbly two-phase flow. Int. J. Multiphase Flow 13, 327-340.
22. Zun, I., 1990. Mechanism of bubble nonhomogeneous distribution in two-phase shear flow. Nucl. Eng. Des. 118, 155-162.

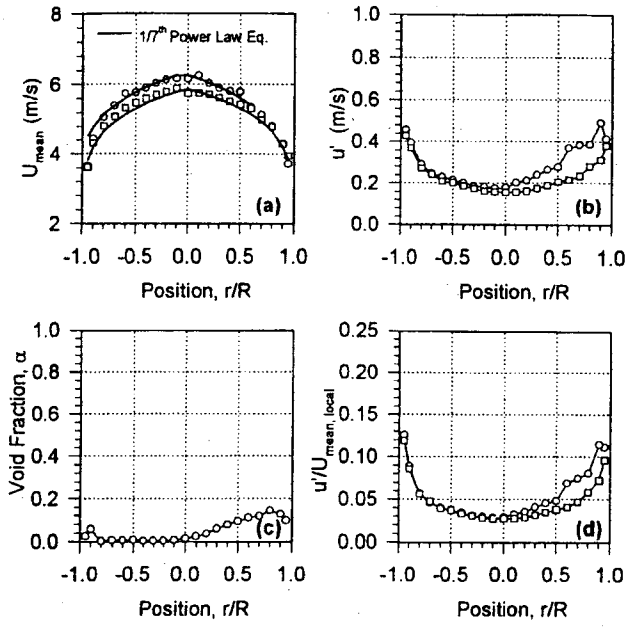

Fig. 1. Two-phase flow data for $\langle j_f \rangle = 5.0$ m s^{-1} and $\langle j_g \rangle = 0.25$ m s^{-1}: (a) local mean velocity; (b) local turbulence velocity; (c) local void fraction; (d) turbulent intensity distribution. □, Single-phase data; ○, two-phase data.

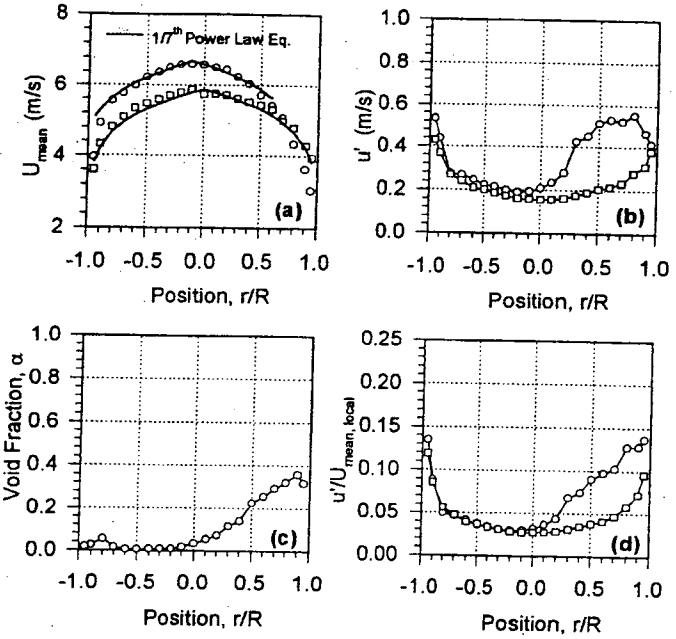

Fig. 2. Two-phase flow data for $\langle j_f \rangle = 5.0$ m s^{-1} and $\langle j_g \rangle = 0.50$ m s^{-1}: (a) local mean velocity; (b) local turbulence velocity; (c) local void fraction; (d) turbulent intensity distribution. □, Single-phase data; ○, two-phase data.

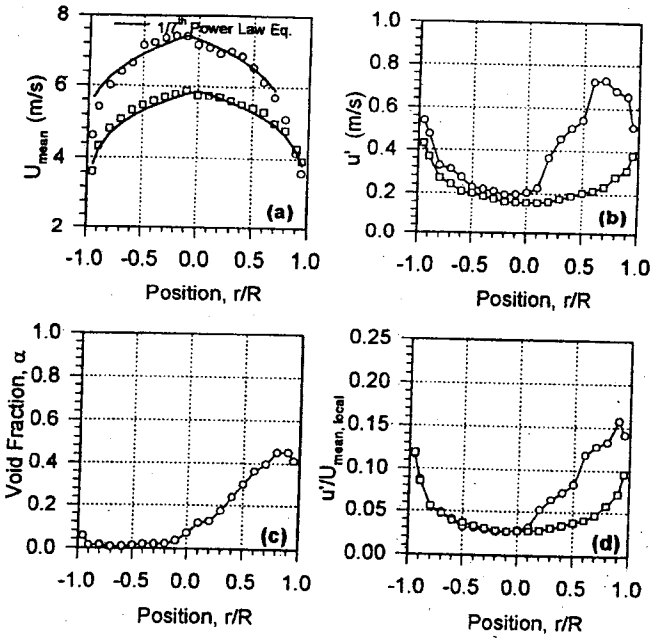

Fig. 3. Two-phase flow data for $\langle j_f \rangle = 5.0$ m s^{-1} and $\langle j_g \rangle = 0.80$ m s^{-1}: (a) local mean velocity; (b) local turbulence velocity; (c) local void fraction; (d) turbulent intensity distribution. □, Single-phase data; ○, two-phase data.

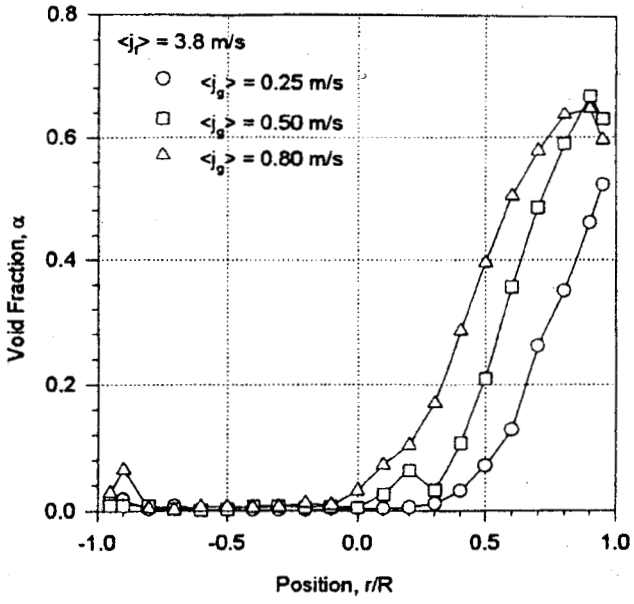

Fig. 4. Influence of gas flow on local void fraction.

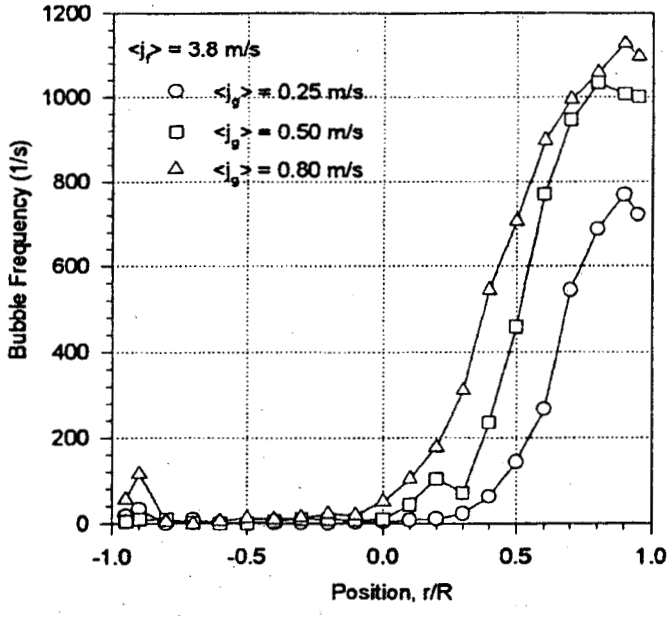

Fig. 5. Influence of gas flow on local bubble-passing frequency.

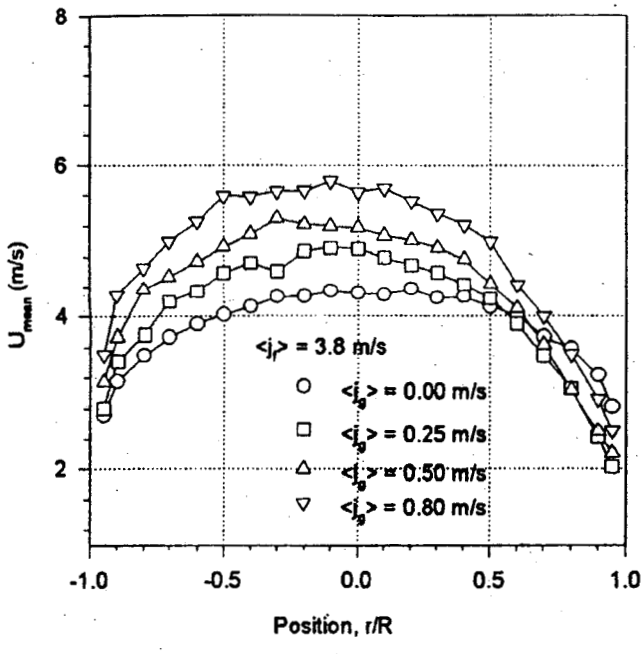

Fig. 6. Influence of gas flow on local mean liquid velocity.

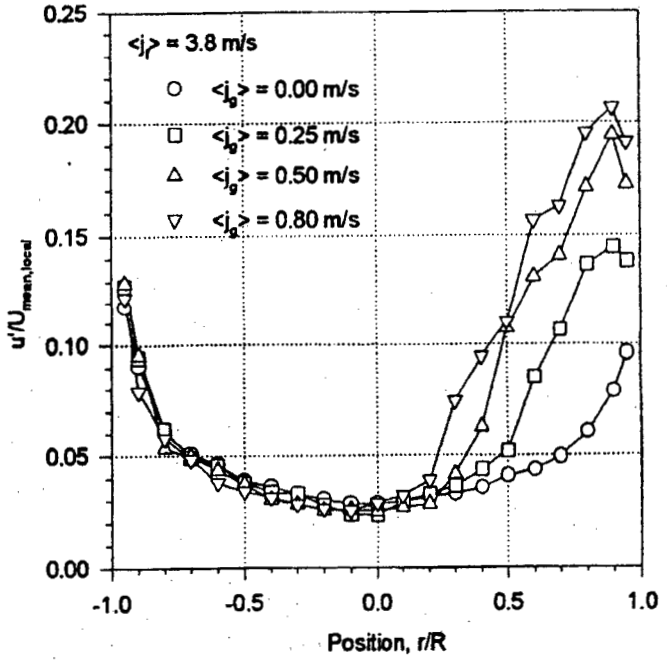

Fig. 7. Influence of gas flow on local turbulent intensity.

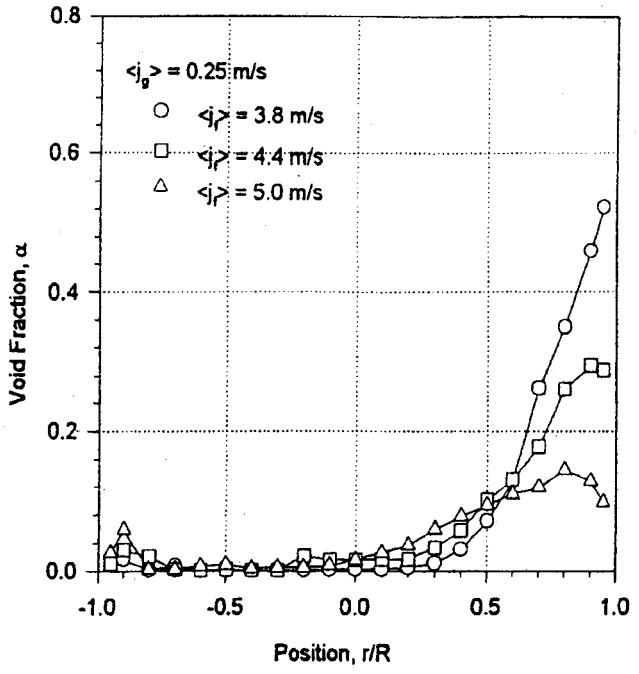

Fig. 8. Influence of liquid flow on local void fraction.

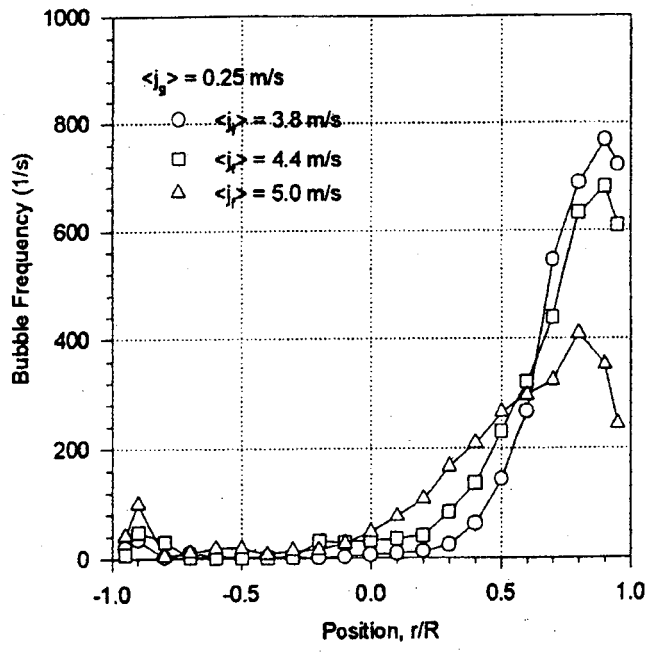

Fig. 9. Influence of liquid flow on local bubble-passing frequency.

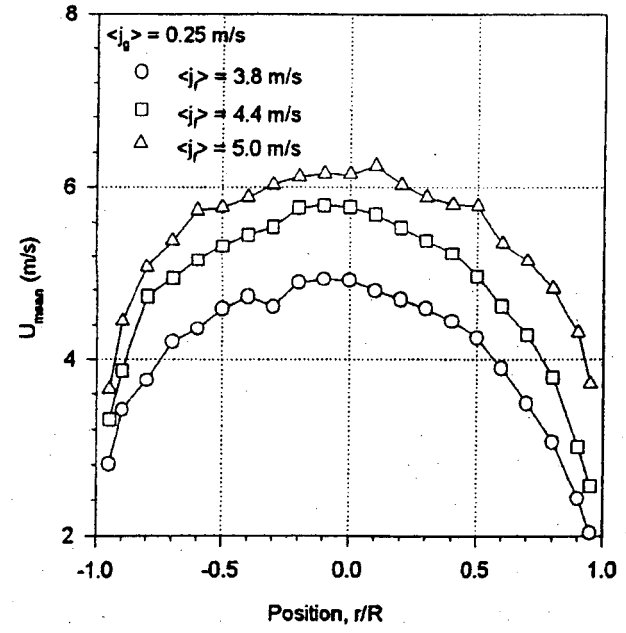

Fig. 10. Influence of liquid flow on local mean liquid velocity.

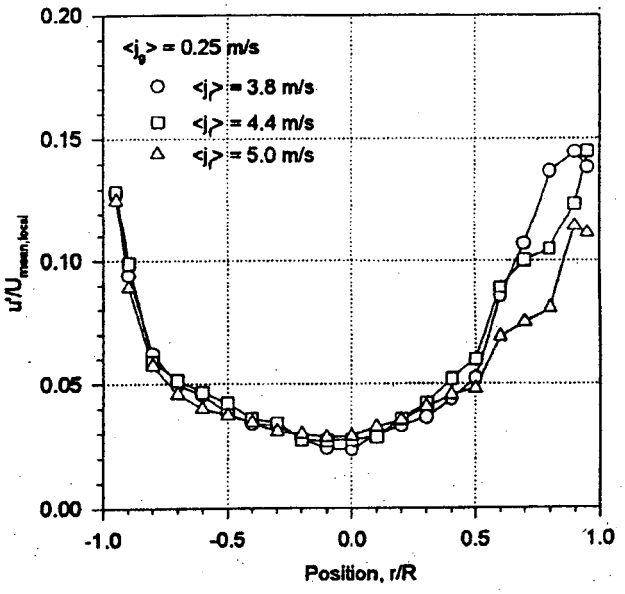

Fig. 11. Influence of liquid flow on local turbulent intensity.

8. DEVELOPMENT OF FOUR-SENSOR PROBE METHOD FOR PLUG/SLUG FLOW MEASUREMENTS

Gunol Kojasoy, Tangwen Guo and Jovica Riznic
Department of Mechanical Engineering
University of Wisconsin-Milwaukee, Milwaukee, Wisconsin 53201, USA

Abstract

The main objective of this work is to investigate the internal flow structure in horizontal slug flow by measuring the local interfacial area concentration, void fraction and interfacial velocity distributions as well as gas bubble transit frequency. The four-sensor and two-sensor electro-resistivity probes and other respective related signal processing programs are developed to measure the time-averaged local void fraction and interfacial area concentration. Experimental studies were performed on the plug/slug flow regimes with an air-water system. Data were acquired at the axial location of L/D=253 from the mixing chamber, which represents the region of quasi fully-developed two-phase flow. The liquid superficial velocity was varied between 0.55 and 2.20 m/s and gas velocity between 0.27 and 2.20m/s. With these experimental conditions, the local void fraction ranged from 10 to 70%. Experimental data showed higher interfacial area concentration in the lower part of a slug bubble with a larger curvature of interface. Radial profiles of interfacial area concentration for slug bubbles show almost a flat profile in the upper part of slug bubble. The larger value of the total interfacial area concentration indicates that the contribution from the small bubbles is increased. It was observed that the size of the slug bubbles in terms of height and shape did not vary much. In the region of transition between plug and slug flow regimes, with an increase in the gas flow rate the number and contribution of the small follow up bubbles increased. For all gas velocities considered in the present investigation, it was observed that the slug frequency increases as the water superficial velocity increases. In contrast, for the range of liquid superficial velocities used in the present investigation the slug frequency increases and then decreases as the air superficial velocity increases.

8.1. Introduction

The thermal hydraulic behavior of gas-liquid flow has been of great interest to practicing engineers, since it is often encountered in many industrial applications such as nuclear and fossil fueled power plants, petrochemical process apparatus and plants, refrigeration equipment, and various multiphase heat exchangers. This type of flow has the advantages of high heat and mass transport rates between the coupling phases at the internal deformable interfaces as well as at the fluid-solid boundaries.

Gas-liquid flow in conduits may take on a wide range of configurations termed as two-phase flow patterns or flow regimes. One of the flow patterns frequently encountered is the intermittent or slug flow pattern. In horizontal and inclined pipes, slugs of liquid that occupy the whole cross section are separated by a elongated gas slug bubble in the upper part of the conduit and a liquid layer at the bottom. The long gas slug is followed by some small gas bubbles in the liquid slug. At lower gas flow rates, the liquid slug is almost free of small follow-up bubbles. This pattern is termed as plug or elongated bubble flow regime. However, at higher gas flow rates, small bubbles may break off the large slug and either reside in the liquid slug or coalesce with the faster moving front of the following gas slug bubble.

Slug flow is a highly complex type of multiphase flow with an unsteady nature and intermittent structure, which is non-periodic either in space or in time, even when the gas and liquid flow to the system is steady. As a result, the processes of heat, mass and momentum transfer are also unsteady with substantial fluctuations in temperature and orientation. This suggests that one should formulate the two-phase flow dynamic model without ignoring the intermittent nature of the flow. Thus the prediction of the pressure drop, void fraction or liquid holdup, and heat and mass transfer for such flow becomes extremely difficult.

A variety of approximate methods have been developed for predicting hydrodynamic parameters of slug flow. The early semi-empirical methods simply used correlations of experimental results [1]. Further development in two-phase flow modeling showed tendency toward formulation of approximate models that are capable of simulating the flow behavior sufficiently accurate so that the evaluation of relevant flow parameters can be performed with a relative high degree of confidence. Wallis[2] introduced the unit-cell modeling concept and used a simplified slug flow model consisting of a gas slug bubble and a liquid slug. Similar models for

horizontal slug flow were also developed by Dukler and Hubbard[3], Nicholson et al.[4] and Malnes[5]. The ranges of gas and liquid flow rates for which slug flow occurs are well known and incorporated in flow regime maps that display the transition boundaries among different flow patterns[6,7,8]. Besides Fershneider[9] and Fabre et al[10] developed a statistical cellular model based on conditional averaging of conservation equations. To develop more accurate models, a better understanding of the internal flow structure of the slug flow is necessary. However, due to experimental difficulties associated with the intermittent nature of slug flow, very few detailed local measurements have been reported in the literature. The problem in obtaining local data is further complicated in horizontal flow by the axial asymmetry of internal structure and the fact that the slug flow does not exhibit a quasi fully-developed equilibrium condition.

The most significant and essential parameters associated with the two-phase slug flow pattern are the distributions of void fraction, available interfacial area, interfacial velocity and gas bubble and liquid transit frequency (or slug length). These variables characterize the local flow structures of the quasi-steady slug flow. Hence, accurate information on these flow parameters, and generalized relationships among them are necessary to understand the complexity of interfacial transport phenomena for such two-phase flow pattern. Modern advances in the study of multiphase flow increasingly demand overcoming the difficulties in obtaining detailed information on internal flow structure upon which theoretical models can be formulated. For example, among the various available formulations of two-phase flow dynamics, the two-fluid model, which treats the two phases separately in the conservation equations, is considered the most accurate formulation because of its detailed treatment of the phase interactions at interfaces. In such a model, the constitutive equation of the interfacial area is indispensable[11].

At present, several methods are available to measure interfacial area concentration in gas-liquid and liquid-liquid two-phase flows. Measurement techniques can be broadly classified into two categories: chemical absorption methods and physical methods. Chemical absorption techniques provide global measurements of interfacial area concentration and thus do not provide the local information of interest in closure models. Physical methods involve techniques such as photography, light attenuation, ultra-sonic attenuation and various intrusive probe techniques(e.g., resistivity or impedance probes, fiber-optic probes, hot-film anemometer probes, etc). However, all these methods have their own limitations. Detailed review of all these methods

have been given by Landau et al.[12] Veteau[13], Ishii and Mishima[14], Kocamustafaogullari and Wang[15], Riznic et al.[16], amongst others.

Kasturi and Stepanek[17], Tomida[18] and De Jesus and Kawaji[19] carried out experiments in vertical circular cross section tubes of inside diameter in the range of 6 to 25.4 mm. The interfacial area was measured by using the chemical absorption technique in slug, churn and annular flow regimes. The liquid superficial velocity varied from 0.05 to 1.3 m/s and the gas superficial velocity from 0 to 15.5 m/s. However, the scatter of experimental data points was considerable. Bensler[20] performed experimental study on both vertical natural recirculation and forced circulation air-water loop. Three square test sections were used (40 x 40; 80 x 80; and 120 x 120 mm). The liquid superficial velocity ranged from 0 to 3 m/s and the gas superficial velocity from 0.001 to 0.25 m/s. No existing correlations for interfacial area concentration were satisfactory when compared with Bensler's extensive set of data. Chang and Morala[21] used the ultrasonic pulse echo technique to measure the interfacial area and time averaged void fraction in a horizontal two-phase flow system. They performed experiments in horizontal pipe of 20 mm id and 63.5 mm inside diameter vertical pipes. The range of superficial velocities covered by the experiment was 0 to 2.7 m/s for air and 0 to 0.18 m/s for water. The results were widely scattered and multi-beam method with two- or three-dimensional analyses was recommended for further interfacial area concentration measurements. Grossetete[22] used a dual-fiber optical probe to measure local interfacial area concentration in 6 meter long, vertical smooth pipe of 38.1mm inside diameter, in developing bubbly flow and at a slug-churn transition. The liquid superficial velocity varied from 0.614 to 1.316 m/s and the gas superficial velocity from 0.06 to 0.47 m/s. Profiles of the interfacial area concentration and void fraction were obtained along the test section at three axial positions located at Z/D=8, 55 and 155.

Revankar and Ishii[24] reported a detailed study of internal structure in vertical two-phase slug flow, in a vertical pipe of 1500 mm in height and inside diameter of 50.8 mm. They employed the four-sensor resistivity probe to measure local interfacial area concentration and void fraction at a superficial gas velocity range of 0.006-0.041m/s. The interfacial area concentration profiles for the cap bubbles showed a higher value near the steep side interface of the cap bubble. The four-sensor probe data showed that in the presence of a large number of small bubbles in a cap or slug flow, the interfacial area concentration is largely determined by the

small bubbles. Kalkach-Navaro et al[25] proposed another method to measure local interfacial area concentration. Their method is based on the measurement of the bubble size probability distribution function and the determination of its moments. Experiments were performed using a dual-sensor resistivity probe in vertical tube of 60 mm inside diameter. Measurements covered bubbly flow regime with the liquid superficial velocity in the range of 0.3 to 1.25 m/s and the gas superficial velocity from 0.081 to 0.148 m/s. Based on our literature survey, there are no other experimental data or fundamental studies available on the local distribution of these parameters in horizontal plug and/or slug two-phase flow.

In our studies(Lewis et al[6] Riznic et al[16]), the internal flow structure of horizontal slug flow was investigated by measuring the local interfacial area concentration, void fraction, interfacial and turbulent velocity distribution. The four-sensor electro-resistivity and the hot-film anemometer probes were used to measure the instantaneous interface velocities and liquid velocities, respectively. The experimental results indicate that the void fraction profile of large slug bubbles shows a sharp increase right above the liquid layer and then flattens gradually, goes through a maximum with a slight decrease toward the top wall of the pipe. On the other hand, the small bubble void fraction increases toward the top wall of the pipe, which indicates a strong small bubble migration toward the top wall within liquid slugs. The mean velocity and absolute turbulence profiles show two distinct turbulent flow regions where the fully-developed turbulent velocity profiles are preserved.

In view of the above discussions, it is evident that much experimental work is still necessary to attain a thorough physical understanding of the internal structure of an intermittent slug flow pattern. In this context, an experimental investigation has been performed at the University of Wisconsin-Milwaukee to clarify the interfacial structure of this flow pattern. In present experiments, the local interfacial parameters in a horizontal plug/slug two-phase flow have been studied experimentally by using the four-sensor resistivity probe methods. More specifically:

- The four-sensor resistivity probe method was developed to measure the local void fraction and interfacial area concentration of large bubbles in a horizontal plug/slug two-phase flow,
- The double-sensor resistivity probe method which was developed to measure local void fraction, interfacial area concentration, interface velocity, local bubble chord-

length, size and frequency distributions of bubbles in a horizontal bubbly flow[15,16], was also used to measure the interfacial characteristics of small bubbles encountered st the wake of large bubbles in a horizontal slug flow.

8. 2. Development of Four-Sensor Resistivity Probe Method

8.2.1. Measurement Principle

The conductivity probe technique was proposed based on the significant differences in conductivity between water and air. In view of its most durable, least expensive and relatively simplest way to implement, the conductivity probe has been extensively used for the measurement of various two-phase flow parameters. The theoretical foundation for its application has been well established.

For a moving gas-liquid interface j represented by $f_j(x,y,z,t)=0$, the local instantaneous interfacial area concentration was defined as[Ishii,1975),

$$a_i(x,y,z,t) = \sum_j |\nabla f_j| \delta(f_j(x,y,z,t)) \tag{1}$$

This representation is valid for any flow regime of gas-liquid flow, but cannot be used in practice since the distribution function $\delta(f_i(x, y, z, t))$ is not observable experimentally. Instead, the time-averaged value of interfacial area concentration is more practical. By averaging the equation (1) over a time interval Ω at position x_0, y_0 and z_0, a measurable formulation of the time-averaged interfacial area concentration resulted[Ishii,1975, Katauka &Ishii,1986),

$$\bar{a}_i^t(x_0,y_0,z_0) = \frac{1}{\Omega}\sum_j \left(|\nabla f_j| \Big/ \frac{\partial f_j}{\partial t} \right) \quad at\ (x_0,y_0,z_0,t_j) \tag{2}$$

which applies for all j satisfying $t < t_j < t + \Omega$. It can be further expressed as,

$$\bar{a}_i^t(x_0,y_0,z_0) = \frac{1}{\Omega}\sum_j \left(\frac{1}{|v_i \cdot n_i|} \right)_j \tag{3}$$

were j denotes the j'th interface passing the position (x_0, y_0, z_0) during time interval Ω, v_i and n_i are the moving velocity and the unit surface normal vector of the j'th interface, respectively. Equation (3) indicates that the local time-averaged interfacial area concentration can be obtained by measuring the interfacial velocity for each passing bubble. Based on Equation (2) and (3),

Kataoka et al(1986) derived the widely used formulations of the time-averaged interfacial area concentration for both two-sensor probe and four-sensor probe. The two sensor probe has been employed in dispersed bubbly flow regimes whereas the four-sensor probe has been adopted in cap or slug flow conditions.

For the application of two-sensor probe, the following equation can be derived based on the assumptions that: 1) The bubbles are spherical in shape, 2) The interfacial velocity v_i is statistically independent of the angle between mean flow direction(z-direction) and normal direction ($\boldsymbol{n}_i$) of the interface, 3) The probe penetrates every part of a bubble with an equal probability, 4) the transverse direction (x or y direction) components of the interfacial velocity are random.

$$\bar{a}_i^t(x_0, y_0, z_0) = \frac{4N_t \left\{ \sum_j \frac{1}{|\overline{v_{szj}}|} / \sum_j \right\}}{1 - \cot\frac{1}{2}\alpha_0 \ln(\cos\frac{1}{2}\alpha_0) - \tan\frac{1}{2}\alpha_0 \ln(\sin\frac{1}{2}\alpha_0)} \tag{4}$$

where N_t, v_{szj}, and α_0 denote the bubble number acquired by sensor per unit time, the passing velocity of the j'th interface in z direction, and the maximum angle between the interfacial velocity and axial direction, respectively. The maximum angle α_0 can be related to the interfacial velocity by assuming that the fluctuations of the bubble interfacial velocity are isotropic.

$$\frac{\sin 2\alpha_0}{2\alpha_0} = \frac{1 - (\sigma_z^2 |\overline{v_{iz}}|^2)}{1 + 3(\sigma_z^2 |\overline{v_{iz}}|^2)} \tag{5}$$

here $|\overline{v_{iz}}|$ is the mean value of z-component of the interfacial velocity, σ_z is the mean square root of the measured velocity fluctuations,

$$\sigma_z^2 = \overline{(v_{iz} - \overline{v_{iz}})^2} = \overline{|v_{iz}|^2} - |\overline{v_{iz}}|^2 \tag{6}$$

Therefore, the time-averaged local interfacial area concentration of the spherical bubbles can be obtained from the measurable quantities v_{szj}, and N_t by means of the two-sensor probe.

On the other hand, when the bubble size is larger and their shapes are no longer spherical, the application of the four-sensor probe becomes necessary. Ideally, with the four-sensor probe, the three components of interfacial velocity can be obtained at a local point by measuring the time

delays between the signals of the front sensor and each rear sensor. Then the time-averaged interfacial area concentration formulation, Eq.(2), can be further reduced as,

$$\bar{a}_i^t = \frac{1}{T}\sum_j \frac{\sqrt{|A_1|^2 + |A_2|^2 + |A_3|^2}}{\sqrt{|A_0|^2}} \tag{7}$$

where,

$$|A_0| = \begin{vmatrix} \cos\eta_{x1} & \cos\eta_{y1} & \cos\eta_{z1} \\ \cos\eta_{x2} & \cos\eta_{y2} & \cos\eta_{z2} \\ \cos\eta_{x3} & \cos\eta_{y3} & \cos\eta_{z3} \end{vmatrix} \tag{8}$$

$$|A_1| = \begin{vmatrix} \frac{1}{v_{s1j}} & \cos\eta_{y1} & \cos\eta_{z1} \\ \frac{1}{v_{s2j}} & \cos\eta_{y2} & \cos\eta_{z2} \\ \frac{1}{v_{s3j}} & \cos\eta_{y3} & \cos\eta_{z3} \end{vmatrix} \tag{9}$$

where v_{skj} denotes the j'th interface passing velocity component measured by front sensor and rear sensor k, and $\cos\eta_{xk}$, $\cos\eta_{yk}$, $\cos\eta_{zk}$ are the direction vector cosines along the direction from the front sensor to rear sensor k.

$|A_2|$ and $|A_3|$, similar to $|A_1|$, can be obtained by replacing the second and third column of the determinant $|A_0|$ by the inverse of the measured passing velocity components. Eqs (7) indicates that the local time-averaged interfacial area concentration can be obtained by the three measured velocity components and the known geometric parameters of the four-sensor probe. When the front sensor and three rear sensors are configured such that they form an orthogonal system, the Eq.(7) can be simplified to,

$$\bar{a}_i^t = \frac{1}{\Omega}\sum_j \left\{ \left(\frac{1}{v_{s1j}}\right)^2 + \left(\frac{1}{v_{s2j}}\right)^2 + \left(\frac{1}{v_{s3j}}\right)^2 \right\} \tag{10}$$

In deriving the Equation (7), no hypothesis for the bubble shape was employed. Therefore, it can be used for bubbles with any shape as long as the local bubble interface is large compared to the probe projection area.

8.2.2. Four-Sensor Probe Design and Signal Processing

The probe sensor is made of an exposed tip of an otherwise electrically insulated metal wire. The material and geometry of the sensor were found to be critical as they affected the quality of the signals and consequently the value of the measured parameters. Each sensor was made of the platinum/13% rhodium or chromel alloy wire which has a good corrosion-proof in the water environment. The thin wire with a selected diameter of 0.127μm minimizes the interference with the bubble surface and its trajectory, yet provides enough strength to withstand the fluctuation. Most of the probes used in the experiment could last for a few weeks and the failure was usually caused by breakdown of the insulating varnish. Another critical factor is the distance between the front and rear sensor tips. The distance is dictated by the possible bubble size and bubble interface velocity. In view of the effect of interface curvature of bubbles, it is evident that the distances between the tips of front sensor and rear sensor should be considerably smaller than the bubble size. However, a very small distance would result in inaccuracies in time duration measurements unless sampling frequency is set very high or the bubble velocity is very low. On the other hand, too large distance will increase the likelihood of misinterpretation of signals, since a series of bubbles may pass the front sensor before they reach the rear sensor. Preliminary experiments were conducted to determine a proper distance between front and rear sensor tips. It was found that 2 - 2.5 mm in lateral direction and 3 - 4 mm in longitudinal direction were the appropriate separation distance for the selected experimental conditions.

Figure 1 gives the typical voltage signals from four-sensor probe in a slug flow. As illustrated in the figure, the signals, even for the large slug bubbles, deviate from the ideal two-state square-wave signals. The trailing edges are generally steeper than the leading edges. This deviation is largely due to the unavoidable formation of thin residual liquid film on the finite sensor tip surface and the possible deformation of the interface when sensor enters from liquid phase to gas. When the sensor tips encounter small gas bubbles in liquid, the residence time in a small bubble is not long enough for the sensors to dewet and dry. As a result, signals for small bubbles do not vary between V_{min} and V_{max} as observed in the case of large bubbles.

8.2.3. Signal Processing

8.2.3.1. Phase Identification

The output voltage signal from the conductivity probe is collected by the data nacquisition system and stored in PC. To obtain local two phase-flow parameters, the correct identification of the signal from bubble interface is critical. A new signal processing program is established and featured with two main improvements in phase identifying. The first one is using the normalization of the raw signal, which is effective as demonstrated by Kim et.al(2000). The second one is the use of signal slope criteria which was proved feasible by Kojasoy and Lewis(2001).

Considering the regression of both the sensor and water conductivities with the time, neither the absolute value of the base voltage(sensor in liquid), nor the voltage drop between air and water is susceptible to variation. To process the signal under same criteria, it is much convenient to normalize the signal. The normalization equation is,

$$V_{norm,i} = \frac{V_i - V_{\min}}{V_{\max} - V_{\min}} \tag{11}$$

where $V_{norm,i}$ is the normalized voltage of the i'th signal, V_i is the i'th signal, V_{max} is the maximum voltage, and V_{min} is the minimum voltage. This minimum voltage can be determined by the average voltage signal in the liquid phase. A simple method to determine the minimum voltage is to divide the total signal range into four quarters and set the most probable voltage in lowest quarter as V_{min}.

After the normalization, a threshold level V_{thres} is set to remove the noises due to the signal fluctuation in water. V_{thres} can be determined by experimental observation. Any voltage fluctuations with amplitude less than V_{thres} will not be counted as bubble signals. Further, due to the finite rise/fall time in signals, ambiguity exists in identifying the bubble interfaces. It is necessary to convert the normalized signal into step signal which represents the bubbles. In present signal processing scheme, two slope threshold levels are introduced for determining the occurrence of the bubble interfaces and converting the normalized signal into square step signal, slope threshold one, S_{thres1}, with a positive value for determining the bubble nose and slope threshold two, S_{thres2}, with a negative value for determining the bubble tail. The signal slope is defined as,

$$S_i = \frac{V_{norm,i} - V_{norm,i-1}}{t_i - t_{i-1}} \tag{12}$$

where, $V_{norm,i}$ and $V_{norm,i-1}$, are the normalized signal voltages at time t_i, t_{i-1},respectively. Evidently, S_i has a positive value for the rising edges and a negative value for the falling edges.

For the normalized signal above the voltage threshold level, once the slope values of two consequent data points exceed the first threshold one, S_{thres1}, i.e., $S_i > S_{thres1}$ and $S_{i+1} > S_{thres1}$, then bubble nose is detected, then the phase identification step signal is set equal to 1. On the other hand, once the slope values exceed the second slope threshold, S_{thres2}, the tail of the bubble is detected, and the phase separation step signal is set equal to 0. The values of S_{thres1} and S_{thres2} are determined by experimental observation. Figure 2 shows the examples of the raw signal, normalized signal and identified step signal.

After distinguishing the phases, the next important step is identifying the signals which originate from the same bubble, because the two subsequent signals detected by the front and rear sensors do not always correspond to the same bubble and the residence time intervals of the bubble at front and rear sensors are not exactly the same. The signal validation was made by judging whether the following criteria are satisfied simultaneously:

(1) By assuming the forward motion of the bubbles, the front sensor signal rises or falls before the rear sensor signals do. Therefore, referring to figure 1, the following conditions should be satisfied

$$t_{orj} < t_{krj}, t_{ofj} < t_{kfj} \quad k = 1,2,3 \tag{13}$$

where the subscript *0* denotes the front sensor and *k=1,2,3* denote the rear sensors, *r* and *f* denote the times of the signal rise and fall, respectively, *j* identifies the *j*'th interface.

(2) The residence time of a same bubble at the front and rear sensors should be comparable, i.e.:

$$t_{ofj} - t_{orj} \cong t_{kfj} - t_{krj} \qquad k = 1,2,3 \tag{14}$$

(3) The time lag between the front sensor and rear sensor for a same interface should satisfy the following condition,

$$\begin{aligned} &\Delta t_{\min} \le t_{krj} - t_{orj} \le \Delta t_{\max} \\ &\Delta t_{\min} \le t_{kfj} - t_{ofj} \le \Delta t_{\max} \qquad k = 1,2,3 \end{aligned} \tag{15}$$

where waiting time limits Δt_{min} and Δt_{max} were determined by the combination of the distances between front and rear sensor tips and flow conditions such as superficial gas velocities.

8.2.3.2. Separation of Large and Small Bubbles

The large bubble is distinguished from the following small bubbles based on the bubble chord lengths. From the phase identification signal(square step signal), residence time for each bubble can be determined. This time multiplied by a representative bubble velocity yields the bubble chord length. In present processing scheme, the representative bubble velocity is estimated using the known sensor distance and the most probable time delay between front sensor and rear sensor. To find out the most probable time delay, the cross-correlation operation between signal from front sensor and that from rear sensor is applied. This representative velocity is then used to estimate the range of bubble chord-length, and hence, the bubble sizes. In present experiments, the maximum small bubble chord-length, is used as the discriminatory criterion for separating small bubbles from large bubbles[Kojasoy & Lewis,2001]. According to the small bubble spectra and the visual observations, the discriminatory criterion is set at 30mm for small bubbles and at 200mm for slug bubbles in present experiments.

8.2.3.3. Calculation of Time-averaged Interfacial Area Concentration

In obtaining the two-phase flow parameters, signal from the front sensor of either two-sensor probe or four-sensor probe is used for the calculation of time-averaged void fraction and the bubble chord length. To obtain the local instantaneous interfacial area concentration, it is necessary to know the passing velocity of bubble interfaces. The same interface should be detected by both the front and rear sensors with two-sensor probe or by all the four sensors with the four-sensor probe so that the passing velocity could be determined. However, because of the finite size of the probe and the finite spacing between the sensors of four-sensor probe as well as the possible distortion of bubble interfaces, especially in horizontal slug flow, some interfaces contact the front sensor and miss one or more of the rear sensors and vice versa. Furthermore in horizontal slug flow, the slug bubbles always pass through the upper portion of the pipe cross section due to the buoyancy, and a very steep interface is formed by the thin liquid film existing near the top wall for each slug bubble. On the other hand, the bottom side interface of the slug bubble is more susceptible to significant distortions. It is hardly for all four sensors to detect such interfaces without one missing.

In view of these, an important issue for signal processing is to device a method for correcting the contribution to the time-averaged interfacial area concentration from those bubbles whose signal is not sufficient enough for calculating the local instantaneous interfacial velocity. As noted by Kim & Ishii(2000), there are three kinds of such bubble signals. The first kind named "missed" or missing bubble signal occurs when small spherical bubble misses one sensor of the two-sensor probe. For such bubble only one signal is registered. The second kind referred as a "non-effective" bubble signal appears when the interface of the slug bubble is highly distorted, the signal from the front sensor may not precede the ones from the rear sensors. Apparently such signals cannot be used to calculate the interfacial velocity and the local interfacial area concentration. The third kind is associated with the steep side interface of the slug bubble as described above. This side interface is parallel to the horizontal orientation of the probe sensors, so one or more of the rear sensors may escape it. The interfacial area of this steep side interface is substantial compared to the front and rear interfaces of the same slug bubble. Therefore it is important to estimate such missing signal properly. For vertical flow, this missing phenomenon mainly occurs near the flow duct wall(Ishii & Revankar, 1993, Kim & Ishii, 2000), while for horizontal flow, this phenomenon can exist in a large area because the slug bubbles with different size always pass through the top portion of the flow duct due to the buoyancy effect.

For the first kind of bubble signals, the local time-averaged interfacial area concentration is first calculated for non-missing bubbles by Eq.(4). The contribution of the missing bubbles is then corrected using the average a_i obtained from the non-missing bubbles and the total small bubble number N_{total} acquired by front sensor. So the total time-averaged a_i for small bubbles is corrected as

$$a_{i,tot} = \left(\frac{N_{total}}{N_{total} - N_{miss}} \right) a_{i,non-miss} \tag{16}$$

For the second kind of bubble signals, also, the local time-averaged interfacial area concentration is first calculated for the bubbles with effective signals by Eq.(7). Considering the irregular interfaces of the large bubbles, the contributions to a_i from the front and rear interface of the slug bubble are calculated separately. The contribution from the non-effective bubble is then corrected in the similar way as for the missing small bubble as,

$$a_{i,tot} = a_{if,eff}\left(\frac{N_{tot}}{N_{f,effl}}\right) + a_{ir,eff}\left(\frac{N_{tot}}{N_{r,effl}}\right) \tag{17}$$

where $a_{i,eff}$ is the average a_i obtained from effective bubble signals, $N_{,eff}$ is the number of the effective bubble signals, $N_{,tot}$ is the sum of the effective and non-effective bubble interfaces detected by the front sensor, and subscripts f and r denote front and rear bubble interfaces, respectively.

For the third kind of missing bubble signals, i.e., the missing signals due to the steep side interfaces of slug bubbles, Ishii and Revankar's(1993) correction method is applied. The interfacial area concentration of such missing interfaces is estimated by the ratio of the bubble side interface area to the volume formed by the projection area of the four-sensor probe in the flow direction. The calculating equation is

$$a_{i,miss} = \frac{\sum_j t_{rj}}{T}\frac{l_s}{A_s} \tag{18}$$

where t_{rj} is the residence time of the j'th missing steep side interface. T is the total sampling time, l_s is the average distance between three rear sensors and A_s is the projection area of the probe.

Finally, the total time-averaged interfacial area concentration of slug bubbles is calculated as follows:

$$a_{i,slug,tot} = a_{if,eff}\left(\frac{N_{tot}}{N_{f,effl}}\right) + a_{ir,eff}\left(\frac{N_{tot}}{N_{r,effl}}\right) + a_{i,miss} \tag{19}$$

8.3. Experimental Results and Discussion

Experimental studies were performed on the plug/slug flow regimes. Data were acquired at the axial location of L/D=253 from the mixing chamber, which represents a region of semi-fully developed two-phase flow. Test conditions include four liquid flow rates in combination with five gas flow rates as follows.

1). Superficial liquid velocity:

j_f=O.55, 1.10, 1.65, and 2.20 m/s, and,

2). Superficial gas velocity:

j_g=0.27, 0.55, 1.10, 1.65, and 2.20 m/s.

With these conditions, the void fraction ranged from 10 to 70 %. The void fraction measurements were checked against the high-speed video recordings and the measurements obtained by the hot film anemometer probe. The agreement between the data confirmed that the four-sensor probe measurements can be performed with a high degree of confidence. Most of the data were within a 15% error range, as documented in author's previous paper[16].

Figure 3 illustrates the typical distribution of the total void fraction including large slugs and small bubbles along the vertical radial direction in the pipe. It is evident that the total void fraction profile increases with the increase in the gas flow rate. Figure 4 illustrates the typical void fraction distribution of the slug bubbles. Comparing Figure 3 with Figure 4, it can be observed that both profile shapes are similar each other, and that the contribution from the slug bubbles dominates in the total void fraction. It is interesting to note that same findings were observed by Revankar and Ishii(24) for the case of vertical two-phase cap bubble flows.

To obtain the local interfacial parameters over the cross sectional plane of the pipe, the test section was rotated with 22.5° intervals, and the four-sensor probe was traced at 17 selected positions along each radial directions. Due to its size limitations the four-sensor resistivity probe cannot be traced beyond r/R = ±0.8 although there is a significant amount of void present beyond r/R > 0.8. This shortage was compensated by using hot-film anemometer void fraction measurements at r/R = 0.9 and 0.95. As shown by Riznic et al[16], the discrepancy of the void fraction measurements between two methods is within ±15%. Figures 5 and 6 present the three-dimensional perspective plots of the total void fraction and slug bubble void fraction distributions over the pipe cross section plane. From these figures, it is evident that buoyancy provokes the migration of small gas bubbles toward the top of the pipe and the void fraction distribution becomes non-symmetric in the pipe cross section. Detailed examination of local profiles showed that with an increase in gas flow, the local void fraction at a given location increases. Irrespective of the gas velocity, the internal flow structure has a general similarity at $\theta=0^{o}$ in terms of local peaking toward the top channel wall.

The interfacial area concentration for the plug/slug bubbles was calculated by Eq.(7). The resultant velocity components v_{skj} were obtained for both the front and tail surfaces of each j'th slug bubble. Then the interfacial area concentration contributions from the front and tail surfaces were added to get the total interfacial area concentration for each slug bubble. In the present

method three passing velocities must be measured for the same interface to estimate the interfacial area concentration. However, when the local orientation of a interface becomes parallel to the sensor orientation, due to the finite size of the probe the interface may contact the front sensor but escape from one or more of the rear sensors, or vice versa. Typically when the probe was close to the top wall of the pipe and to the bottom side of the slug bubble, one or more of the sensors would not detect an interface. In fact the contribution of the interfacial area from these interfaces would be substantial for the slug bubble and must be accounted for[16,24]. This contribution can be estimated by the ratio of the bubble side interface area to the volume formed by the projection area of the four-sensor probe in the flow direction, as given by Eq.(18) and (19).

For small bubbles following a slug bubble, the two-sensor resistivity probe was used. Measurement principle of the two-sensor probe was illustrated in reference[15]. The total interfacial area concentration was obtained by adding the contribution from small bubbles to that from the slug bubbles.

Figure 7 shows the interfacial area concentration profiles along the vertical axis for slug and small follow-up bubbles at given flow conditions. A higher interfacial area concentration appears in the lower part of a slug bubble with a larger curvature of interface. This is expected since the long slug bubble has relative large local interface area along its bottom surface. Similar qualitative trend is observed near the pipe wall in vertical slug flow, too[24]. These profiles show almost a flat profile in the upper part of slug bubble. Due to the finite probe size, the measurement close to the pipe wall is impossible. (However, near the pipe top wall the value of interfacial area concentration should go down asymptotically to zero.) The contribution from the small bubbles increases with an increase of gas flow rates. This observation is quite expected, since the number of small follow-up bubbles increases. Experiment results show that in the horizontal slug flow, the contribution of the small follow-up bubbles to the total interfacial area concentration is as important as that of the slug bubbles. This is quite in contrast to the case of vertical slug flow where the total interfacial area concentration is dominated by the contribution from the small bubbles.

Figure 8 depicts perspective plot of the slug bubble interfacial area concentration over the cross section. Since the local transport of mass, momentum and energy are directly proportional

to the interfacial area concentration, the figure shows a non-symmetric interfacial transport in a horizontal two-phase flow configuration.

For the flow conditions considered in the present study the slug bubbles obtained, in most cases, were smooth and isolated from the small bubbles that follow the slug bubble. This simplified the problem of distinguishing the plug/slug and small follow-up bubbles during the data processing. The size of the slug bubbles in terms of height and shape do not vary much. However, the length of the slug bubbles varies from 250 to 5,500 mm, depending on the gas flow rate. In the region of transition between plug and slug flow regimes, with an increase in the gas flow rate the number and contribution of the small follow-up bubbles increase. The increase in the liquid flow rate has similar effects. Figures 9 and 10, respectively, show the dependences of the slug frequency on liquid and gas superficial velocities. For all gas velocities the slug frequency increases as the liquid superficial velocity increases. In contrast, for all liquid superficial velocities the slug frequency increases and then decreases as the gas superficial velocity increases. This peculiar feature of slug frequency curves has also been observed in analyzing the data derived from some other studies. Nicholson et al[4] observed a sharp peak in the measured values of slug frequency at gas superficial velocities between 0.1 and 0.2 m/s for a slug flow at liquid superficial velocity of 0.12m/s. Taitel and Dukler[30] in their discussion of Chu's experimental data on slug frequency identified this phenomenon as slug suppression at low gas rates. Tronconi[31] attributed the appearance of the maximum in the slug frequency at low gas rates to the laminar-turbulent regime transition of the gas flow in the inlet region. Since our data are taken at the distance of L/D=253 from the mixing chamber, it seems that Tronconi's argument does not hold. Present experimental study shows that maximum slug frequency appears at the air superficial velocity close to 0.55 m/s. This velocity approximately corresponds to the transition from plug to slug flow pattern for the present flow conditions. It may be reasonable to postulate a mechanism of plug to slug flow regime transition as a cause for the existence of the slug frequency maximum at low gas rates. Certainly, a more detailed study is needed to clarify this peculiarity and eventually determine a more precise flow condition at which that maximum exists.

8. 4. Conclusions

The survey of the previous work shows that very few data exist on the local interfacial area concentration for two-phase flow systems. This is particularly true for two-phase flow in horizontal conduits. In the present study, the local void fraction, interfacial area concentration and slug bubble transit frequency for the co-current air-water plug/slug flow in a horizontal pipe have been experimentally investigated. The four-sensor electro resistivity probe was used to detect the instantaneous interface velocities and interfacial area of large gas slug bubbles whereas the two- sensor probe method was used for small bubble contributions to the interfacial area. The theoretical foundation for using the four-sensor probe was described. The experimental data were obtained for plug/slug flow regimes at the liquid superficial velocity ranging from 0.55 to 2.20 m/s and the gas superficial velocity from 0.27 m/*s* to 2.20 m/s.

The shapes of the void fraction profiles for different liquid flow rates are similar, however higher void fractions are recorded with a decrease in the liquid flow rate. The interfacial area concentration profiles for slugs clearly show a higher interfacial area along the slug bottom surface with a larger curvature. It is evident that in horizontal slug flow, the contribution of slug and small follow-up bubbles to total interfacial area concentration are equally important. The three-dimensional presentations show that the void fraction and interfacial area distribution become non-symmetric over the pipe cross section, indicating non-symmetric interfacial transport in a horizontal two-phase flow configuration. For all gas velocities used, the slug frequency increases as the water superficial velocity increases. However, the slug frequency first increases and then decreases as the air superficial velocity increases.

Acknowledgment

The work reported in this paper was performed under the auspices of U.S. Department of Energy, Office of Basic Energy Science.

Nomenclature

a_i	Interfacial area concentration
j	Superficial volumetric flux
N_{eff}	Number of the effective bubble signals
N_t	Total number of bubbles

N_{tot} Sym of effective and noneffective bubble interfaces

N_i Unit normal vector at the interface

S Signal slope

V Voltage

V_{norm} Normalized voltage

V_{thres} Threshold voltage

V_i Interfacial velocity

x,y,z Coordinates

Greek symbols

αo Maximum angle between the interfacial velocity & axialdirection

δ Kronecker delta function

Ω Sampling time

σ Mean square root of the measured velocity fluctuations

Subscripts

f Liquid phase

g Gaseous phase

i i'_{th} signal

j j'_{th} interface

o front sensor

k Rear sensors, k=1,2,3

References

1. Bretherton, F. P., "The Motion of Long Bubbles in Tubes," *Jour. Fluid Mechanics,* 10(2), pp. 166-188, 1961.
2. Wallis, G. B., *One-Dimensional Two-Phase Flow,* McGraw Hill, New York, 1969.
3. Dukler, A E:, Hubbard, M. G., A Mod~ for Gas-Liquid Slug Flow in Horizontal and Near Horizontal Tubes, *Ind. Eng. Chem. Fundam.,* 14. 337-347, 1975.

4. Nicholson, M.K., Aziz, K.A., Gregory, G. A., Intermittent Two-Phase Flow in Horizontal Pipes: Predictive Models, *Can.* J: *Chem. Eng.,* 56, 653-663, 1978.
5. Malnes, D., Slug Flow in Vertical, Horizontal and Inclined Pipes, Institutt for Energiteknikk Report, IFE/KRJE-83/002, Kjeller, Norway, 1987.
6. Baker, 0., Simultaneous Flow of Oil and Gas, *Oil and Gas, J.,* 53(12), pp. 185-190, 1954.
7. Mandhane, J. M., Gregory, G. A., Aziz, K .A., A Flow Pattern Map for Gas-Liquid Flow in Horizontal Pipe Line, *Int. J. Multiphase Flow,* 1,537-554, 1974.
8. Taitel, y ., Dukler, A. E., A Model for Predicting Flow Regime Transitions in Horizontal and Near Horizontal Gas-Liquid Flow, *AIChEJ.,* 22(1), pp. 47-55, 1976.
9. Ferschneider, G., Ecoulemnents Gaz-Liquide a Poches et a Bouchons en Conduite, *Rev. d'Inst. Franr;ais du Petrole,* 38(2), pp.153-182, 1982.
10. Fabre, J., Ferschneider, G., Masbernat, L., Intermittent Gas-Liquid Flow Modeling in Horizontal or Weakly Inclined Pipes, *Paper, Int. Conf. on Physical Modeling of Multiphase Flow,* 19-21, April Coventry, 1983.
11. Kocamustafaogullari, G., Ishii, M., Interfacial Area and Nucleation Site Density in Boiling Systems, *Int. J. Heat and Mass Transfer,* 26, pp. 1377-1387, 1983.
12. Landau, I., Boyle, I., Gomaa, Ho G., Al Tawell, A. M., Comparison of Methods for Measuring Interfacial Areas in Gas-Liquid Dispersions, *Canadian.J. of Chem. Eng.,*55, pp. 13-28, 1977.
13. Veteau,J.M., Contribution a l'etude des techniques de mesure de l'aire intetfaciale dans 1es ecoulements a bu11es, These de Doctorat es Sciences, Universite Scientifique et Medicale et Institut National Po1ytechnique de Grenob1e , 1981.
14. Ishii, M., Mishima, K., Study of Two- Fluid Model and Interfacial Area, Argonne National Laboratory Report, ANL- 80- 111, *NUREG/CR*-1873, 1980.
15. Kocamustafaogullari, G. and Wang, Z, An Experimental Study on Local Interfacial Parameters in a Horizontal Air-Water Bubbly Two-Phase Flow, *Int. J. Multiphase Flow,* 17, pp.553-572, 1991.
16. Riznic, J.R, Lewis, S., Kojasoy, G., Experimental Studies of Interfacial Area in Horizontal Two-Phase Flow, *Symposium on Experimental Studies in Multiphase Flow of the ASME International Mechanical Engineering Congress and Exposition- IMECE'96,* Proceedings of

the ASME Heat Transfer Division, Vol.3, HTD-Vol.334, pp. 27-37, Atlanta, GA, November 17-22, 1996.

17. Kasturi, G., Stepanek, J. B., Two-Phase Flow-III. Interfacial Area in Co-current Gas-Liquid Flow , *Chem. Eng. Sci.,* 29, pp.713-719, 1974.
18. Tomida, T., Yuse, F., Okezaki, O., Effective Interfacial Area and Liquid-Side Mass Transfer Coefficient in the Upward Two-Phase Flow of Gas-Liquid Mixture, *Chem. Eng. J.,* 16, pp. 81-88, 1978.
19. De Jesus, J. M., Kawaji, M., Measurement of Interfacial Area and Voids Fraction in Upward, Cocurrent Gas-Liquid Flow, *National Heat Transfer Conference, ANS Proceedings* ,4, pp. 137-146, 1989.
20. Bensler, H. P., Delhaye, J. M., Favre, C., Detennination of the Volumetric Interfacial Area, Volumetric Void Fraction and Sauter Mean Diameter in Bubbly Flow by Means of Ultrasound Attenuation, *Second World Experimental Heat Transfer, Fluid Mechanics and Thermodynamics,* Dubrovnik, June 23- 28, 1991.
21. Chang, J. S., Morala, E. C., Detennination of Two- Phase Interfacial Areas by an Ultrasonic Technique, *Nuclear Engineering and Design,* 122, pp.143-156, 1990.
22. Grossetete, C., Experimental Investigation and Preliminary Numerical Simulations of Void Profile Development in a Vertical Cylindrical Pipe, paper pres. at Second Int. Conf. on Multiphase Flow Kyoto '95, 1995.
23. Zeitoun, O., Shoukri, M., Chatoorgoon, V., Measurement of Interfacial Area Concentration in Subcooled Liquid-Vapor Flow, *Nuclear Engineering and Design,* 152, pp. 243-255, 1994.
24. Kataoka, I., Ishii, M. and Serizawa, A., Local Formulation and Measurements of Interfacial Area Concentration in Two-Phase Flow, *Int. J Multiphase Flow,* 12(4), 505-529, 1986.
25. Revankar, S. T ., Ishii, M., Theory and Measurement of Local Interfacial Area using a Four-sensor Probe in Two-phase Flow, *Int. J. Heat and Mass Transfer,* 36(12), pp. 2997-3007, 1993.
26. Kataoka, I., Ishii, M. and Serizawa, A., Sensitive Analysis of Bubble Size and Probe Geometry on the Measurements of Interfacial Area Concentration in Gas-Liquid Two-Phase Flow, *Proc. of the Fifth Int. Top. Meeting on Reactor Thermal Hydraulics NURETH-5,* Sept. 21-24, Salt Lake City, 1287-1294, American Nuclear Society, 1992.

27. Ishii, M., Thermal-Fluid Dynamic Theory of Two-Phase Flow, Eyrolles, Paris, Scientific and Medical Publications of France, NY, 1975.
28. Kim, S., Fu, X.Y.,Wang, X. and Ishii,M., Development of the Miniaturized Four-sensor Conductivity Probe and the Signal Processing Scheme, Intl Journal of Heat and Mass Transfer, 43, 4101-4118, 2000,
29. Lewis, S., Fu, W.L. and Kojasoy G., Internal Flow Structure Description of Slug Flow-Pattern in a Horizontal Pipe, Int. J. Heat and Mass Transfer(under review), 2001.

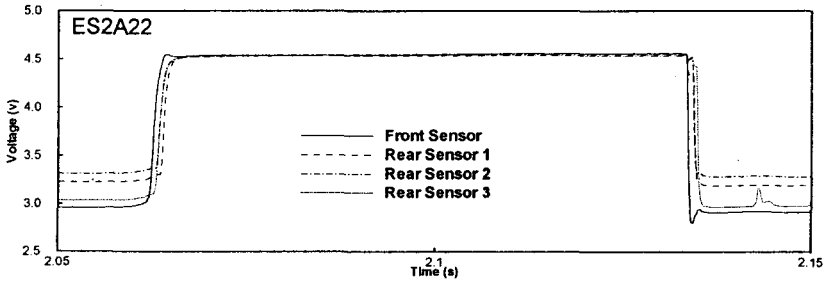

Figure 1. Typical Signals of Four-Sensor Probe

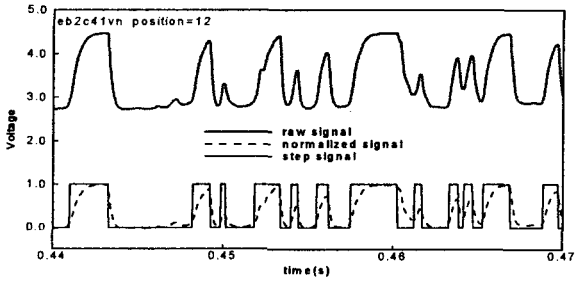

Figure 2. Phase Identification

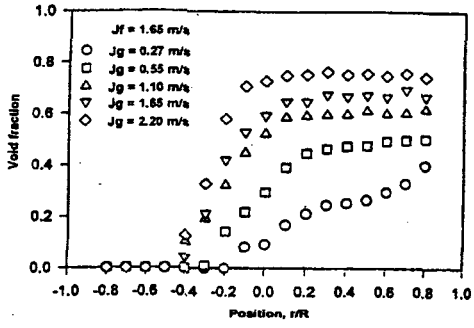

Figure 3 Total Void Fraction Distribution Along Vertical Diameter

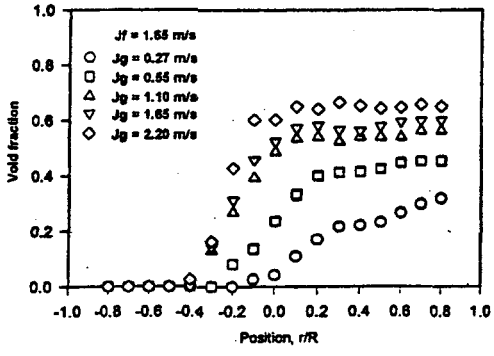

Figure 4. Slug Void Fraction Distribution Along Vertical Diameter

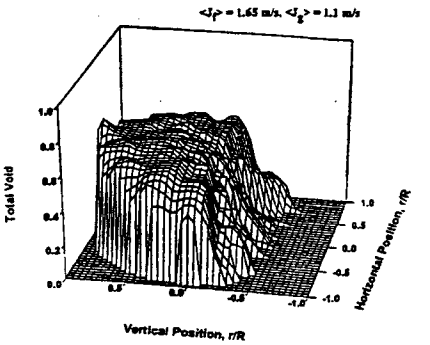

Figure 5. Total Void Fraction Distribution
Over Pipe Cross Section

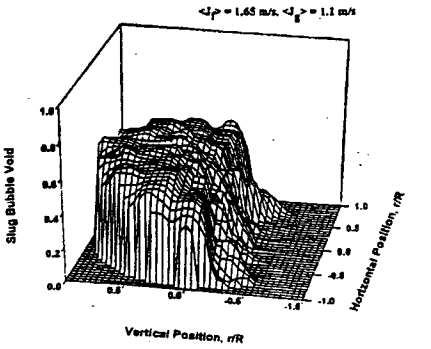

Figure 6. Slug Void Fraction Distribution
Over Pipe Cross Section

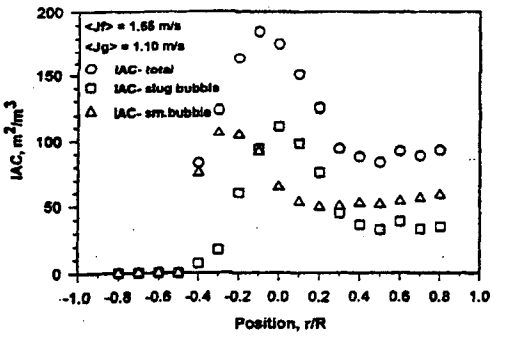

Figure 7. Interfacial Area Concentration
Along Vertical Diameter

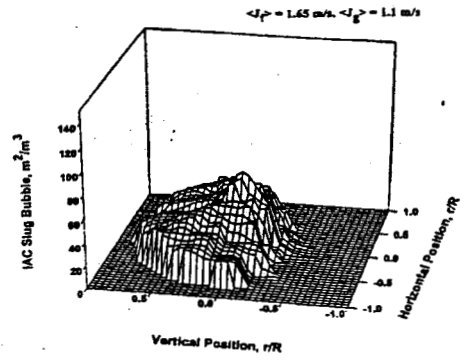

Figure 8. Slug Bubble Interfacial Area Concentration Over Pipe Cross Section

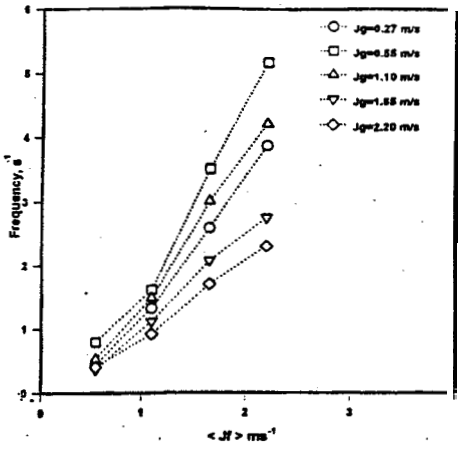

Figure 9 Slug Bubble Frequency Dependence on Liquid Superficial Velocity

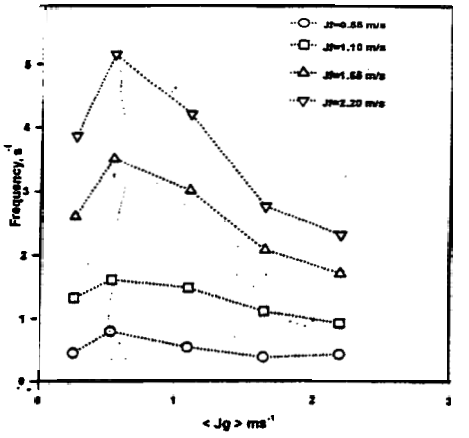

Figure 10 Slug Bubble Frequency Dependence on Gas Superficial Velocity

9. USE OF HOT-FILM ANEMOMETRY TECHNIQUE IN PLUG/SLUG MEASUREMENTS

S. Lewis, W.L. Fu and G. Kojasoy
Department of Mechanical Engineering, University of Wisconsin-Milwaukee
P.O Box 784, Milwaukee, WI 53201 USA

ABSTRACT

Utility of the hot-film anemometry technique in describing the internal flow structure of a horizontal slug flow-pattern is discussed within the scope of intermittent nature of slug flow. It is shown that a single probe can be used for identifying the gas and liquid phases and for differentiating the large elongated bubble group from the small bubbles present in the liquid slug. Analyzing the nature of voltage signals, a signal processing scheme is developed for measurements of time-averaged void fractions of small and large bubbles as well as for the measurements of local mean axial velocity and turbulent intensity in the liquid phase. Some results of local measurements of time-averaged void fractions of small and large bubble groups, axial mean velocity and turbulent intensity are presented at relatively low and high gas and liquid flows for a horizontal slug flow-pattern in a 50.3-mm ID pipe.

9.1 Introduction

The intermittent flow pattern, which are commonly defined as plug and slug flow, exists a wide-range of gas and liquid flow rates in a horizontal two-phase flow configuration. The plug flow-pattern is formed at very low gas velocities: it is characterized by elongated bubbles that move along the top of the pipe. At relatively high gas velocities for a given liquid flow a transition from plug to slug flow-pattern occurs. The slug flow is described by the intermittent appearance of aerated liquid slug occupying the entire cross section, that are separated from one another by a large elongated gas bubble moving on top of a liquid layer. In order to advance the study of such a two phase flow structure, it is essential to experimentally obtain detailed local values of fundamental parameters, which can be used for phenomenologically based flow structure modeling.

The most significant and essential parameters for the plug/slug flow-pattern are the distribution of gas and liquid phases, the liquid velocity and its fluctuating components, the gas bubble and liquid transit frequency (or slug length), and the turbulent characteristics of interfacial transport of mass, momentum, and energy. These variables describe the local flow conditions of the quasi-steady slug flow, both qualitatively and quantitatively. Hence, accurate information about these parameters and relationships among them are necessary to understand the turbulent transport phenomena of the two-phase flow pattern.

A comprehensive physical model describing horizontal gas-liquid slug flow was first initiated by Dukler and Hubbard [1]. This model has been modified and extended over the years by Barnea and Brauner [2], Ruder et al. [3], Taitel and Barnea [4], Fabre and Line [5], Andreussi et al. [6] and Fan et al. [7] to apply to the entire intermittent flow-pattern and the slug flow transition. The predictive models developed by these investigators make it possible to obtain average liquid velocities both in the liquid slug and the liquid region underneath a large bubble, pressure drops, length of liquid slug, and slug frequencies, if the gas and liquid mass fluxes are provided. These models seem to give reasonable results when compared to experimental data of global measurements. However, these models cannot give the detailed

void fraction distribution due to small and large bubbles, local velocity distribution, and the turbulent structure throughout the liquid phase. This information is of great importance to the eventual understanding and modeling of the basic hydrodynamics of two-phase slug flow. Due to the experimental difficulties associated with the intermittent nature of slug flow, very few detailed data have been reported in the literature. The problem of obtaining local data is complicated in horizontal flow configurations by the facts of axial asymmetry of the internal structure and that the slug flows do not exhibit a quasi-fully-developed equilibrium condition.

Kvernvold et al. [8] used the combination of LDV and optical two-phase probes to measure the axial velocity distribution throughout a slug flow unit in a 24-mm ID horizontal tube of atmospheric pressure. Although the method gives good results at relatively low gas velocities, the application of LDV induces technical difficulties in regions with high concentrations of small gas bubbles in the liquid slug occurring at higher gas flow rates. Andreussi et al. [6] successfully used local (optical) and cross-sectional (conductance) probes to measure the radial void fraction distribution in the liquid slugs, the size of the dispersed bubbles in the liquid slug and the aeration of the liquid layer underneath the slug bubble. Kawaji et al. [9] used the photochromatic dye activation technique to visualize the instantaneous motion of the liquid and gas slugs, and to successfully measure axial and vertical velocity profiles of the liquid phase in a horizontal slug flow. The experimental data were obtained for both circular and rectangular channels, and the liquid flow structure was found to be quite similar between the two channels. These previous studies have provided detailed basic information on the internal structure of the intermittent flow pattern in a horizontal configuration. However, issues associated with the local void fraction contributions due to elongated large bubbles and small bubbles, the turbulent structure, and interactions between dispersed and continuous phases are not addressed in these previous studies. Accurate prediction of flow requires detailed understanding of the local instantaneous interactions between continuous and dispersed phase. The horizontal slug flow-pattern introduces additional challenges because the dispersed phase by itself can only be

characterized by two internal length scales and the velocity scales-one due to small bubbles in the liquid slugs and another associated with the large bubbles between two liquid slugs. Due to the complexity of interactions between dispersed and continuous phases and among dispersed phase bubbles, experimental approach remains fundamental in their analysis.

In view of the above discussion, it is evident that much experimental work is still necessary to attain a thorough physical understanding of the internal structure of an intermittent two-phase slug flow-pattern. In this context, an experimental investigation has been underway at the University of Wisconsin-Milwaukee to obtain local void fraction and velocity distributions and to clarify the turbulence structure of this flow pattern. In these experiments it is shown that the hot-film anemometry method can be used

- to identify liquid and gas phases, i.e., phase separation,
- to measure the local time-averaged void fractions due to large and small bubbles,
- to construct the local time-averaged, liquid velocity and turbulent intensity distributions,
- to investigate the dependence of the these parameters on the gas and liquid flow for an air-water intermittent flow in a 50.3-mm ID horizontal channel.

In the following, the hot film probe method, proper signal processing technique and the test facility are described, and based on the data, results are documented in terms of the local velocity, turbulent structure and void fraction distributions.

9.2 Hot-film Anemometry Method

9.2.1 Measurement Principle

Hsu et al. [10] was the first to initiate the possible application of the hot-film anemometry technique to water-steam two-phase flows to identify the flow patterns and to measure the void fraction in an upward vertical flow channel. The probe temperature was raised above the saturation temperature of the water to induce nucleate boiling on the sensor. This allowed more sensitive measurements of the phase change, but removed the capability of measuring velocities. Delhaye [11] studied the response of hot-wire and hot-film probes in a liquid-gas two-phase flow. He found that although the hot-wire probes have given

satisfactory results in measuring velocities and turbulence in single-phase flows, their fragility makes them impractical for two-phase flow measurements. The design is susceptible to the formation of deposits and the collection of debris on the sensor. In addition, the hot-wire probe is not electrically insulated from the surroundings and, therefore, large eddy currents could cause a signal shift. The hot-film probe relieves the problem of durability by replacing the wire with a thin film on the surface of a strong quartz rod. Delhaye [11] showed that local measurements of void fraction, liquid velocity and turbulence intensity in the liquid phase could be achieved by a proper use of the hot-film anemometry in air-water flows.

Since then, this technique has been used by Serizawa et al. [12], Abel and Resch [13], Wang et al. [14,15], Liu and Bankoff [16,17], Lance and Bataille [18] and Roig et al. [19] for describing the internal turbulence structure and phase distributions in vertical bubbly flow patterns. Theofaneous and Sullivan [20] demonstrated the utility of LDV to measure the turbulence structure in bubbly two-phase flow. Recently, Suzanne et al. [21] examined the application of LDV and hot-film anemometry methods for the liquid field velocity and void fraction measurements in plane bubbly mixing layer in vertical configurations. They concluded that at relatively higher void fractions (>2%), the LDV signal was no longer suitable because of the increase of the beam interruption rate by the bubble crossing. In this case, use of hot-film anemometry method was recommended. The utility of hot-film probes, particularly in relatively high-void fraction, provided information on the basic characteristics of bubbly flow in vertical configurations. However, only limited efforts were made to examine two-phase flow characteristics in large-scale experiments of the slug flow-pattern.

In principle, the hot-film anemometry method consists of the instantaneous measurement of the change in heat transfer from an electrically heated sensor. As the fluid flows past the constant temperature hot-film probe, changes in the fluid velocity, including turbulent fluctuations, cools the sensor at different rates. These changes in cooling rates result in voltage changes in the anemometer. In the case of an air-water two phase flow, the heat transfer rate between the two fluids is dramatically different. This results in abrupt voltage

changes as the probe encounters phase interfaces. A typical sensor output for a horizontal two-phase slug flow is illustrated in Fig. 1. In order to illustrate the peculiarity of the hot-film probe signals in a horizontal slug flow the signals appearing in Fig. 1 were recorded simultaneously by two probes, one located at the upper portion of the pipe (r/R = 0.8) while the other located well below the passing large elongated bubbles.

As seen in Fig. 1a, when the probe is located in the upper portion of the pipe the sensor encounters the bubbles dispersed in the liquid slug. After the sharp initial drop, caused by the probe piercing the nose of a large bubble, the voltage gradually continues to decrease while the sensor is inside the gas bubble. This gradual decrease is due to the evaporation of a thin film of liquid that remains on the sensor. The probe is wetted immediately upon exiting the bubble, and the output signal from the probe shows a sharp increase to the previous level as it enters the liquid slug. When encountering a small gas bubble, in the liquid slug, the signal shows a sharp drop followed immediately by a sharp increase. These small bubble signals are quite different from those of large bubbles since the residence time in a small bubble is much shorter than those in a large bubble. On the other hand, the probe does not encounter any small bubbles when it is positioned in the lower portion of the pipe (Fig. 1b). In this case, the voltage signal shows an overall irregular wave motion believed to be caused by the passage of large bubbles over the top of the probe.

9.2.2 Signal Processing

9.2.2.1 Phase Identification

To process the anemometer voltage signal output for calculating the time-averaged void fraction and the flow field parameters, such as the time-averaged liquid phase mean velocity and turbulence intensity, the gas and liquid phases must be distinguished form each other and phase signals must be separated. Since the liquid and gas phases have significantly different heat transfer characteristics, the power required to maintain the probe temperature in each phase would be significantly different. Based on the drastic voltage change from one phase to another a number of methods have been developed. These methods have either

analyzed the pure analog output from the probe or post-processed a digital record of this output. In both cases, however, the methods basically consisted of detecting the voltage changes associated with a change in phase.

Delhaye [11] used the method of classifying the voltage signals according to amplitude. He then related the void fraction to the areas of distribution in the amplitude histogram. Abel and Resch [13] proposed a method of using the digital output. Their method consisted of comparing each pair of successive voltage increases and decreases against pre-determined liquid level threshold values. With this method the data had to be processed several times in order to determine the correct threshold values. These threshold values, therefore, were only valid for that particular data set. This method worked successfully for identifying the large bubbles. A second method was suggested for identifying the small bubbles.

In the present study Lance and Bataille [18] method, which was devised for a very low void fraction vertical bubbly flow, is modified for the intermittent flow-pattern for distinguishing phases. In this method signal processing is not only applied to the hot-film voltage e(t) but also to its derivative ($\partial e/\partial t$). This method based on the derivative of the hot-film signal greatly magnifies the signals associated with the passage of bubbles and allow a better discrimination between bubbles and turbulence than a threshold method only applied to the signal e(t). By plotting the anemometer voltage output and the slope on the same time scale (Fig. 2), effects of a bubble piercing the probe can be easily identified.

For each bubble passage, the slope signal shows a sharp negative spike for the nose of the bubble followed by a sharp positive spike for the tail of the bubble. Since the power required to heat the sensor to maintain its temperature in the gas phase is considerably less than in the liquid phase, the signal shows a decrease in the power to the sensor as a bubble is pierced by the probe. This decrease is responsible for the negative spike in the slope signal. Similarly, the positive spike in the voltage output slope is induced by a sharp increase in power required by the liquid phase. At this point, it is a matter of determining the proper threshold values to detect the spikes in the slope signal.

It is important to note that to accurately detect the gas bubbles, the threshold must also distinguish between the peaks induced by the probe sensor entering gas bubbles and those caused by the turbulent fluctuations in the liquid phase. By plotting the anemometer output voltage data and the corresponding slope as seen in Fig. 2 for the experimental data covering the entire range of gas and liquid flow rates, three threshold slope values were identified. The first one is set as an indicator for the arrival of the gas phase at the probe sensor whereas the second one is used for determining the transition back to the liquid phase. The third threshold is needed to distinguish the turbulent fluctuations from the phase identification thresholds. The slope threshold is simply a scale in terms of two consecutive samples of voltage difference. For a fixed sampling rate each slope threshold value can be fixed satisfying all of the flow conditions. However, it is well known that the anemometer responds with a different level of liquid voltage signal for different flow conditions. Therefore, before processing a particular data set the level threshold value should be determined. Since a combination of the level and a series of slope thresholds are used in the present studies, it was not necessary to restrict the setting of level threshold to a value very close to the liquid signal.

Once the first slope threshold value is reached or exceeded on the negative plane, the phase separation step signal, δ; is set equal to unity, indicating the gas phase as shown in Fig. 2c. Once the slope signal exceeds the second threshold following the first one, the tail of the bubble is detected. However, the third threshold is also used to delay the detection of the liquid phase until the slope value decreases to the magnitude of the liquid phase turbulence threshold value. This indicates that the probe has fully reentered the liquid phase, and the phase separation signal, δ, is assigned a value of zero as observed on Fig. 2c.

The maximum time derivative of the signal induced by turbulence in the continuous phase remains very low in comparison with the time derivative associated with bubble when the gas-liquid interface impacts the hot-film sensor. However, this discrimination sometimes becomes difficult, especially for high void-fraction bubbly flow as observed by Suzanne et al.

[21]. It is also the case when a high turbulent level is associated with a non-uniform bubble size distribution because the passage of small bubbles can be mistaken with turbulent fluctuations. Thus, the sampling frequency must be high enough in order to provide satisfactory information about whether the probe is located in liquid or in gas. In the present experiments conical type probes of TSI model 1231W was used, and after preliminary sensitivity studies the sampling frequency was optimized to be 5 kHz level. This frequency was much higher than the liquid turbulence frequency and allowed a statistically meaningful sampling time.

9.2.2.2 Separation of Large and Small Gas Bubbles

The second part of the phase discrimination process is to distinguish the elongated large bubbles from the small bubble group concentrated in liquid slugs. Only then the void fraction can be divided into contributions from small and large bubble groups, which is essential for understanding and modeling the local interfacial transport processes. The shape of elongated bubble being controlled by the tube diameter, their length is typically greater than a few pipe diameters. Thus, knowing their residence time and estimating their velocity would be useful for an objective criterion. However, the hot-film probe used in the present experiments is directed to measure the liquid velocity not the interfacial or gas velocities. There exist no satisfactory predictive methods for the elongated large bubble length. Furthermore, depending on the flow rates of each phase the size of each group varies requiring use of different criteria of the separation at each two-phase flow condition. We used the maximum small bubble chord-length, i.e., the maximum small bubble size, to differentiate the small bubbles signals from the elongated large bubble signals. Such an approach summarized below was enable us to determine a global threshold value that would be usable throughout the test matrix.

The phase separation signal gives the residence time for each bubble encountered. Then, when the residence time multiplied by a representative small bubble velocity yields the bubble chord-length: Here, the representative small bubble velocity in a liquid slug can be

characterized by the liquid velocity, which is measured in the present experiments. This approach assumes a homogeneous two-phase flow model within the liquid slug, which is a good approximation for the horizontal slug flow configurations. The local measurements of liquid velocities are area-averaged from top of the tube to the maximum liquid velocity. This approximates the average velocity in the liquid slug where small bubbles mostly present. The maximum is found to be located at r/R of 0.1 to 0.2 but not below centerline for the entire range of experiments performed for the present study.

The averaged slug velocity is then used to estimate the range of bubble chord-length, and hence, the small bubble sizes. A histogram is created to identify the bubble count and range of bubble chord-length by their respective residence time. An example of such histograms is illustrated on Fig. 3 for varying gas velocities at (a) $\langle j_f \rangle$=1.1 m/s, (b) $\langle j_f \rangle$=1.65 m/s, (c) $\langle j_f \rangle$=2.2 m/s, where u_{LS} appearing on each figure refers to the average liquid slug velocity. From these figures the small bubble chord-length distribution is evident for varying gas and liquid superficial velocities. Due to presence of a few large bubbles in a given record, their location in the figure cannot be seen unless the time scale is drastically reduced.

Studying the small bubble size spectra figures and the visual observations made during each experimental conditions, a maximum threshold residence time is determined that would separate the large bubbles from the small bubble group. This characteristic residence time is ranged from 0.005 to 0.019 seconds for the entire range of present experiments. A global threshold residence time is set at 0.02 seconds. Such an approach of estimating a global threshold bubble chord-length or residence time was necessary since at each experimental condition the average liquid slug velocity was not available until after the probe signal is analyzed by the signal processing scheme developed in this study. When the entire conditioned signals have been analyzed as described above, the data processing returns the phase separation signal. This signal is used to remove the liquid phase data for analysis of velocity and turbulence in the liquid phase and the gas phase data for void fraction analysis.

The local void fraction, $\alpha(r)$, at any probe location, r, can be obtained by the gas-phase data of hot-film probe sensor. It is defined as the local time-averaged void fraction by

$$\alpha(r) \equiv \lim_{T\to\infty} \int_0^T \delta(r,t)dt \tag{1}$$

where δ, as a function of the space coordinate, r, and time, t, is equal to 1 if the probe sensor is in the gas phase and δ is equal to 0 if the sensor is in the liquid phase. As the signal is given in discrete form, Eq. (1) can be written as follows:

$$\alpha(r) \equiv \frac{1}{T}\sum_{m=1}^{N}(t_{2m} - t_{2m-1}) \tag{2}$$

where T is the total sampling time, N is the number of bubbles in the sample, t_{2m-1} is the time when the probe sensor enters into a bubble, and t_{2m} is the time the sensor enters into the liquid phase. Since the characteristic signal can be split into the large elongated bubble and small bubble group contributions, the void fractions for each bubble group are distinguished by classifying each bubble either in the large or small bubble group as follows:

$$\alpha(r) \equiv \frac{1}{T}[\sum_{i=1}^{N_{lb}}(t_{2i} - t_{2i-1})_{lb} + \sum_{j=1}^{N_{sb}}(t_{2j} - t_{2j-1})_{sb}] \tag{3}$$

where t_{2j-1} is the time when the probe sensor enters into the small bubble, and t_{2j} is the time the sensor enters into the liquid phase. Similarly, the subscript i identifies large elongated slug bubbles. N_{lb} and N_{sb}, respectively, are the number of large and small bubbles passing the probe sensor in the total sampling time, T. It is to be noted that

$$i = 1, \ldots \; N_{lb} \text{ for large bubble group} \tag{4}$$

and

$$j = 1, \ldots \; N_{sb} \text{ for small bubble group} \tag{5}$$

It is important to note that the void fraction, $\alpha(r)$ appearing in Eq. (3) is the total void fraction at a location r, which consists of the large bubble group defined by

$$\alpha_{lb}(r) \equiv \frac{1}{T}\sum_{i=1}^{N_{lb}}(t_{2i} - t_{2i-1}) \tag{6}$$

and the small bubble group defined by

$$\alpha_{sb}(r) \equiv \frac{1}{T}\sum_{j=1}^{N_{sb}}(t_{2j} - t_{2j-1}) \tag{7}$$

In view of Eqs. (3), (6) and (7), it is evident that

$$\alpha(r) \equiv \alpha_{lb}(r) + \alpha_{sb}(r) \tag{8}$$

It is to be noted here that both the small bubble and large bubble void fraction contributions are defined as the time-averaged void fraction based on the total sampling time T. There may be other forms of definitions in terms of weighting factors associated with the occurrence of each group. However, the way it is defined here makes more physical sense in terms of the unit-cell concept which has been frequently used in modeling the slug flow.

9.2.2.3 Liquid Velocity Field

After phase separation algorithm was performed to identify phases and to calculate the local time-averaged void fraction, the gas phase data is taken away and the liquid-phase data is analyzed further for the local time-averaged axial velocity and turbulent intensity evaluations. The time-averaged velocity $u_{ave}(r)$ is given by

$$u_{ave}(r) = [\sum_{i=1}^{N} u_i(r,t)] / N \tag{9}$$

where $u_i(r,t)$ is the instantaneous liquid velocity, and N is the total number of discrete data points in the liquid phase.

As it was shown in a great detail by Sharma et al. [22], where two hot-film probes were used simultaneously to investigate the intermittent and transient characteristics of the slug flow-pattern, there exist short transition zones within liquid slugs right behind and ahead of large bubbles causing temporal variations on the mean velocity. In the mean time as it is observed on Fig. 1b, within the liquid layer below a passing large bubble, the velocity gradually decelerates from the large bubble nose. However, right before the large bubble tail a rapid acceleration is observed toward the wake region. An example of these observations at a probe location of r/R= -0.6 is illustrated in Fig. 4 for the case of $\langle j_f \rangle$ = 1.65 m/s and $\langle j_g \rangle$ = 0.55 m/s. The experimental data shown on this figure was obtained by simultaneous use of

two hot-film probes. One of the probes was held at a fixed position r/R=0.8 throughout the experiment while the other probe was traced through the vertical axis of the pipe, stopping at 18 positions to take measurements. With this arrangement of two probes, the local, instantaneous liquid velocity was measured at each location by the bottom probe, and the top probe was exclusively used to determine whether the bottom probe was in the liquid slug or in the liquid film underneath passing large bubbles. Since liquid slug length and the length of large bubbles vary even at a given flow conditions, the time variation within the liquid slug is normalized by the liquid slug passage time, t_{ls}, and within the liquid layer by the large bubble passage time, t_{lb}. The ever developing nature of the liquid layer flow and the relatively uniform behavior of the liquid slug flow are clearly demonstrated from Fig. 4.

In view of the above it is evident that the mean liquid flow in a unit cell of a slug flow, i. e., a large bubble plus a liquid slug highly aerated by small bubbles, undergoes a series of changes. Although not quantitatively, these changes repeat themselves qualitatively for the next unit slug cell indicating that such a two-phase flow-pattern is inherently unsteady with large variations of mean velocity at any given location. Therefore, the transient nature of this two-phase flow-pattern introduces problems in decomposing the velocity field into a time-averaged motion and a random fluctuation due to turbulence as follows:

$$u'(r,t) = u(r,t) - u_{ave}(r) \tag{10}$$

where $u'(r,t)$ is the instantaneous turbulent velocity fluctuating component. The root-mean-square values of turbulent velocity fluctuations calculated in a traditional way for separating the random from organized motion would be in grave error due to undeterministic motion linked to the movement of the large and small bubbles. A frequency-based filtering process would not correct the situation. Therefore, a time-domain filtering method is introduced to remove the apparent unsteadiness in the mean liquid motion. The idea is that the mean flow varies on a time scale much larger than the turbulent fluctuations. This requires a sampling time of much smaller than the period of the unsteadiness in the mean flow.

In the present study, at each local measurement location the liquid-phase data are divided into several blocks. Each data block is analyzed separately to ensure statistically stationary results. In this way, the time-dependent mean velocity field is removed from the signal of each block without loosing or changing the basic characteristics of the local turbulence. The root-mean-square values of the velocity fluctuations for each block are calculated by

$$\overline{u_k'}(r) = \{\sum_{k=1}^{n_k} [u_k(r,t) - u_{ave,k}(r,t)]^2 / n_k\}^{1/2} \tag{11}$$

where $u_{ave,k}$ (r,t) is the time-dependent mean velocity in the k'_{th} block, and the n_k is the number of data points in the k'_{th} block. Finally, the overall root-mean-square value at a given location is calculated by

$$\overline{u'}(r) = \{\sum_{k=1}^{N_k} [n_k (\overline{u_k'})^2] / \sum_{k=1}^{N_k} n_k\}^{1/2} \tag{12}$$

where N_k is the number of blocks. As it was shown by Evans [23] such an approach is justified for homogeneous, isotropic turbulence, and in this case ensemble averages may be replaced by time averages.

9.3 Experimental Setup and Procedure

9.3.1 Experimental Setup

A schematic diagram of the experimental flow system is shown in Fig. 5. The flow loop consists of a horizontal line of 50.3-mm ID and 15.4 meter Pyrex glass tubings with pressure tabs installed between them. The flow loop is entirely transparent to allow for flow visualization, high-speed photography and cinematography.

The air and distilled water are used as the two-phase coupling fluids. The air to the test section is supplied from a high-pressure university central air system and filtered as it enters a 0.95 m^3 capacity, high-pressure storage tank. The pressure is then stepped down, and the air flow is regulated by valves in parallel. The air flow is re-filtered and measured by series of well-calibrated turbine flow meters before air enters the mixing chamber. The distilled water

is stored in a 1.9 m^3 capacity storage tank which containing cooling coils to control the water temperature. It is pumped from the tank by a stainless steel centrifugal pump and regulated from 0 to 100 % of the pump capacity by a transistor inverter. This temperature control is essential in minimizing the temperature drift of the hot-film sensor.

The water flow rate is measured by a series of paddlewheel flow meters assembled in a parallel configuration. The air enters the two-phase mixing chamber from a 90° vertical leg and injected axially into the water flow through a cylindrical porous media of 100 μm porosity to achieve a uniform mixing. The two-phase mixture from the test section is directed to an air-water separator. The air is then vented to atmosphere, whereas the water is returned to the water storage tank to for re-circulation.

Six diaphragm type pressure transducers along with six U-tube monometers are used to measure the pressure drop. The pressure transducers have a natural frequency of 5 Hz, with a range of 0 to 34.4 kPa, and an accuracy of ±0.3 % of the full scale. The pressure of the air at the location of the flow meter and the two-phase system pressure at the test section are both measured.

9.3.2 Experimental Procedure

The experiments were carried out using hot-film anemometry and conical shaped (TSI 1231-W) hot-film probes. The liquid and gas volumetric superficial velocities ranged from 1.1 to 2.2 m/s and 0.27 to 2.2 m/s, respectively. For all the flow conditions, the system pressure was near atmospheric and the temperature about 20°C.

A Vernier, with graduations to an accuracy of 0.01 mm, was used to traverse the probe in a direction perpendicular to the axis of the tube. The position of the probe was read on a digital linear scale. The high resolution was necessary to evaluate probe positions in the flow stream accurately and to ensure reproducible results. The hot-film probe was traced through the vertical axis of the pipe, stopping at twenty-one positions to take measurements.

Before beginning the two-phase measurements, single-phase liquid measurements were made to calibrate the instrumentation, verify their consistency with known results, and to

serve as a reference for later comparison with two-phase flow measurements. The local mean axial velocity and the turbulent fluctuations in the axial direction were measured along the radial direction at z/D = 253 from the mixing chamber. The measured velocity profiles and turbulent fluctuations were non-dimensionalized with respect to the characteristic velocities of centerline velocity and friction velocity, respectively, for the purpose of comparing with Laufer's [24] benchmark data and Liu and Bankoff's [16,17] single-phase liquid flow data. The axial symmetry in fluctuations in $u_{ave}(r)$, and the root-mean-square values of the turbulent fluctuations, u'(r), was found to be reasonably satisfied when compared with those results provided in these references.

The hot-film probe was calibrated in the single-phase liquid flow by comparing the sensor voltage level with the centerline velocity and fully-developed turbulent flow pressure-drop information for each flow condition. The data was collected by the anemometer and stored into a computer. A FORTRAN program was used to process the data, separating the phases, converting the liquid phase voltage histogram to velocities, and calculating the essential parameters as described.

9.4 Experimental Results and Discussion

A sample of the time-averaged local void fraction, α, liquid phase mean axial velocity, u_{ave}, and the turbulence structure as presented by the turbulent intensity, defined as $\overline{u'}/u_{ave}$, are described in Fig. 6 for relatively low, medium and high values of $\langle j_g \rangle$ at a fixed value of $\langle j_f \rangle$=1.65m/s. Here, r/R is the normalized radial position of the hot-film sensor in the pipe, r, measured along the vertical axis from the pipe center to the probe, and R is the pipe radius. Thus, r/R = -1.0 and 1.0, respectively, identify the bottom and the top of the pipe. The single-phase liquid flow measurements of axial velocity and turbulence structure corresponding to the same liquid flow rates are also shown on these figures. When respective two-phase flow profiles are compared in these figures, it is evident that the void fraction, mean axial velocity, and turbulence structure distributions have similar behaviors. These results demonstrate interesting characteristics of a horizontal, slug flow pattern.

(a) Void Fraction

As it is indicated by Eqs. (3) and (8), the void fraction measurement distinguishes the large bubble contributions from those of the small bubbles present in the liquid slug. Thus, the total void fraction is composed of these two contributions. The small bubble, large bubble and total void fraction distributions are illustrated in Fig. 6 for different $\langle j_g \rangle$ values.

It is evident from these figures that the void fraction distribution shows a sharp decrease toward the bottom of the pipe and practically becomes zero at a certain r/R location indicating the existence of a liquid layer free of voids. Visual observations showed that there are always some small bubble voids within the bottom liquid layer. However, the small bubble population is too small to be detected by the finite size probe. This liquid layer thickness, which is referred as the liquid film in the literature, decreases by increasing gas flow rates at a given liquid flow. It covers a liquid region below r/R = -0.3 at $\langle j_g \rangle$=0.55 m/s and below r/R = -0.6 at $\langle j_g \rangle$=2.2 m/s. This behavior points to the fact that small bubbles distribute more homogeneously as the gas flow increases.

The large bubble void fraction profile shows a sharp increase right after the liquid layer and then flattens gradually, going through a maximum, with a slight decrease toward the pipe wall. This decrease must be due to the interfacial curvature observed at the front and rear of a large bubble. The maximum, which moves downward as the gas flow rate increases, corresponds to the elongated large bubble nose position. On the other hand, the small bubble void fraction increases toward the top of the pipe indicating a strong small bubble migration toward the upper wall under the influence of gravitational segregation. Although the cumulative effect of small bubbles seems to be small, it drastically increases and becomes more homogeneously distributed with increasing gas flow as illustrated in Fig. 6. Considering the fact that the liquid slug length is much smaller than the gas slug length then it becomes obvious that the small bubble void fraction relative to the liquid slug volume may become extremely large at high gas flow rates.

(b) Mean Velocity Profiles

The mean liquid velocity , u_{ave}, profiles illustrated in Fig. 6 show an asymmetric character of the liquid velocity profiles with the largest velocities located at the upper part of the pipe. The degree of asymmetry is shown to increase with increasing gas flows and seems to be well correlated with corresponding void fraction profiles. An interesting feature of the velocity distribution is that the profiles for all the cases exhibit a strong shear layer. When the velocity profiles are analyzed together with the void fraction distributions it is evident that the location of the shear layer corresponds well to the thickness of the respective liquid layer underneath the large bubble. Instantaneous velocity profiles, as measured by Kvernvold et al. [8], show a similar trend with regard to the appearance of the shear layer.

Another interesting feature of the velocity profile is that the velocity distribution within the bottom liquid layer exhibits a fully-developed turbulent flow character as demonstrated by the $1/n'_{th}$ power law profile, which was fitted by the experimentally measured maximum velocity located in the liquid layer. Obviously, the maximum velocity profile in this liquid layer corresponds to the location where the void fraction nearly goes to zero. A similar fully-developed turbulent velocity profile is also observed within the liquid slug across the upper portion of the pipe. In this case, however, the maximum velocity in the liquid slug is used for fitting the $1/n'_{th}$ power law profile. The profiles shown in Fig. 6 have the same character as for fully-developed turbulent flow profile with a transition zone from one to another. For the cases investigated during the course of present experiments we find that the area-averaged mixture superficial velocity is well correlated with the maximum liquid velocity. It is given by

$$< j_f > + < j_g > \cong (0.77 \sim 0.8)\, U_{\max} \qquad (13)$$

A kind of flow adjustment layer occurs between these two distinctive turbulent flow regions. This adjustment layer thickness decreases as the gas flow increases. In fact, the adjustment, or transition layer, is almost completely absorbed by the two turbulent profiles as shown in Fig. 6c, where the superficial gas velocity is much higher than the first two cases shown in Figs. 6a-6b. This unique feature is somewhat similar to the recent observations of

Kawaji et al. [9]. Even though, time-averaged, mean velocities are used here instead of the instantaneous velocity profiles presented by Kawaji et al. [9].

From the local values of $\alpha(r)$ and $u_{ave}(r)$ measured along the vertical axis, the area-averaged liquid superficial velocity $<j_f>$ was calculated as follows:

$$< j_f >\equiv \frac{1}{A}\int_A [1-\alpha(r)]\, u_{ave}(r) dA \qquad (14)$$

where A is the cross-sectional area of the pipe.

In order to check the accuracy of both local void fraction and the mean axial liquid velocity measurements, the area-averaged liquid superficial velocity calculated by Eq. (14) was compared with corresponding liquid superficial velocity as measured by the flow meter. It was observed that the calculated superficial velocity was consistently over-estimated by a margin of ±4.2% to 12%. There may be several reasons for such a consistency. First, as noted by Delhaye [11] and Wang et al. [14] the void fraction measured by the conical hot-film probe technique is underestimated due to the deformation and the deflection of the bubbles by the probe. Such an experimental error is expected to be more pronounced in measuring the small bubble contribution toward the total void fraction expressed by Eqs. (3) and (8). Secondly, as demonstrated by Fig. 1b, the data show a wavy pattern when the probe is located underneath the slug bubble. Although a correction on the time domain was performed to smooth out the behavior, this may still cause some errors in calculating the mean velocity in the liquid phase. Finally, the small-amplitude peaks due to incomplete piercing of small bubbles or due to the bubble sliding on the probe are difficult to detect by the present data processing scheme. This is again expected to be the case in the small bubble encounter of the probe. These series of experimental errors are probably the main causes of the systematic error observed in matching the liquid superficial velocities.

(c) Turbulence Structure

The turbulence structure is presented in Fig. 6 in terms of the turbulent intensity as defined by $\overline{u'}/u_{ave}$, where $\overline{u'}$ is the root-mean-square value of instantaneous local velocity

fluctuation. Both the axial turbulent fluctuations and turbulent intensities generally increased toward the bottom wall and go through a minimum at the top edge of the bottom liquid layer. Furthermore, it is interesting to note that both profiles follow very closely to the corresponding single-phase flow turbulent fluctuations and intensities within the bottom liquid layer, which is practically free of voids as discussed above. As it is expected, the turbulence in this region is slightly enhanced by the passage of large bubbles. But it preserves the general character of single-phase flow turbulence intensity.

On the other hand, the turbulence drastically increases as the probe is moved away form the bottom liquid layer toward the bubbly liquid slug region, and reaches a local maximum at the maximum mean velocity level. In the core of the liquid slug, the turbulence stays nearly constant and shows a sharp increase toward the top wall. This enhanced turbulence might be related to the observed trend of small bubble void fraction profiles, which also shows a sharp increase toward the top of the pipe as shown on Fig. 6. Parallel to the mean velocity behavior, the local axial turbulence structure shows a two regions behavior, the liquid layer and bubbly liquid slug regions. This consistent tendency of turbulence points to the fact that the local turbulent motion is directly related to the local two-phase flow motion.

Probably not the most distinctive, but certainly the most surprising observation from Fig. 6 is the variation of turbulence intensity in the lower part of the pipe. A careful inspection of the first two figures in the lower part indicates that the turbulence intensity is slightly, but consistently, lower than the corresponding single-phase intensity. This phenomenon is observed only at relatively low gas and liquid flows. As discussed above with regard to the void fraction profiles, always there exist small bubbles in the lower part. However, the population and frequency of small bubbles are too small to detect with a finite size probe and, therefore, cannot be traceable on Fig. 6. It seems that the extremely small values of void fraction tend to lower the turbulence intensity. This is so-called "lubrication" effect of a very small bubble population was observed in vertical bubbly flow configuration by Serizawa et al. [12] and Wang et al. [15].

It is customary practice in vertical bubbly two-phase flow experiments to express the bubble-induced turbulence components as the difference between the two-phase bubbly flow turbulence and the corresponding single-phase wall-generated components. Based on this type of superposition hypothesis, the enhanced two-phase flow fluctuation $\overline{u'_{tp}}$ can be expressed as the sum of the single-phase turbulence, $\overline{u'_{sp}}$, and the bubble-induced turbulence, $\Delta\overline{u'}$. Thus,

$$\overline{u'_{tp}} = \overline{u'_{sp}} + \Delta\overline{u'} \tag{15}$$

With this hypothesis the relative effect of bubble-induced turbulence in the axial direction can be calculated from the measured data of two-phase and corresponding single-phase flows. Results are shown in dimensionless form on Fig. 7. It is evident from this figure that the ratio of bubble-induced turbulence to the total turbulence strongly depends on the local flow conditions. Generally, this ratio increases with increasing gas flow, and follows very closely the two-layer velocity profile structures. The lubrication effect of very small bubble population is evident at relatively low gas flow of $\langle j_g \rangle$=0.27 m/s. At relatively high gas flows, the bubble-induced turbulence contribution accounts for more than 80% of the total turbulence toward the top of the pipe where the void fraction is high. However, this generally increasing trend with the local void fraction distribution does not reflect the wall peaking void fraction as observed on Fig. 6. On the other hand, increasing the liquid flow at constant gas flow generally decreases the ratio of $\Delta\overline{u'}/\overline{u'_{tp}}$ within the liquid layer region and has a minimal effect in the high void fraction region above the liquid layer. This damping effect of liquid flow in vertical bubbly two-phase flow was also observed by Liu and Bankoff [16].

(d) Effect of Flow Variable

The profiles of the local void fraction, liquid phase mean velocity and turbulent intensity are shown for the case of an increasing gas flow rate at a constant value of the liquid flow. The large bubble void fraction drastically increases with increasing gas flow. An

increase in the small bubble void fraction can also be noted. However, the bottom liquid layer thickness decrease with increasing gas flow. The introduction of gas into a water flow generally accelerates the velocities, with a relatively steeper increase at the upper portion of the pipe than in the liquid layer. As noted with regard to Fig. 6, a consistent shear layer appears on all the flow conditions at the same location, namely, where the void fraction profile goes to zero. With increasing gas flow, the slope of the mean velocity profile above the shear layer increases along with the overall magnitude. It is evident that the turbulence increases significantly upon increasing the gas flow. At the bottom liquid layer, the relative turbulence, as characterized by the local turbulent intensity, follows very closely the single-phase flow intensity. However, after the shear layer, the turbulence is strongly enhanced with the increasing gas flow. This enhancement may be attributed to the increased population of small bubbles in the liquid slug toward the top of the pipe.

The influence of increasing liquid flow at a constant flow is demonstrated in Fig. 8b. The effect of increasing liquid flow is to decrease the large bubble void fraction. However, the small bubble void fraction shows a sharp increase. This may be due to the increase in the local turbulence and interfacial instability both of which result in disintegration and generation of small bubbles. With increasing liquid flow, the mean velocity profile develops toward a symmetric behavior. The turbulent intensity in the bottom liquid layer is almost indistinguishable for a wide range of gas flow rate. On the other hand the axial turbulent intensity generally increased toward the wall and became flat in the core region. An interesting conclusion can be drawn when Fig. 7b is compared to Fig. 8b. Even though the absolute turbulence level is enhanced with the increasing liquid flow, the rate of increase of $\overline{u'_{tp}}$ is less than that of $\overline{u'_{sp}}$.

9.5 Summary and Conclusions

It is demonstrated that the hot-film anemometry technique can be successfully utilized in a horizontal two-phase slug flow-pattern (a) to distinguish the gas and liquid phases, (b) to differentiate the large bubble group from the small bubble group present in the liquid slug, (c)

to measure the time averaged local void fractions of small and large bubble groups and (d) to measure the local axial mean velocity and turbulent intensity in the liquid phase.

The experimental results for a 50.3-mm ID horizontal slug flow indicate that the large bubble void fraction profile shows a sharp increase right after the liquid layer and then flattens gradually, going through a maximum, with a slight decrease toward the pipe wall. On the other hand, the small bubble void fraction increases toward the top of the pipe indicating a strong small bubble migration toward the upper wall. It was found that increasing the gas flow at a fixed liquid flow would increase the local slug bubble void fraction.

The mean velocity profiles showed an asymmetric behavior with the largest velocities located at the upper part of the pipe. The degree of asymmetry was shown to increase with increasing gas flow. An interesting feature of the liquid velocity distribution is that the profiles, for all the cases studied, exhibited a strong shear layer starting at the top of the bottom liquid layer. The most interesting feature of the slug flow was that the bottom liquid layer and the top portion of the liquid slug tended toward a fully-developed turbulent pipe-flow profile.

Increasing the gas flow rate, increased not only the absolute turbulence, but also the turbulent intensity over the whole cross-section. This effect of the gas superficial velocity was more pronounced within the liquid slug than the bottom liquid layer. In general, it was concluded that the local turbulence and the bubble-induced turbulence components were directly related to the main stream motion within the liquid phase.

Acknowledgement

The work reported in this paper was performed under the auspices of the U.S. Department of Energy, Office of Basic Energy Science. The authors would like to express their sincere appreciation for the encouragement, support and technical comments on this program from Dr. R. Price and Dr. R. Goulard of the U.S. DOE/BES.

References

[1] A.E. Dukler, M.G. Hubbard, A Model for Gas-Liquid Flow in Horizontal and Near Horizontal Tubes, Ind. Engng. Chem. Fundam. 14 (1975) 337-347.

[2] D. Barnea, N. Brauner, Holdup of the Liquid Slug in Two-Phase Intermittent Flow, Int. J. Multiphase Flow 11 (1985) 43-49.

[3] Z. Ruder, P.J. Hanratty, T.J. Hanratty, Necessary Conditions for the Existence of Stable Slugs, Int. J. Multiphase Flow 15 (1989) 209-226.

[4] Y. Taitel, D. Barnea, Two-Phase Slug Flow. Advances in Heat Transfer 20 (1990) 83-132, Hartnett, J. P. and Irvine, T. F. Eds., Academic Press.

[5] J. Fabre, Line, Modeling of Slug Flow, Annu. Rev. Fluid Mech. 24 (1992) 21-46, J.L. Lamley, M. Van Dayke, and H.L. Reed, Eds., Annu. Rev. Inc.

[6] P. Andreussi, K.H. Bendiksen, O.J. Nydal, Void Distribution in Slug Flow, Int. J. Multiphase Flow 19 (1993) 817-828.

[7] Z. Fan, F. Lusseyran, T.J. Hanratty, Initiation of Slugs in Horizontal Gas-Liquid Flows, AIChE J. 39 (1993) 1742-1753.

[8] O. Kvernvold, V. Vindoy, T. Sontvedt, A. Saasen, S. Selmer-Olsen, Velocity Distribution in Horizontal Slug Flow, Int. J. Multiphase Flow 10 (1984) 441-457.

[9] M.Kawaji, M. Ali, A. Ciastek, C. Lorencez, Study of Liquid Flow Structure in Horizontal Cocurrent Gas-Liquid Slug Flow, Proc. ANS-THD 8 (1995) 79-88, 1995 Natl. Heat Transfer Conf., August 5-9, Portland, Oregon.

[10] Y.Y. Hsu, F.F. Simon, R.W. Graham, Application of Hot-Wire Anemometry for Two-Phase Flow Measurements such as Void Fraction and Slip Velocity, Proc. ASME Winter Meeting, Philadelphia, PA. 1963.

[11] J.M. Delhaye, Hot-Film Anemometry in Two-Phase Flow, Two-Phase Flow Instrumentation, B.W. Le Tourneau and A.E. Bergles, Eds., ASME, 1969, pp. 58-69.

[12] A. Serizawa, I. Kataoka, L. Michiyoshi, Turbulence Structure of Air-Water Bubbly Flow - I. Measuring Techniques, Int. J. Multiphase Flow 2 (1975) 221-233.

[13] R. Abel, F.J. Resch, A Method for the Analysis of Hot Film Anemometer Signals in Two-Phase Flows, Int. J. Multiphase Flow 4 (1978) 523-533.

[14] S.K. Wang, S.J. Lee, O.C. Jones, R.T. Lahey, Local Void Fraction Measurement Techniques in Two-Phase Bubbly Flow Using Hot-Film Anemometry, Proc. 22nd Heat Transfer Conf, Niagara Falls, August 5-8,1984.

[15] S.K. Wang, S.J. Lee, O.C. Jones, R.T. Lahey, 3-D Turbulence Structure and Phase Distribution Measurements in Bubbly Two-Phase Flows, Int. J. Multiphase Flow 8 (1987) 327-343.

[16] T.J. Liu, S.G. Bankoff, Structure of Air-Water Bubbly Flow in a Vertical Pipe - I. Liquid Mean Velocity and Turbulence Measurements, Int. J. Heat & Mass Transfer 36 (1993a) 1049-1060.

[17] T.J. Liu, S.G Bankoff, Structure of Air-Water Bubbly Flow in a Vertical Pipe II. Void Fraction, Bubble Velocity and Bubble Size Distributions, Int. J. Heat & Mass Transfer 36 (1993b) 1061-1072.

[18] M. Lance, J.M. Bataille, Turbulence in the Liquid Phase in a Uniform Bubbly Air-Water Flow, J. Fluid Mech. 222 (1991) 95-118.

[19] V. Roig. C. Suzanne, L. Masbernat, Measurement in Two-Phase Mixing Layer, 3rd. World Conf. Exp. Heat Trans., Fluid Mech Therm., Honolulu, Hawaii, 1993, pp. 1342-1348.

[20] T.G. Theofaneous, J. Sullivan, Turbulence in Two-Phase Dispersed Flows, J. Fluid Mech.116 (1982) 343-362.

[21] C. Suzanne, K. Ellingsen, F. Risso, V. Roig, Local Measurements in Turbulent Bubbly Flows, Nucl. Eng. & Design, (1998) 319-327

[22] S. Sharma, S. Lewis, G. Kojasoy, Local Studies in Horizontal Gas-Liquid Slug Flow, J. Nucl. Engr. & Design, 184 (1998) 305-318.

[23] R.L. Evans, Turbulence and Unsteadiness Measurements Downstream of a Moving Blade Row, Journal of Engineering for Power, Trans. ASME, Jan. 1975, pp. 131-139.

[24] J. Laufer, The Structure of Turbulence in Fully-Developed Pipe Flow, NACA Report 1174, 1954.

Nomenclature

A	cross-sectional area (m^2)
D	diameter of pipe (m)
j_f, j_g	local, time-averaged superficial velocities of liquid and gas
$\langle j_f \rangle$, $\langle j_g \rangle$	cross-sectional area-average value of j_f and j_g (m/s)
R	radius of pipe (m)
r	radial coordinate (m)
N_{lb}, N_{sb}	number of large and small bubbles (-)
t	time (s)
u	instantaneous axial velocity component (m/s)
u_{ave}	time-averaged local velocity (m/s)
u′	instantaneous local velocity fluctuation in axial direction (m/s)
$\overline{u'}$	root-mean square values of u′ (m/s)
u_{LS}	average liquid slug velocity (m/s)

Greek Symbols

α	local void fraction

Subscripts

f	liquid phase
g	gaseous phase
lb	large bubble
sb	small bubble
sp	single-phase flow
tp	two-phase flow
LS	liquid slug

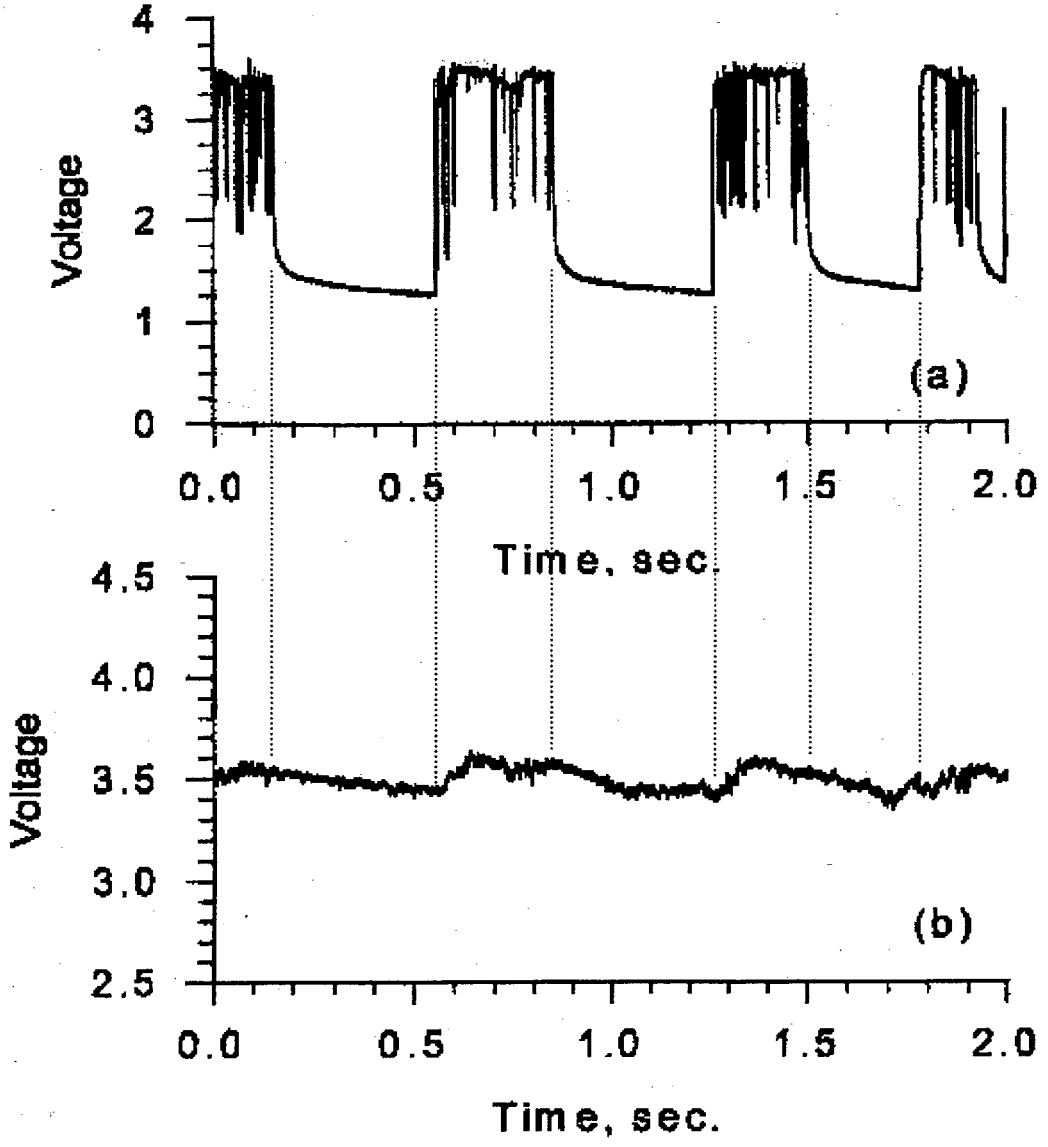

Fig. 1. Typical Probe Signals of Two-Probe Measurements for $\langle j_f \rangle$ = 2.2 m/s and $\langle j_g \rangle$=1.1 m/s,

(a) Probe Pierces Through Elongated Large Bubbles at r/R = 0.8

(b) Probe Located in Liquid Layer Below Passing Large Bubbles

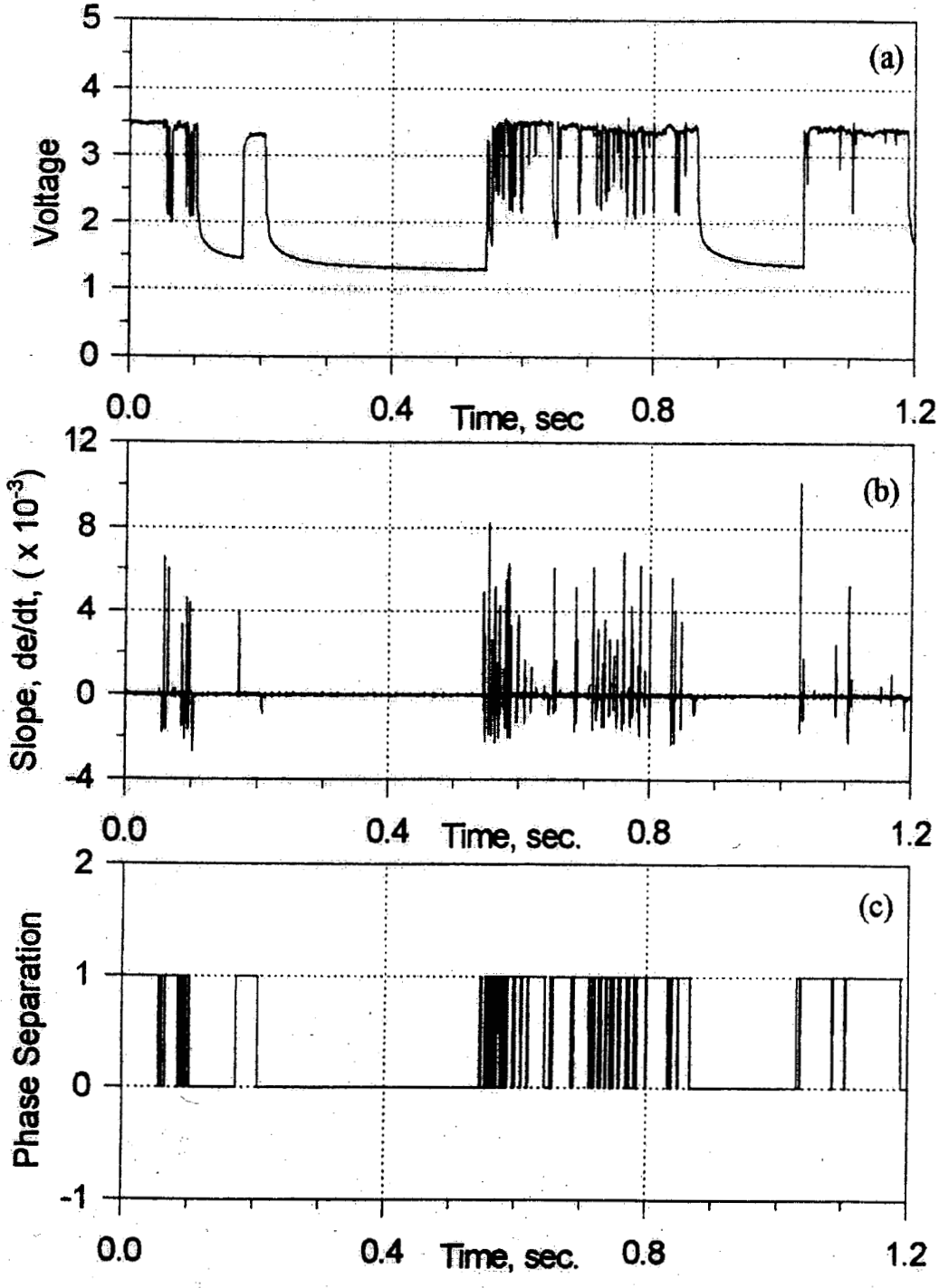

Fig. 2. Typical Anemometer Output and Signal Processing

(a) Anemometer Output Signals

(b) Slope of Voltage Signals

(c) Phase Separation Step Signals

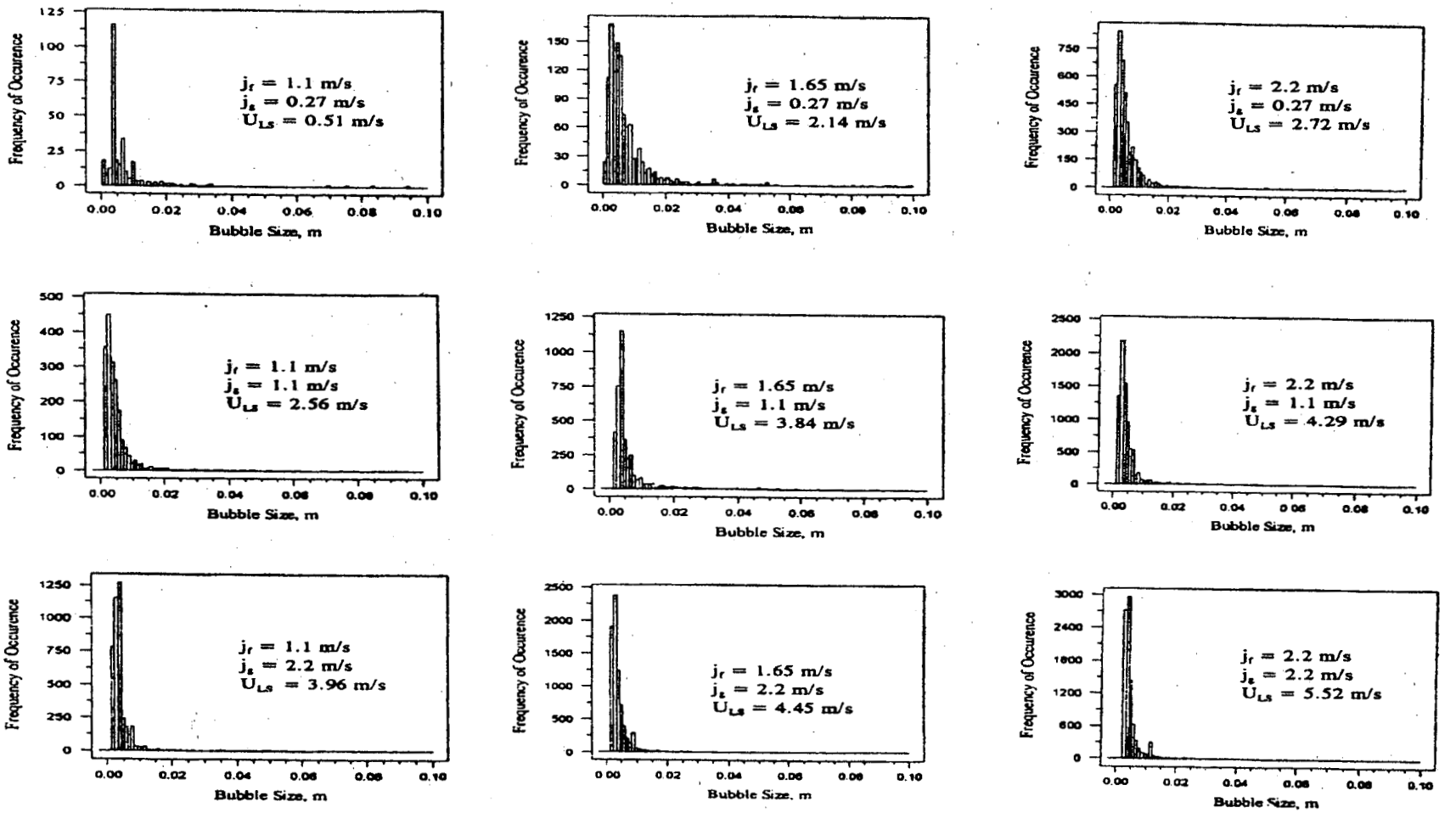

Fig. 3. Bubble Size Spectrum for varying gas velocities at

(a) $< j_f > = 1.1$ m/s and $< u_{LS} > = 2.14$ m/s,

(b) $< j_f > = 1.65$ m/s and $< u_{LS} > = 3.84$ m/s,

(c) $< j_f > = 2.2$ m/s and $< u_{LS} > = 4.45$ m/s

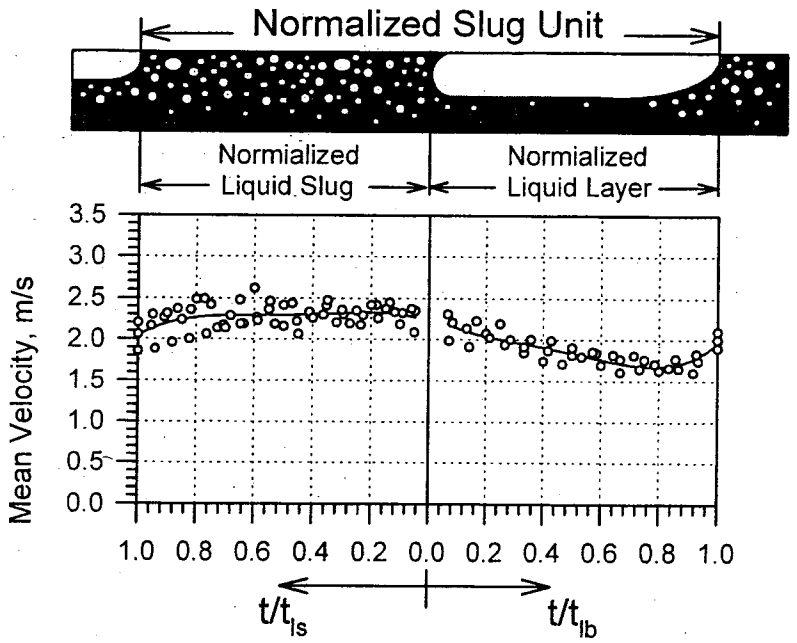

Fig. 4. Axial Velocity Variation in the Liquid Slug and the Liquid Layer under Passing Large Bubbles

A - Interchangeable Air-Water mixing chambers
B - Water flow meters of appropriate size
C - Water flow meter control valves
D - Air flow meters of appropriate size
E - Air flow meter control valves
F - Air flow regulating valves
G- Air pressure regulator
H - Air filter
I - Water pressure relief valves
J - Water flow regulating valves
K - Pneumatic operated ball valves
L - Motor control
M - computer and data acquisition system
N - 250 gal. Air tank
P - 500 gal. Water tank
Q - Air-Water separator, with internal baffles
R - Water shut-off valve
S - 20 hp. 750 gpm Water pump
T - Glass pipe couplings with pressure taps

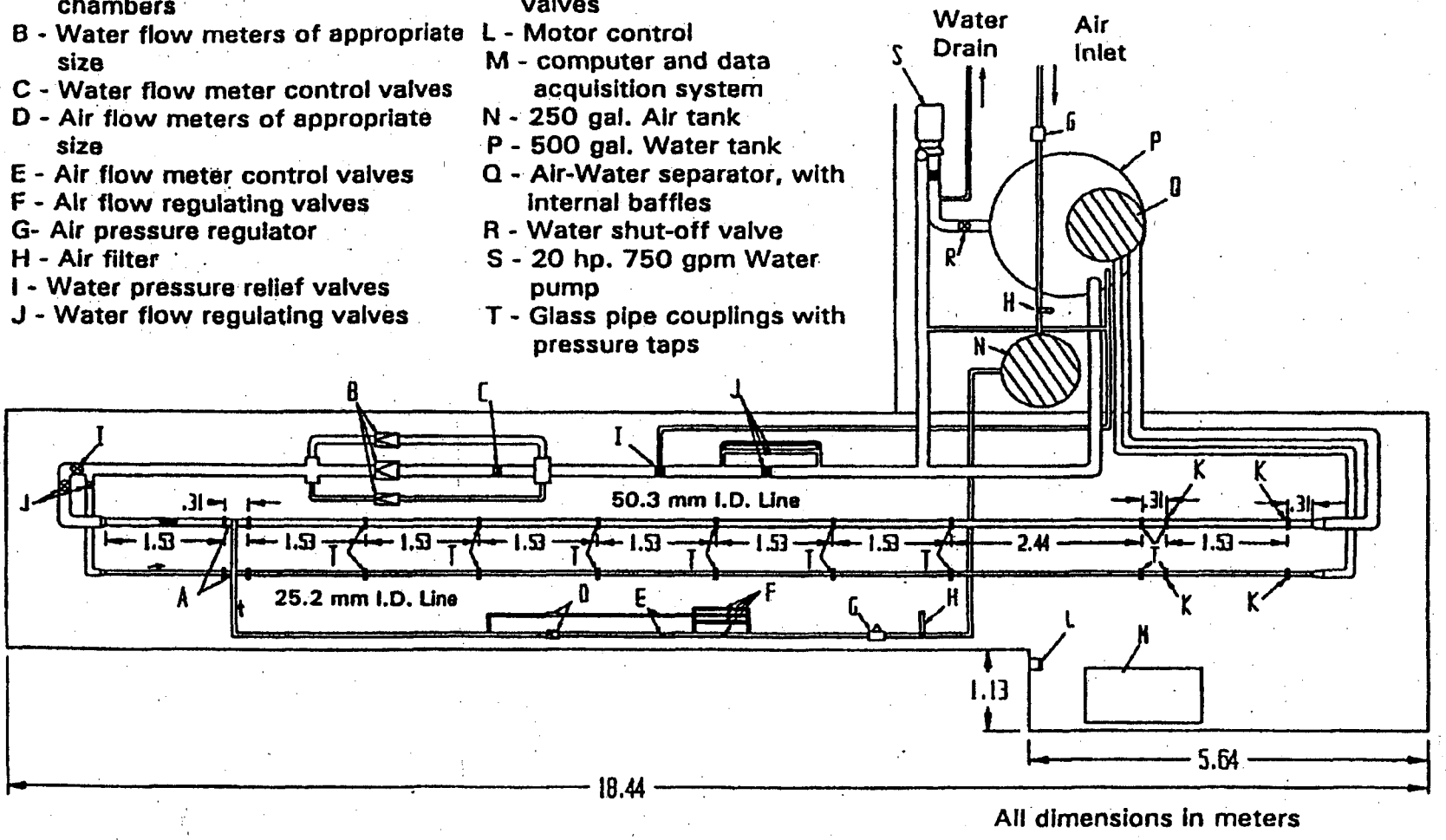

Fig. 5. Schematic of the Experimental Flow Loop

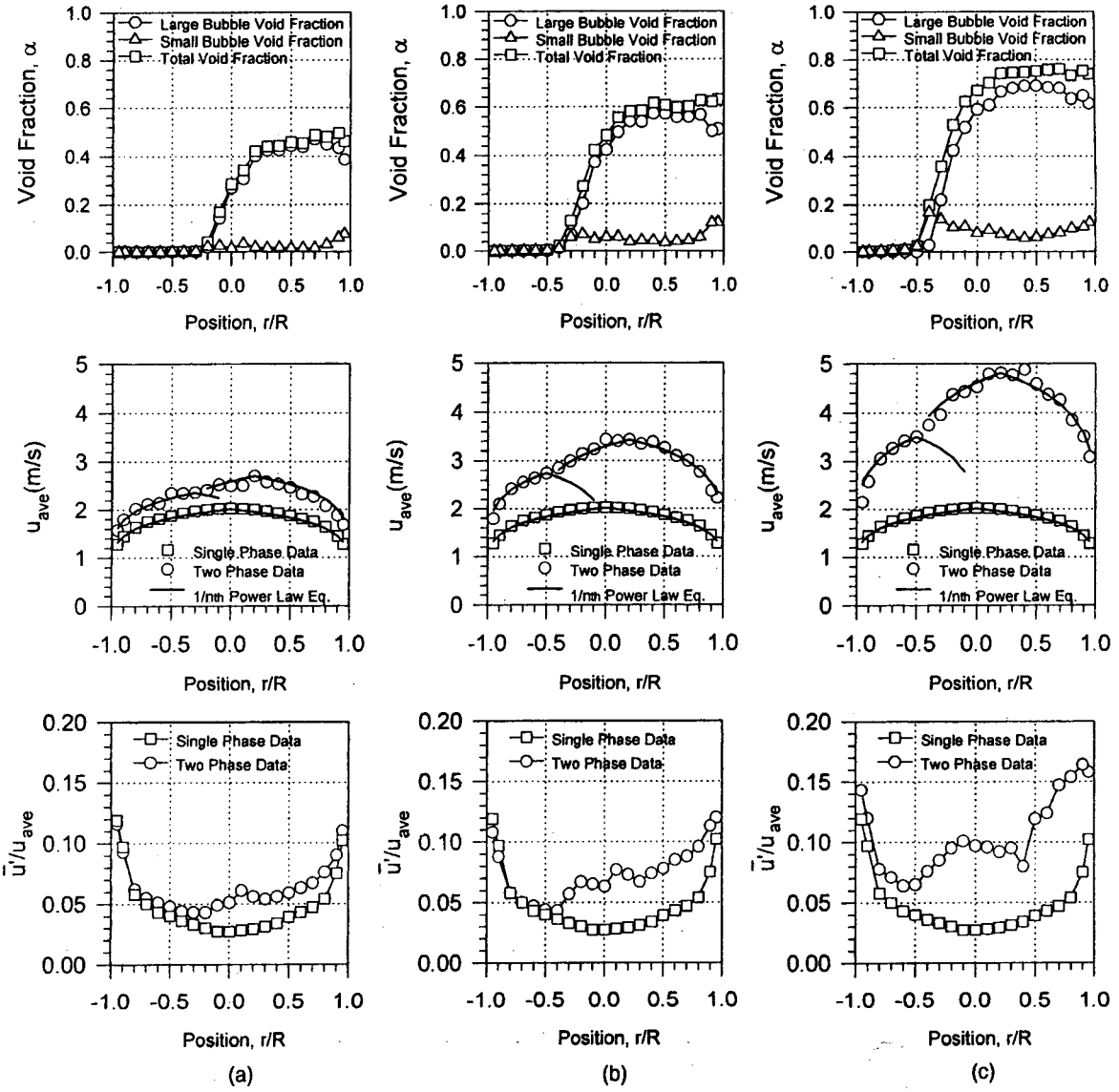

Fig. 6. Local Void Fraction, Mean Velocity and Turbulence Structure Distributions

(a) $< j_f > = 1.65$ m/s and $< j_g > = 0.55$ m/s

(b) $< j_f > = 1.65$ m/s and $< j_g > = 1.1$ m/s

(c) $< j_f > = 1.65$ m/s and $< j_g > = 2.2$ m/s

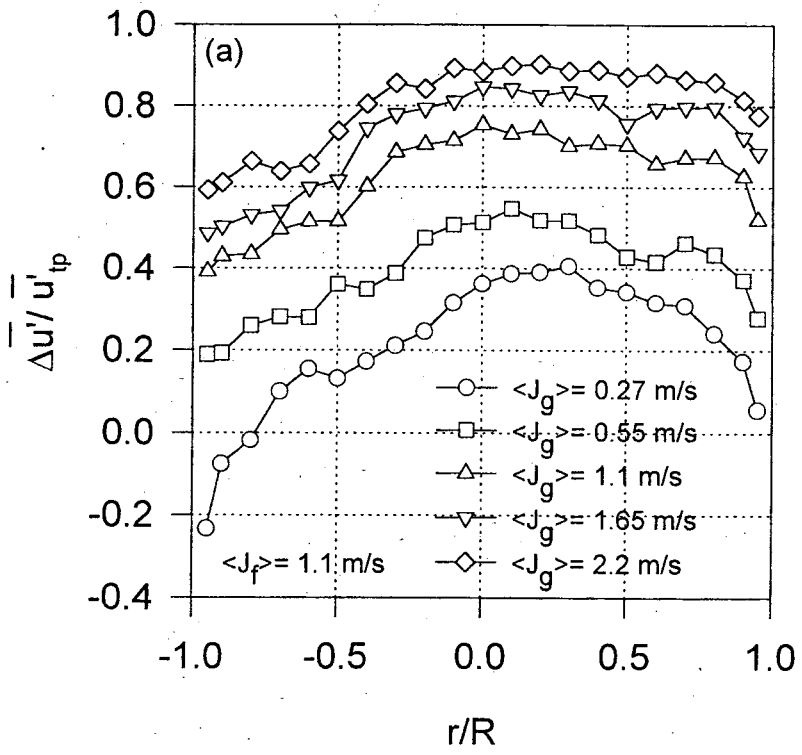

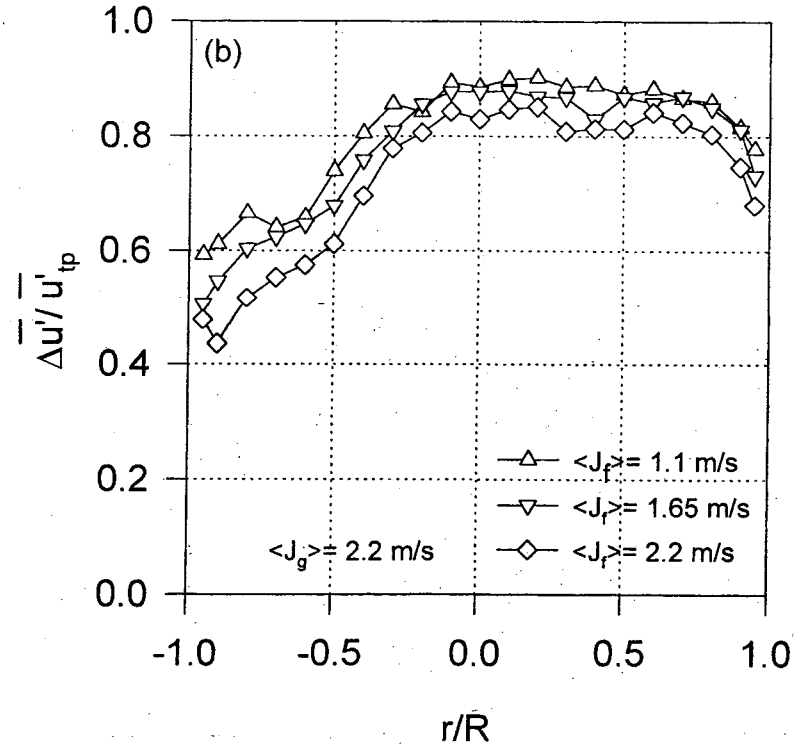

Fig. 7. Local Variation of Bubble-Induced Axial Turbulence

(a) Effect of Gas Flow at $< j_f > = 1.1$ m/s

(b) Effect of Liquid Flow at $< j_g > = 2.2$ m/s

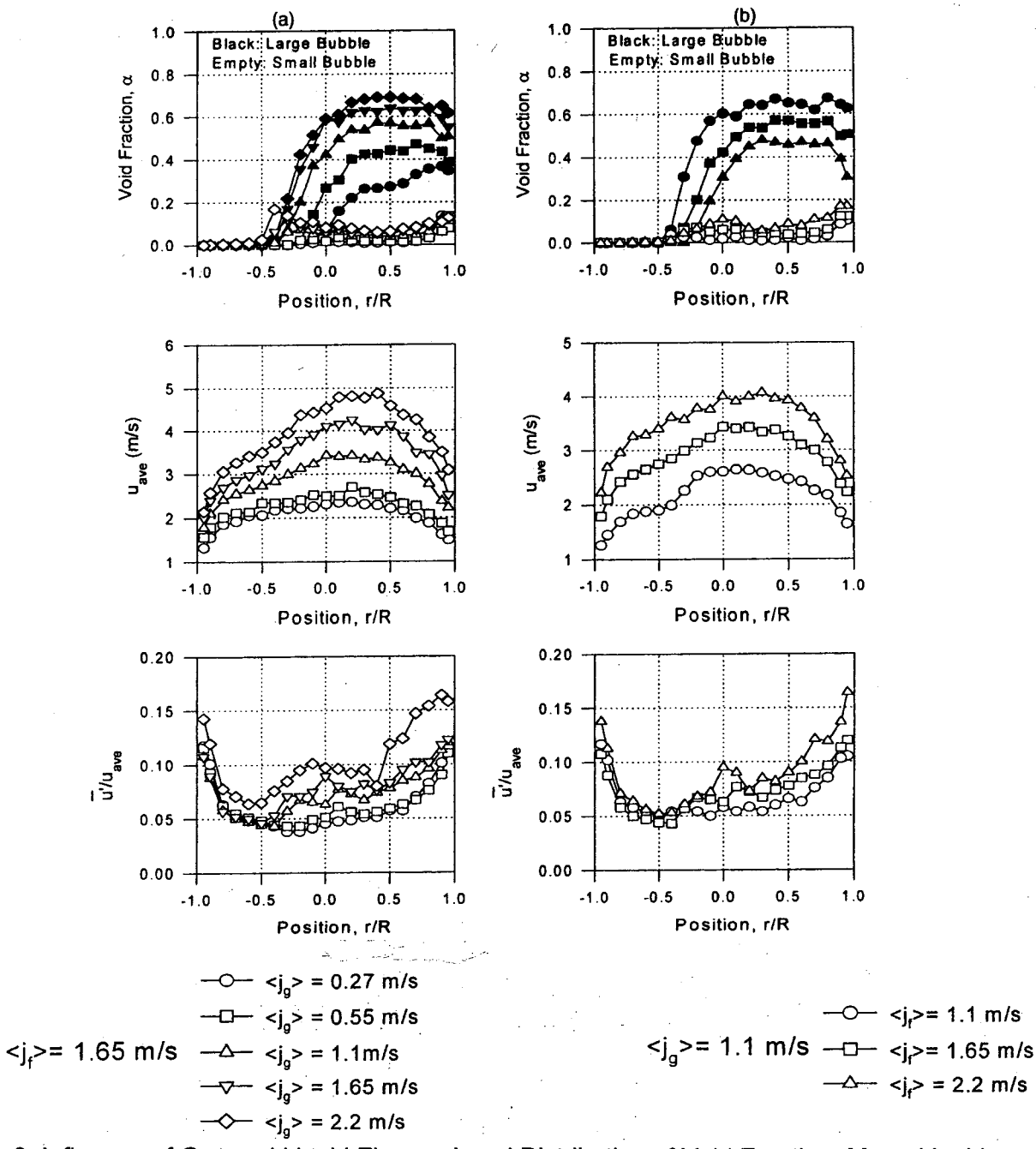

Fig. 8. Influence of Gas and Liquid Flow on Local Distribution of Void Fraction, Mean Liquid Velocity and Turbulent Intensity

(a) Effect of Gas Flow at $< j_f > = 1.65$ m/s

(b) Effect of Liquid Flow at $< j_g > = 1.1$ m/s

10. SIMULTANEOUS USE OF TWO HOT-FILM PROBES FOR LOCAL STUDIES IN SLUG FLOW

S. Sharma, S. Lewis, and G. Kojasoy
Department of Mechanical Engineering, University of Wisconsin-Milwaukee
P.O Box 784 Milwaukee, WI 53201 USA

ABSTRACT

The local axial velocity profile development in a horizontal air-water slug flow-pattern was experimentally investigated by simultaneously using two hot-film anemometers. One of the probes was exclusively used as phase identifier while the other probe was traversed for local velocity measurements. It was shown that the velocity rapidly develops into an asymmetric but nearly fully-developed profiles within the liquid slugs whereas the velocity never develops into quasi-fully-developed profiles within the liquid layer underneath passing gas slugs. Transient nature of velocity at a given location was demonstrated.

10.1 Introduction

As it is demonstrated by classical flow-pattern maps [1 - 4], the intermittent slug flow-pattern exists over a wide range of flow rates in a horizontal two-phase flow configuration. This two-phase flow pattern is described as a gas slug in the form of a large elongated gas bubble in the upper part of the pipe followed by a liquid slug occupying the entire cross section. Based on the flow rates of the gas and liquid, small bubbles may break off of the large slug bubble and either reside in the liquid slug or coalesce with the front of the following gas bubble. In order to advance the study of such a

two phase flow structure, it is essential to experimentally obtain detailed local values of fundamental parameters.

The most significant and essential parameters associated with the slug flow pattern are the distribution of gas and liquid phases, the liquid velocity and its fluctuating components, the gas bubble and liquid transit frequency (or slug length), and the turbulent transport characteristics of interfacial mass, momentum, and energy. These variables describe the local flow conditions of the quasi-steady slug flow, both qualitatively and quantitatively. Hence, accurate information about such flow parameters and generalized relationships among them are necessary to understand the turbulent transport phenomena of the two-phase flow pattern.

A comprehensive physical model describing horizontal gas-liquid slug flow was first initiated by Dukler and Hubbard [5]. This model has been modified and extended over the years by Nicholson et al. [6], Fabre et al. [7], Bornea and Brauner [8], Andreussi and Bendiksen [9], Andreussi et al. [10] and Moalem Maron et al. [11], to apply to the entire intermittent flow-pattern. The predictive models developed by these investigators make it possible to obtain average liquid velocities both in the liquid slug and the liquid region underneath a slug bubble, pressure drops, length of liquid slug, and slug frequencies, if the gas and liquid mass fluxes are provided. These models seem to give reasonable results when compared to experimental data of global measurements. However, these models cannot give the detailed void fraction distribution due to small and large bubbles, local velocity distribution, and the turbulent structure throughout the liquid phase. This information is of great importance to the eventual understanding and modeling of the basic hydrodynamics of two-phase slug flow.

A large number of experimental investigations have been carried out to develop and verify global slug flow models in horizontal flow configurations [10, 12 - 17]. These investigations have been

concerned with measurements of pressure drop, overall void fraction and of statistical characteristics such as slug length, slug frequency and liquid film thickness underneath the large slug bubbles. However, due to the experimental difficulties associated with the intermittent nature of slug flow, very few detailed, local measurements have been reported in the literature. The problem of obtaining local data is further complicated in horizontal flow configurations by the facts of axial asymmetry of the internal structure and that the slug flows do not exhibit a quasi-fully-developed equilibrium condition.

Kvernvold et al. [17] used the combination of LDV and optical two-phase probes to measure the axial velocity distribution throughout a slug flow unit in a 24 mm ID horizontal tube of atmospheric pressure. However, the method is limited to relatively low gas velocities since the application of LDV induces technical difficulties in regions with high concentrations of small gas bubbles in the liquid slug occurring at higher gas flow rates. Andreussi et al. [10] used local (optical) and cross-sectional (conductance) probes to measure the radial void fraction distribution in the liquid slugs, the size of the dispersed bubbles in the liquid slug and the aeration of the liquid layer underneath the slug bubble. Kawaji et al. [19] used the photochromatic dye activation technique to visualize the instantaneous motion of the liquid and gas slugs, and to successfully measure axial and vertical velocity profiles of the liquid phase in a horizontal slug flow. The experimental data were obtained for both circular and rectangular channels, and the liquid flow structure was found to be quite similar between the two channels. These recent studies have provided detailed basic information on the internal structure of the intermittent flow pattern in a horizontal configuration. Information associated with the turbulent structure and the local void fraction contributions due to elongated large bubbles and small bubbles are not addressed in these studies.

In view of the above discussion, it is evident that much experimental work is still necessary to attain a thorough physical understanding of the internal structure of an intermittent two-phase slug flow-pattern. In this context, an experimental investigation has been underway at the University of Wisconsin–Milwaukee to clarify the local velocity behavior and the turbulence structure of this flow pattern. In these experiments the hot-film anemometry technique was used to measure the time-averaged local void fractions due to small and large slug bubbles, as well as, the local axial velocity and turbulence in the liquid phase of an air-water intermittent flow in a 50.3 mm ID horizontal channel. In the following, the test facility is described, and based on the data, preliminary results are documented in terms of the local axial velocity behavior within the liquid slug and the liquid film underneath the large gas slug bubbles.

10.2 Hot-Film Anemometry Method

10.2.1 Measurement Principle

Hsu et al. [20] were the first to propose the possible application of the hot-film anemometry technique to water-steam two-phase flows to identify the two-phase flow patterns and to measure the local void fraction. Delhaye [21] studied the response of hot-film probes in a liquid-gas two-phase flow, and described the probe behavior in great detail under various flow patterns. With a careful treatment of the data, he showed that local measurements of void fraction, liquid velocity and turbulence intensity in the liquid phase could be achieved by a proper use of the hot-film anemometry in air-water flows. Since then, this technique has been used by Serizawa et al. [22, 23], Abel and Resch [24], Wang et al. [25, 26], Liu and Bankoff [27, 28], Lance and Bataille [29] and Grossetete [30] for describing the internal turbulence structure and phase distributions in vertical bubbly flow patterns. The pioneering studies of Theofaneous and Sullivan [31] demonstrated the utility of LDV to measure the turbulence structure in bubbly two-phase flow. However, only limited

efforts were made to examine two-phase flow characteristics in large scale experiments of the slug flow-pattern.

In principle, the hot-film anemometry method consists of the instantaneous measurement of the change in heat transfer from an electrically heated sensor. As the fluid flows past the constant temperature hot-film probe, changes in the fluid velocity, including turbulent fluctuations, cools the sensor at different rates. These changes in cooling rates result in voltage changes in the anemometer. The voltages are digitized and recorded in a PC, where they can later be converted into fluid velocities. In the case of an air-water two phase flow, the heat transfer rate between the two fluids is dramatically different. This results in abrupt voltage changes as the probe encounters phase interfaces. A typical sensor output for a two-phase slug flow is illustrated in Figure 1a and b.

As seen in Figure 1a, when the probe resides in the upper portion of the pipe the sensor encounters the slug bubbles. After the sharp initial drop, caused by the probe piercing the nose of a slug bubble, the voltage gradually continues to decrease while the sensor is inside the gas slug. This is due to the evaporation of a thin film of liquid that remains on the sensor. When encountering a small gas bubble, the signal shows a sharp drop followed immediately by a sharp increase. The probe does not encounter any slug bubbles when positioned in the lower portion of the pipe (Figure 1b). However, the voltage signal shows a quasi-periodic wave motion believed to be caused by the passage of slug bubbles over the top of the probe.

10.2.2 Signal Processing

Before the two-phase voltage output data can be converted to velocities, the portion of the signal related to the gas phase must be removed. Therefore, a phase separation technique was developed. As has been demonstrated by Lance and Bataille [29], the peaks associated with the sensor encountering an interface can be amplified by calculating the slope of the voltage signal,

(de/dt), where e is the voltage level and t is the time. By careful comparison of the voltage and slope values at the nose and tail interfaces, threshold values were set that distinguish the interface from normal liquid or gas turbulence signals. Once the interfaces were found, a phase identifying signal ($\delta = 1$ in gas phase and $\delta = 0$ in liquid phase) was created for use in phase separation of the voltage signal and calculation of the local time-averaged void fraction. The voltage signal corresponding to the liquid phase was then calibrated into velocities.

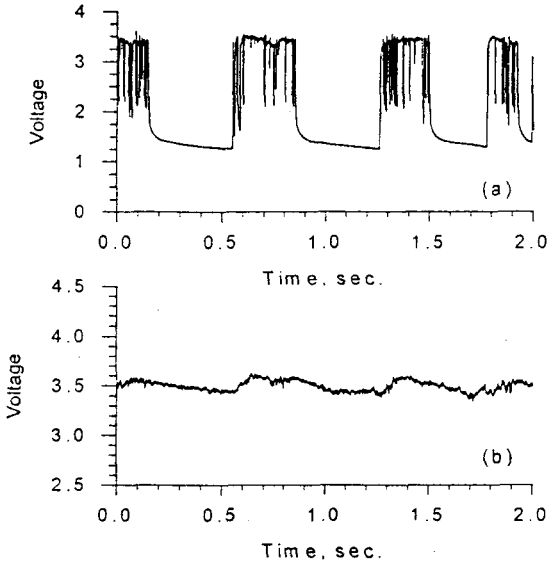

Figure 1. Typical Probe Signals of Two-Probe measurements for $\langle j_f \rangle = 2.2$ m/s and $\langle j_g \rangle = 1.1$ m/s,
(a) Probe Pierces through Slug Bubbles at r/R = 0.8
(b) Probe Located Below Passing Slug Bubbles.

As was seen in Figure 1b, when the probe is positioned near the bottom of the pipe, the voltage signal shows a wave motion induced by the intermittent nature of slug bubble passage over the probe. This wave causes errors in the calculation of the turbulent fluctuations. A time-domain filtering method was introduced to remove the wave.

10.3 Experimental Setup and Procedure

10.3.1 Experimental Setup

The two phase flow loop schematic is illustrated in Figure 2. The loop is made up of sections of pyrex tube, 50.3 mm ID. x 1.53 m in length, flanged together. Between each section, a pressure tab is installed to measure pressure drop. The flow loop is about 15.4 m in total length, and is entirely transparent to allow for flow visualization, high-speed photography, and high-speed cinematography.

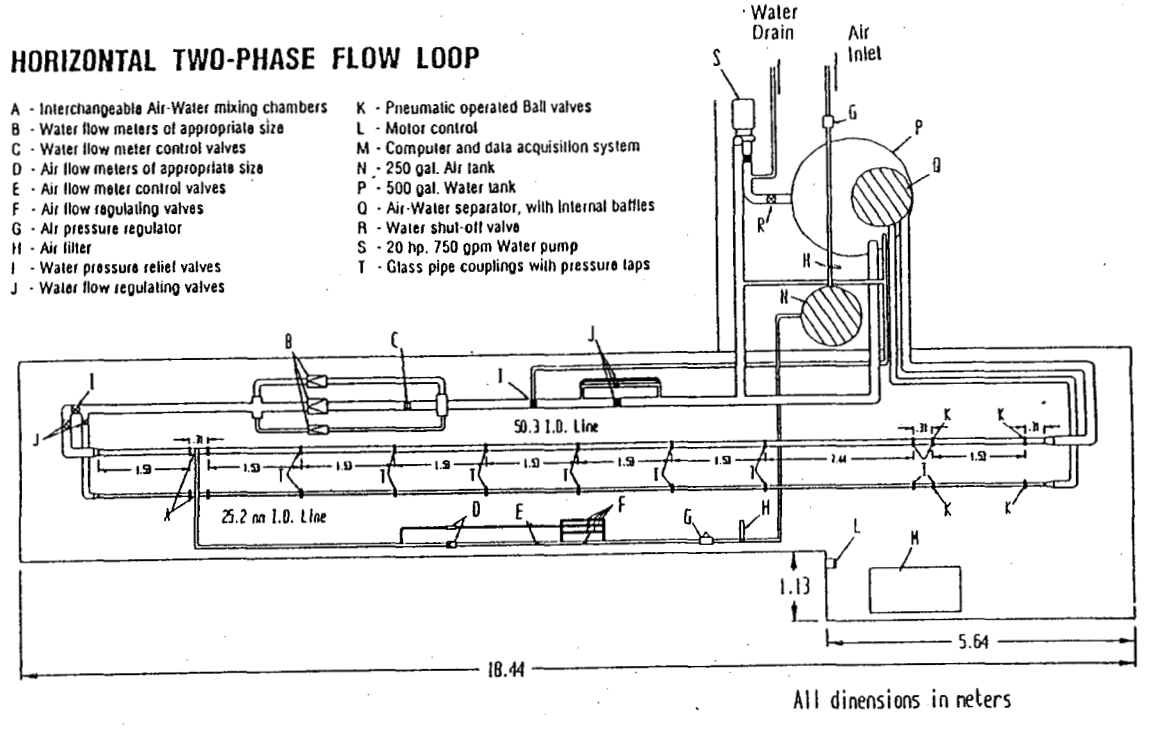

Figure 2. Schematic of Experimental Flow Loop

Air and water are the working fluids used to develop two phase flow. The air is supplied by the university's main air system. The air is filtered as it enters a 0.95 m^3 capacity, high-pressure, storage tank. The air pressure is then stepped down where the flow rate is regulated by a series of valves in parallel. The flow rate is measured by a series of turbine flow meters. Distilled water is stored in a 1.9 m^3 capacity tank. A stainless steel centrifugal pump, regulated by a transistor inverter,

is used to force the water through the loop. The water flow rate is measured by a series of paddle-wheel flow meters.

A T-joint in the glass tubing is used for the air/water mixing chamber (Figure 3). Air is injected into the water through a cylindrical porous media of 100 μm porosity. At the other end of the flow loop the two phase mixture enters a separator where the air is vented to the atmosphere and the water is returned to the storage tank. In the water storage tank, the water temperature is maintained by a tap water cooling system.

Seven pressure taps are mounted along the flow loop. Six diaphragm type pressure transducers along with six U-tube manometers are used to measure the pressure drop. The pressure transducers have a natural frequency of 5 Hz. with a range of 0 to 34.4 kPa, and an accuracy of ±0.3% of the full scale. The pressure of the air at the location of the flow meter and the two-phase system pressure measured at the test section are both measured and used to correct for the compressibility effects of air.

10.3.2 Experimental Procedure

The experiments were carried out using hot-film anemometry and conical shaped (TSI 1264 AW) miniature platinum hot-film probes. The base of the cone is 0.75 mm in diameter. Frequency response of the probe is rated as 150 kHz in air. It is expected greater in water. The liquid and gas volumetric superficial velocities ranged from 1.10 to 2.20 m s^{-1} and 0.27 to 2.20 m s^{-1}, respectively, to develop plug and slug flow regimes. For all the flow conditions, the system pressure was near atmospheric and the temperature about 20-22 °C. The uncertainty for every flow condition was within ± 7.8% for small bubble void fraction and less than ± 1% for slug bubble measurements. The uncertainty for the velocity measurements was better than ± 4%.

As shown in Figure 4, two hot-film anemometers were used in this experiment. One probe was used exclusively to identify the gas and liquid phase while the other probe measured the instantaneous axial velocity components. Each probe was attached to a Vernier scale, with graduations to an accuracy of 0.01 mm. Each of them, further, were mounted on a screw-rod mechanism, fitted with a dial to facilitate traversing linearly. The two probes were mounted diametrically opposite to each other along the vertical axis. For each probe, after the probe was centered along the axis of the tube, the position of the probe was read on a digital linear scale. The high resolution was necessary to evaluate probe positions in the flow stream accurately and to ensure reproducible results. To begin with, the top probe was positioned at r/R value of 0.8 and the bottom probe was positioned at r/R value of 0.7. The top probe was held at this location throughout the experiment. The bottom probe was traced through the vertical axis of the pipe, stopping at 18 positions to take measurements. The local, instantaneous liquid velocity was measured at each location by the bottom probe and the top probe was used to determine whether the bottom probe was in the liquid slug or in the liquid film underneath passing gas slug.

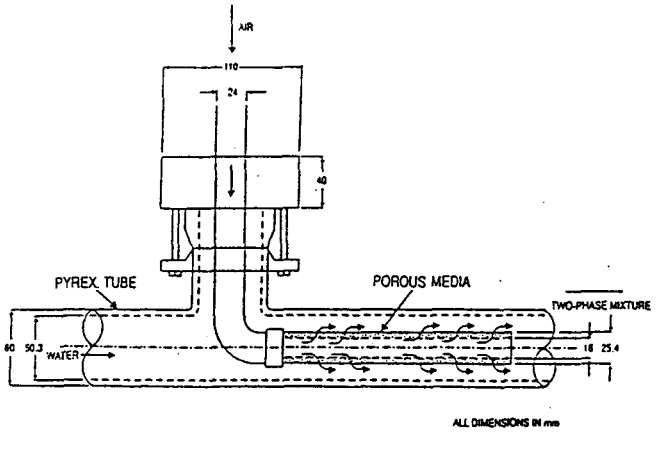

Figure 3. Schematic of Air-Water Mixing Chamber

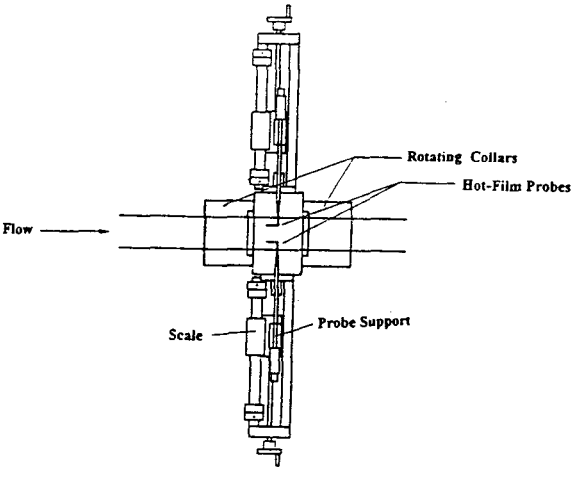

Figure 4. Use of Two Hot-Film Probes

For each preset experimental condition, the pressure drop along six sections of pipe was recorded using electronic pressure transducers and verified by U-tube manometer measurements. In addition to the liquid and gas flow rates, the liquid temperature, gas absolute pressure, and system absolute pressure were recorded.

Before beginning the two-phase measurements, single-phase liquid measurements were made in the same loop to calibrate the instrumentation, verify their consistency with known results, and to serve as a reference for later comparison with two-phase flow measurements. The local mean axial velocity and the turbulent fluctuations in the axial direction were measured along the radial direction. The measured velocity profiles and turbulent fluctuations were non-dimensionalized with respect to the characteristic velocities of centerline velocity and friction velocity, respectively, for the purpose of comparing with Laufer's [32] and Liu and Bankoff's [27] data. The time averaged local axial velocity $U_{ave}(r)$, and the root-mean-square values of the turbulent fluctuations, $u'(r)$, were found to be reasonably satisfied when compared with those results provided in these references. These comparisons can be found in Mr. S. Lewis' thesis [33].

To begin each two-phase flow experiment, the hot-film probe was calibrated in the single-phase liquid flow by comparison of the sensor voltage level with the centerline velocity and fully-developed turbulent flow pressure-drop information. Following this calibration, the pipe was filled with single-phase liquid flowing at an area-averaged mean velocity, $\langle U_{ave} \rangle$, equal to the mean superficial liquid velocity, $\langle j_f \rangle$, desired in the two-phase experiment.

The data from the probe was collected by the anemometer and stored in a PC computer. Due to the limitations of the computer, the sampling rate was set to 5 kHz which allowed a statistically meaningful sampling time. Once the data are stored in the memory of the computer, a FORTRAN

program was used to process the data, separating the phases, converting the voltages to velocities, and calculating the essential parameters.

The local void fraction, α, at any point, r, can be obtained by the hot-film probe sensor. It is defined as a time-averaged void fraction by

$$\alpha(r) \equiv \lim_{T \to \infty} \int_0^T \delta(r,t)\,dt \tag{1}$$

where δ, as a function of the space coordinate, r, and time, t, is equal to 1 if the probe sensor is in the gas phase and δ is equal to 0 if the sensor is in the liquid phase. As the signal is given in discrete form, Eq. (1) can be written as follows:

$$\alpha(r) = \frac{1}{T}\left[\sum_{i=1}^{N_{lb}} (t_{2i} - t_{2i-1}) + \sum_{j=1}^{N_{sb}} (t_{2j} - t_{2j-1})_{sb}\right] \tag{2}$$

where t_{2j-1} is the time when the probe sensor enters into the small bubble, and t_{2j} is the time the sensor enters into the liquid phase. Similarly, the subscript i identifies large elongated slug bubbles. N_{lb} and N_{sb}, respectively, are the number of large and small bubbles passing the probe sensor in the total sampling time, T. It is to be noted that

$$i = 1, \cdots N_{lb}, \tag{3}$$

and

$$j = 1, \cdots N_{sb}, \tag{4}$$

The local, mean axial velocity and the root-mean-square values of turbulent fluctuations were calculated using

$$U_{ave}(r) = \left[\sum_{k=1}^{N} u_k(r,t)\right]/N \tag{5}$$

$$u'(r) = \left\{\sum_{k=1}^{N} [u_k(r,t) - U_{ave}(r)]^2/N\right\}^{1/2} \tag{6}$$

respectively. In Eq. (6), $u_k(r,t)$ is the instantaneous axial velocity for the k'th data point in the liquid phase, and N is the total number of data points in the liquid phase of the digital sample, k = 1, . . ., N. As described above, to remove the error caused by the intermittent wave motion, the time averaged, mean velocity in Eq. (6), $U_{ave}(r)$, is replaced with a curve fit, time dependent mean velocity, $U_{ave,\,CF}(r,t)$, as

$$u'(r) = \left\{ \sum_{k=1}^{N} [u_k(r,t) - U_{ave,CF}(r,t)]^2 / N \right\}^{1/2} \tag{7}$$

From the local values of $\alpha(r)$ and $U_{ave}(r)$ measured along the vertical axis, and with the hypothesis that the flow variables are invariant at a given horizontal slice located at $-1 < r/R < 1$, the area- averaged liquid superficial velocity $\langle j_f \rangle$ was calculated as follows:

$$\langle j_f \rangle \equiv \frac{1}{A} \int_A [1 - \alpha(r)]\, U_{ave}(r)\, dA \tag{8}$$

where A is the cross-sectional area of the pipe.

In order to check the accuracy of both local void fraction and the mean axial liquid velocity measurements, the area-averaged liquid superficial velocity calculated by Eq. (8) was compared with corresponding liquid superficial velocity as given by the flow meter. It was observed that the calculated superficial velocity was consistently over-estimated by a margin of 5 to 12%. There may be several reasons for such a consistency. First, as noted by Wang et al. [25] the void fraction measured by the conical hot-film probe technique is underestimated due to the deformation and the deflection of the bubbles by the probe. Such an experimental error is expected to be more pronounced in measuring the small bubble contribution toward the total void fraction expressed by Eq. (2). Secondly, as demonstrated by Figure 1b, the data shows a wavy pattern when the probe is located underneath the slug bubble. Although a correction on the time domain was performed to

smooth out the behavior, this may still cause some errors in calculating the mean velocity in the liquid phase. Finally, the small-amplitude peaks due to the incomplete piercing of small bubbles or to the bubble sliding on the probe are difficult to detect by the present data processing. This is again expected to be the case in the small bubble encounter of the probe. These series of experimental errors are probably the main causes of the systematic error observed in matching the liquid superficial velocities.

Once the statistical data is extracted from the raw data, the results are then graphed for visual investigation of characteristics. In the graphs the instantaneous velocity values of several slug units are plotted and a best curve is fitted to these points. The absence of points indicate either slug units were fewer than the minimum selected during the sampling time or there were data points which could not be considered for analysis. The time-averaged local values of the void fraction due to small and large bubbles, the overall mean liquid velocity, and the local turbulence fluctuations were presented elsewhere [34]. Here we are presenting preliminary results in terms of the local axial velocity within the liquid slug and the liquid film underneath the large gas slug bubbles. Additional data analysis is expected to lead to a more detailed understanding of two-phase slug flow.

10.4 Experimental Results and Discussions

Considering the unit cell concept, where a lump of liquid which travels over a thin substrate film separating liquid lumps, as illustrated in Figure 5, the flow structure was investigated in the following four distinctive regions:

1) Liquid ahead of gas slug nose,
2) Liquid in the wake region,
3) Liquid layer below the gas slug, which is subdivided into two regions, namely
   3.1) Near the gas slug nose, and

3.2) Near the gas slug wake.

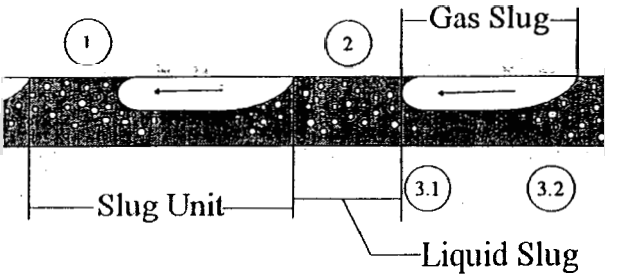

Figure 5. Basic Flow Unit in Slug Flow

The preliminary experimental observations are detailed as below:

10.4.1 Liquid Ahead of the Gas Slug Nose

The local time-averaged axial velocity profiles in the liquid slug are presented in Figure 6. The first figure shows the instantaneous velocity profile at 0.02 seconds ahead of incoming gas slugs. The successive frames are presented in such a way that local liquid velocity profiles in liquid slugs can be analyzed at every 0.02-seconds intervals in front of incoming gas slugs. At least three moving liquid slugs are used to construct these figures. In presenting these experimental data no other statistical averaging techniques were used. The solid lines indicate simple fourth-order curve fittings.

The gas slug interfacial velocities which were measured by the four-sensor resistivity probe technique [35] showed that the interfacial velocity of these gas slugs ranged between 2.7 to 3.25 m/s. The frequency of gas slugs was about 3 to 4, whereas, the average gas slug length was about 50 ~ 60 cm. From the first few figures it is evident that there exists an acceleration region very close to the nose of gas slugs. This initial acceleration of the liquid could be attributed to the faster moving gas slugs. In this region the location of the maximum velocity moves from about center line downward below the center line of the pipe. Here the liquid moves downward due to the downward curvature of faster moving gas slug-liquid interface near the nose resulting in the appearance of the

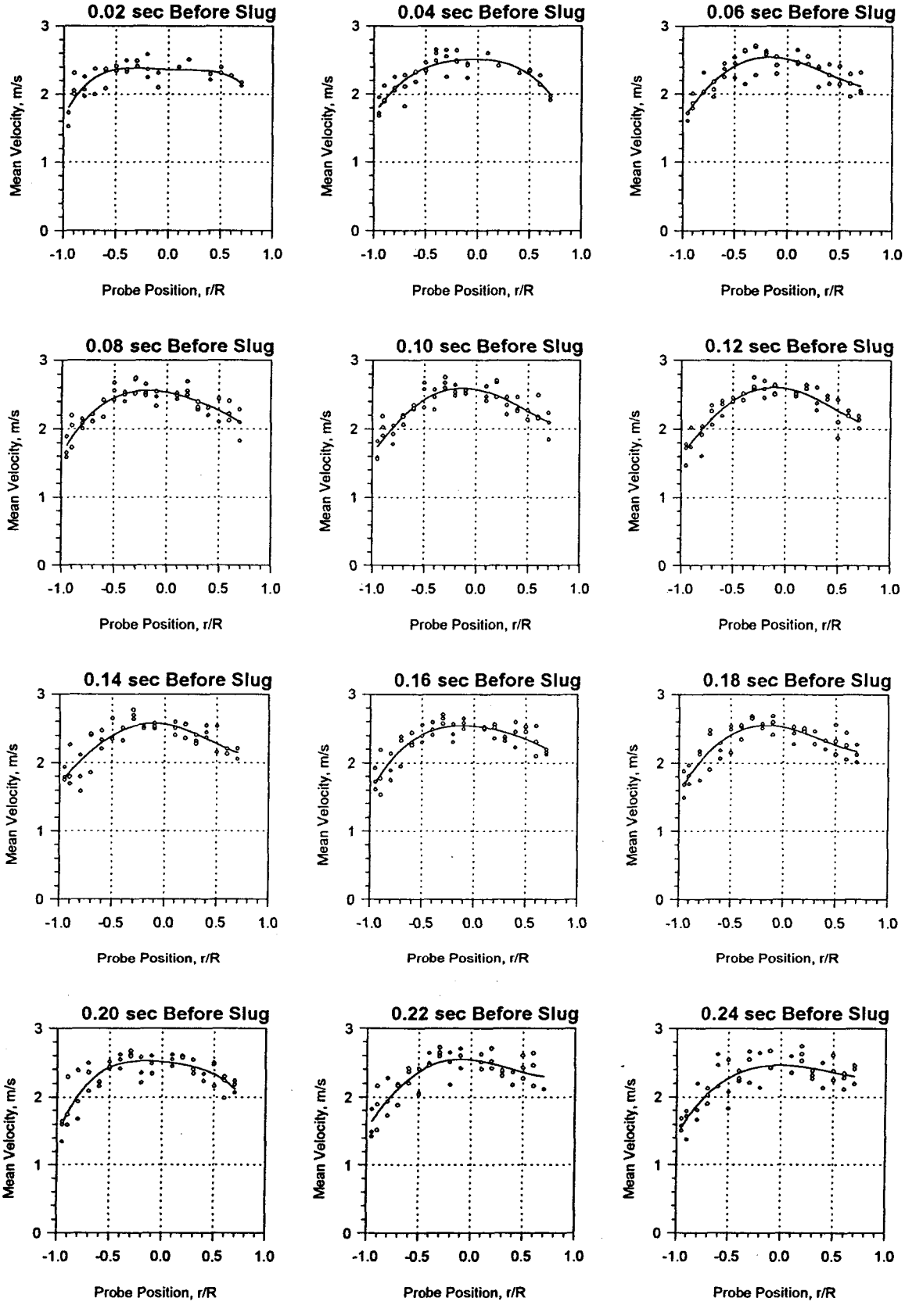

Figure 6. A Typical Velocity Profile Development for Liquid Ahead of Gas Slug Nose.

maximum velocity below the center line. Although it is not seen here this acceleration region is much more pronounced when the gas superficial velocity is higher than 0.55 m/s.

Beyond the transition region of 0.06 ~ 0.08 seconds in front of gas slugs the flow is much like a single-phase liquid flow. Although it is not axially symmetric the velocity profile attains a semi-fully developed condition. This shows that the beyond the transition region the axial velocity is relatively unaffected by the approaching gas slugs. The immediate influence of incoming slugs is confined to a very small region in front of the gas slugs. This observation is consistent with those of Kawaji et al. [19]. However, this uniform flow situation is altered when the probe position approached to the immediate wake region of the gas slug in front of the liquid slug. Such a case can be observed around 0.24-second frame where one can see a slight deceleration. This may be attributed to the vortex generated in front of liquid slugs at the wake of gas slugs. Detailed study of this region will be given below.

10.4.2 Liquid in the Wake Region

The velocity profiles recorded in the slug at 0.02, 0.04, 0.06, ----- 0.24-second downstream of gas slug tails are shown in Figure 7. The figures thus show how the velocity profiles evolves within the liquid slug from a completely unsymmetric profile to a nearly symmetric profile at about 0.12 seconds.

It is evident from the first four or five figures, there is a rapid axial velocity acceleration zone behind a gas slug. It is interesting to observe that in the tip of the liquid slug, the acceleration is much higher than the other parts. This is probably due to the suction caused by the wake region of the faster moving gas slugs. Out of the acceleration zone the velocity profile exhibits a nearly fully-developed single-phase liquid flow character with the maximum velocity occurring slightly below the center line.

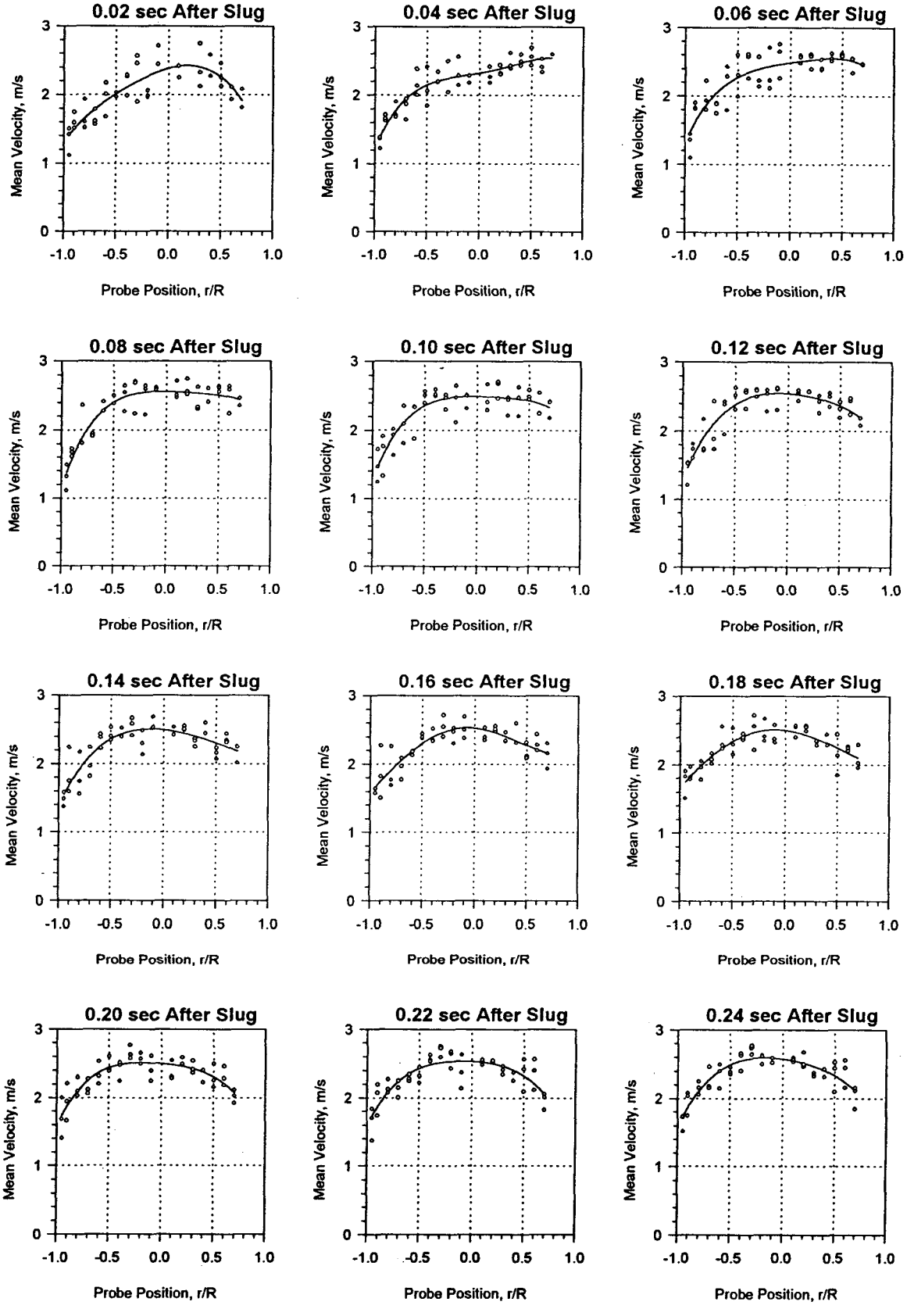

Figure 7. A Typical Velocity Profile Development for Liquid in the Wake Region of the Gas Slug

10.4.3 Liquid Layer Below the Gas Slug

Figure 8 illustrates the liquid behavior within the liquid layer close to the gas slug nose whereas Figure 9 shows the liquid velocity behavior within the liquid layer close to the gas slug tail. From these figures it is clear that axial velocity profile never develops into a fully-developed profile. As indicated in Figure 8, the liquid gradually decelerates from the gas slug nose. The effect of interfacial shear exerted by the faster moving gas slug seems to be confined to the very vicinity of the interface. Such an effect causes a peculiar velocity profile with a point of inflection occurring between the wall and gas-liquid interface. Figure 9 displays a very rapid deceleration in the liquid layer toward the upstream of the slug tail. However, this brief deceleration is followed by a gradual acceleration toward the slug nose.

The velocity evolution at location r/R = -0.6 is shown on Figure 10 where the time is normalized by the liquid slug passage time T_{slug} and the gas slug passage time T_{film} within the liquid slug and liquid layer, respectively. The ever developing nature of the liquid layer flow and the relatively uniform flow behavior of the liquid slug flow are displayed from this figure. Within the liquid layer the liquid gradually decelerates from the slug nose. However, right before the slug tail a rapid acceleration is observed. On the other hand, out of the transition zones after the gas slug nose and before the slug tail within the liquid slug, the velocity stays constant at this r/R = -0.6 location. It is interesting to note that there exists significant differences between the liquid slug and liquid layer velocity behaviors.

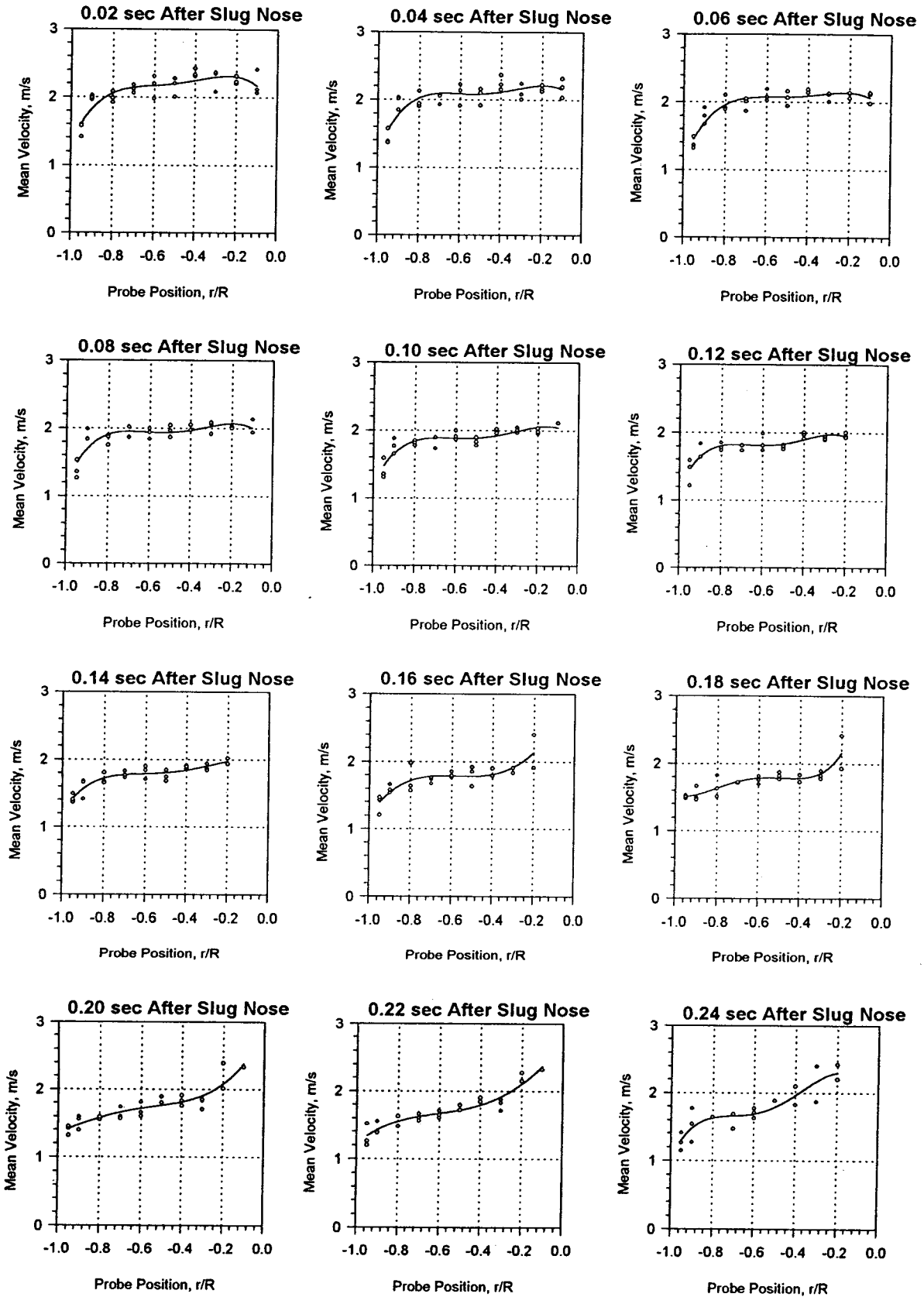

Figure 8. A Typical Velocity Profile Development for Liquid Layer Near Gas Slug Nose.

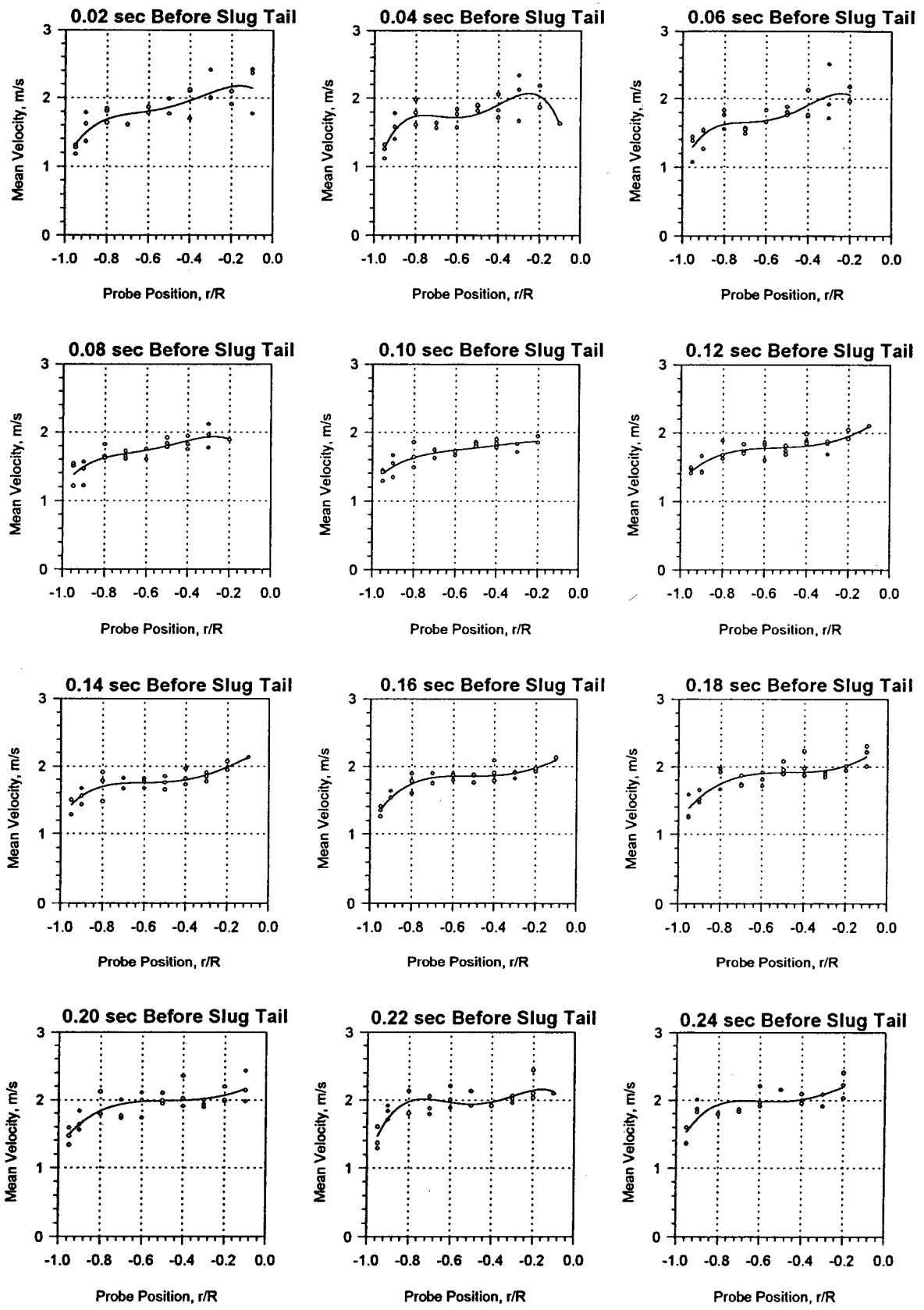

Figure 9. A Typical Velocity Profile Development for Liquid Layer Near Gas Slug Wake

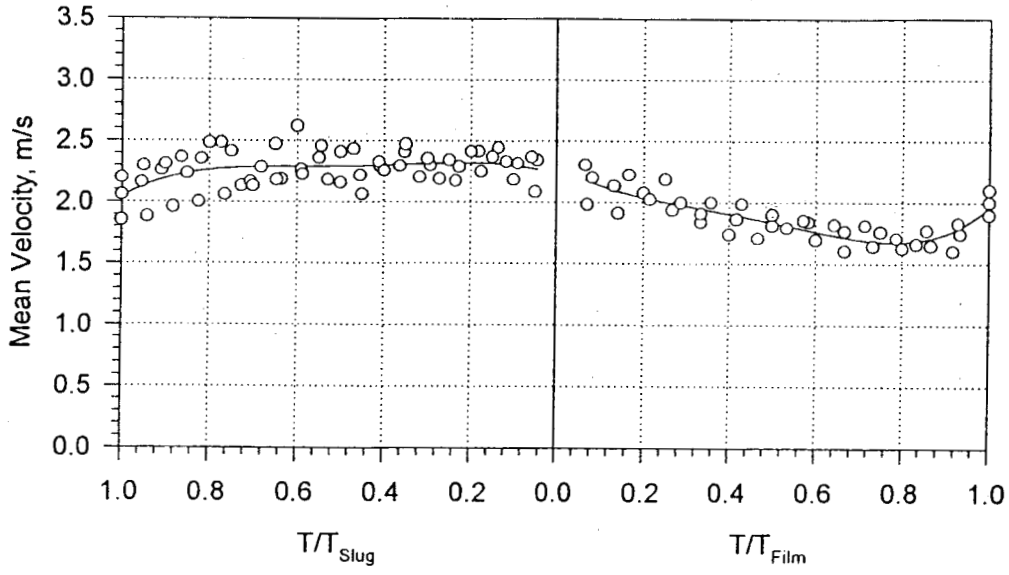

Figure 10. Axial Velocity Variations in Liquid Slug and Liquid Layer Under Gas Slug.

10.5 Summary and Conclusions

The local velocity profile development for a horizontal air-water, two-phase slug flow-pattern in a 50.3 mm-ID transparent pipeline has been experimentally investigated by simultaneously using two hot-film anemometers. One of the probes which was kept at a fixed location was exclusively used as a phase identifier while the other probe was traversed vertically for local velocity measurements.

Experimental observations were focused on the intermittent and transient characteristics of the slug flow-pattern. For this purpose a unit-cell concept of a typical slug flow was used to document the experimental data. It was shown that the velocity rapidly develops into an asymmetric but nearly fully-developed profiles within liquid slugs with the maximum value occurring below the pipe center line. Although there exists short transition zones behind and ahead of gas slugs, the velocity profile remain uniform within the liquid slugs. On the other hand it was documented that the velocity never develops into a quasi-fully-developed profiles within the liquid layer below a passing gas slug. At

a given location the velocity gradually decelerates toward the gas slug tail. But it rapidly accelerates towards the wake of the gas slug.

Nomenclature

A	Cross-sectional area of the pipe
e	Voltage level
i	Subscript identifying the index number for large elongated slug bubbles
j	Subscript identifying the index number for small bubbles
$<j_f>$	Mean superficial liquid velocity
$<j_g>$	Mean superficial gas velocity
N	Total number of data points in the liquid phase
$N_{\ell b}$	Number of slug bubbles passing the probe in the total sampling time
N_{sb}	Number of small bubbles passing the probe in the total sampling time
R	Pipe radius
r	Hot film sensor location measured along the vertical axis from the pipe center
T	Total sampling time
T_{film}	Gas slug passage time
T_{slug}	Liquid slug passage time
t_{2j-1}	Time when the probe sensor enters into small bubble
t_{2j}	Time when the probe sensor leaves gas bubble
t	Time
$U_{ave}(r)$	Time-averaged mean velocity at r
$<U_{ave}>$	Area-averaged mean velocity
$u_k(r,t)$	Instantaneous axial velocity for the kth data point in the liquid phase

$u'(r)$	Root mean square value of turbulent fluctuations
$\alpha(r)$	Local void fraction
$<\alpha(r)>$	Area averaged void fraction
δ	Kronecker delta

Acknowledgement

The work reported in this paper was performed under the auspices of the U.S. Department of Energy, Office of Basic Energy Science. The authors would like to express their sincere appreciation for the encouragement, support and technical comments on this program from Dr. O.P. Manley of the U.S. DOE/BES.

References

1. O. Baker, "Simultaneous Flow of Oil and Gas," Oil and Gas Journal, Vol. 53, pp. 185-190 (1954).

2. J. M. Mandhane, G.A. Gregory, and K. A. Aziz, "A Flow-Pattern Map for Gas-Liquid in Horizontal Pipeline," Int. J. Multiphase Flow, Vol. 1, pp. 537-554 (1954).

3. Y. Taitel and A. E. Dukler, "A Model for Predicting Flow Regime Transitions in Horizontal and Near Horizontal Gas-Liquid Flow," AICHE J. , Vol. 22, pp. 47-55 (1976).

4. J. Weisman, D.Duncan, J. Gibson, and T. Crawford, "Effect of Fluid Properties and Pipe Diameter on Two-Phase Flow Pattern in Horizontal Lines," Int. J. Multiphase Flow, Vol. 5, pp. 437-462 (1979).

5. A.E. Dukler and M.G. Hubbard, "A Model for Gas-Liquid Flow in Horizontal and Near Horizontal Tubes," Ind. Engng. Chem. Fundam., Vol. 14, pp. 337-347 (1975).

6. M.K. Nicholson, K. Aziz and G.A. Gregory, "Intermittent Two-Phase Flow in Horizontal Pipes, Predictive Models," Can. J. Chem. Engng., Vol. 56, pp. 653-663 (1978).

7. J. Fabre, G. Ferschneider and L. Masbernat, "Intermittent Gas Liquid Flow Modeling in Horizontal or Weakly Inclined Pipes," Proc. Int. Conf. Phys. Modeling of Multiphase Flow, Coventary, Cranfield: BHRA, pp. 233-254 (1983).

8. D. Bornea and N. Brauner, "Holdup of the Liquid Slug in Two-Phase Intermittent Flow," Int. J. Multiphase Flow, Vol. 11, pp. 43-49 (1985).

9. P. Andreussi and K.H. Bendiksen, "An Investigation of Void Fraction in Liquid Slugs for Horizontal and Inclined Gas-Liquid Pipe Flow," Int. J. Multiphase Flow, Vol. 15, pp. 937-946 (1989).

10. P. Andreussi, K.H. Bendiksen and O.J. Nydal, "Void Distribution in Slug Flow," Int. J. Multiphase Flow, Vol. 19, pp. 817-828 (1993).

11. D. Moalem Maron, N. Brauner and D. Naot, "Hydrodynamic Mechanisms in the Horizontal Slug Pattern," Int. J. Multiphase Flow, Vol. 17, pp. 227-245 (1991).

12. Z. Ruder, P. J. Hanratty and T. J. Hanratty, "Necessary Conditions for the Existence of Stable Slugs," Int. J. Multiphase Flow, Vol. 15, pp. 209-226 (1989).

13. Z. Ruder and T. J. Hanratty, "A Definition of Gas-Liquid Plug Flow in Horizontal Pipes," Int. J. Multiphase Flow, Vol. 16, pp. 233-242 (1990).

14. G. Saether, K. Bendiksen, J. Muller and E. Froland, "The Fractal Statistics of Liquid Slug Lengths," Int. J. Multiphase Flow, Vol. 16, pp. 1117-1126 (1990).u

15. O. J. Nydal, S. Pintus and P. Andreussi, "Statistical Characterization of Slug Flow in Horizontal Pipes," Int. J. Multiphase Flow, Vol. 18, pp. 439-453 (1992).

16. Z. Fan, W. P. Jepson and T. J. Hanratty, "A Model for Stationary Slugs," Int. J. Multiphase Flow, Vol.18, pp. 477-494 (1992).

17. Z. Fan, Z. Ruder and T. J. Hanratty, "Pressure Profiles for Slugs in Horizontal Pipelines," Int. J. Multiphase Flow, Vol. 19, pp. 421-437 (1993).

18. O. Kvernvold, V. Vindoy, T. Sontvedt, A. Saasen and S. Selmer-Olsen, "Velocity Distribution in Horizontal Slug Flow," Int. J. Multiphase Flow, Vol. 10, pp. 441-457 (1984).

19. M. Kawaji, M. Ali, A. Ciastek, and C. Lorencez, "Study of Liquid Flow Structure in Horizontal Cocurrent Gas-Liquid Slug Flow," Proc. ANS-THD, Vol. 8, pp. 79-88, 1995, Natl. Heat Transfer Conf., August 5-9, 1995, Portland, Oregon.

20. Y.Y. Hsu, F.F. Simon, and R.W. Graham, "Application of Hot-Wire Anemometry for Two-Phase Flow Measurements such as Void Fraction and Slip Velocity," Proc. ASME Winter Meeting, Philadelphia, PA (1963).

21. J.M. Delhaye, "Hot-Film Anemometry in Two-Phase Flow," Two-Phase Flow Instrumentation, B.W. Le Tourneau and A.E. Bergles, Eds., ASME, pp. 58-69 (1969).

22. A. Serizawa, I. Kataoka and I. Michiyoshi, "Turbulence Structure of Air-Water Bubbly Flow - I. Measuring Techniques," Int. J. Multiphase Flow, Vol. 2, pp. 221-233 (1975).

23. A. Serizawa, I. Kataoka and I. Michiyoshi, "Turbulence Structure of Air-Water Bubbly Flow - II. Local Properties," Int. J. Multiphase Flow, Vol. 2, pp. 235-246.

24. R. Abel and F.J. Resch, "A Method for the Analysis of Hot Film Anemometer Signals in Two-Phase Flows," Int. J. Multiphase Flow, Vol. 4, pp. 523-533 (1978).

25. S.K. Wang, S.J. Lee, O.C. Jones and R.T. Lahey, "Local Void Fraction Measurement Techniques in Two-Phase Bubbly Flow Using Hot-Film Anemometry," Proc. 22nd Heat Transfer Conf., Niagara Falls, August 5-8, 1984.

26. S.K. Wang, S.J. Lee, O.C. Jones and R.T. Lahey, "3-D Turbulence Structure and Phase Distribution Measurements in Bubbly Two-Phase Flows," Int. J. Multiphase Flow, Vol. 8, pp. 327-343, (1987).

27. T.J. Liu and S.G. Bankoff, "Structure of Air-Water Bubbly Flow in a Vertical Pipe - I. Liquid Mean Velocity and Turbulence Measurements," Int. J. Heat & Mass Transfer, Vol. 36, pp. 1049-1060, (1993).

28. T.J. Liu and S.G. Bankoff, "Structure of Air-Water Bubbly Flow in a Vertical Pipe - II. Void Fraction, Bubble Velocity and Bubble Size Distributions," Int. J. Heat & Mass Transfer, Vol. 36, pp. 1061-1072, (1993).

29. M. Lance and J.M. Bataille, "Turbulence in the Liquid Phase in a Uniform Bubbly Air-Water Flow," J. Fluid Mech., Vol. 222, pp. 95-118 (1991).

30. C. Grossetete, "Experimental Investigation and Preliminary Numerical Simulation of Void Profile Development in a Vertical Cylindrical Pipe," Proc. 2nd Int. Conf. on Multiphase Flow, Kyoto, Japan, (1995).

31. T.G. Theofaneous and J. Sullivan, "Turbulence in Two-Phase Dispersed Flows," J. Fluid Mech., Vol. 116, pp. 343-362 (1982).

32. J. Laufer, "The Structure of Turbulence in Fully-Developed Pipe Flow," NACA Report 1174 (1954).

33. S. Lewis, "Use of Hot-Film Anemometry in Horizontal Gas-Liquid Slug Flow," MS Thesis, University of Wisconsin–Milwaukee, May 1996.

34. S. Lewis, M. Herre, V. Davenport, J. Riznic and G. Kojasoy, "Use of Hot-Film Anemometry in Horizontal Gas-Liquid Flow," Nat'l. Heat Transfer Conf., August 3-6, 1996, Houston, Texas.

35. J. R. Riznic, S. Lewis and G. Kojasoy, "Experimental Studies of Interfacial Area in a Horizontal Slug Flow," Proc. ASME-THD-334, pp. 27-37, 1996, Int. Mech. Engr. Congress & Exposition, November 16-22, 1996, Atlanta, Georgia.